

DEVELOPMENT OF A MULTIDIMENSIONAL FLUORESCENCE
MICROSCOPE USING MULTIPOINT CONFOCAL SCANNING

DEVELOPMENT OF A MULTIDIMENSIONAL FLUORESCENCE
MICROSCOPE USING MULTIPOINT CONFOCAL SCANNING

By
Morgan Richards

A Thesis
Submitted to the School of Graduate Studies
In Partial Fulfillment of the Requirements for the Degree
Doctor of Philosophy

McMaster University

© Copyright by Morgan Richards, December 2024

DOCTOR OF PHILOSOPHY (2024)

Department of Engineering Physics

McMaster University

Hamilton, Ontario

TITLE: DEVELOPMENT OF A MULTIPOINT MULTIDIMENSIONAL
CONFOCAL MICROSCOPE

AUTHOR: Morgan Richards, McMaster University

SUPERVISOR: Qiyin Fang, Ph.D.

NUMBER OF PAGES: xvi, 99

Lay Abstract

Microscopes are essential tools in biology that allow scientists to visualize microscopic structures and processes within cells. Scientists use glowing molecules called fluorophores to color the different parts of the cell to better understand its function. One function of interest is how proteins interact with each other, as this is one of the core processes of a cell's function in life. To measure these interactions, scientists need to make many measurements over time, but these glowing molecules only work for a short period of time before they fade. Building a microscope that can carefully take these measurements all at once and fast enough to see changes would allow careful measurement and might help explain what is happening within the cell. The different methods of measurement are spatial (3D), spectral (Color), dynamic (Time), and a special temporal quantum measurement known as the fluorescence lifetime (FLIM). Together, these measurements form a multidimensional description of the protein's behavior. In this thesis, I present the tools developed to address these issues and create a fast, multi-dimensional microscope.

Abstract

Capturing cellular dynamics is key to understanding cell behavior, but this task is challenging due to the weak fluorescence signal in live cells. This signal scarcity becomes more pronounced when divided across multiple contrast dimensions, pushing the boundaries of detector sensitivity. This complexity of measurement is essential for revealing the intricate mechanisms governing cellular function. By using spatial, spectral, and fluorescence lifetime imaging contrasts, we can more precisely isolate species and interactions, uncovering previously hidden aspects of cellular behavior.

In this work, we present the development of multiple prototypes for multi-dimensional multipoint confocal microscopy, designed to optimize the use of these faint signals and advance the study of cellular dynamics. Our prototype systems, unmatched in speed and spectral resolution, utilize a pinhole array for efficient confocal multiplexing and dense time-resolved detectors, such as a gated optical intensifier, to measure multipoint confocal time-resolved fluorescence spectra. We demonstrate an enhanced optical design using a 32x32 pinhole array and a SPAD array to capture 960x960 pixel images at a frame rate of 4 Hz. Additionally, we present a 10x10 point multispectral FLIM system, representing the first highly multiplexed multispectral confocal FLIM microscope.

A novel optical design further improves the acquisition rate by reducing the sensor readout rate requirements from a quadratic sampling problem to a linear sampling problem. This new optical system can capture 22 spectral bands simultaneously across the 450 nm to 650 nm spectral range at a 1Hz frame rate with a final image resolution of 960x1920. These advancements mark a significant step towards realizing a high-speed multipoint multispectral confocal FLIM microscope and lay the groundwork for future improvements and research.

Acknowledgments

I want to express my deepest gratitude to my supervisor, Dr. Qiyin Fang. You challenged me with a task that truly tested my abilities and, in doing so, provided me with an invaluable opportunity for personal and professional growth. Working with someone so approachable and open to discussing research and the broader aspects of graduate studies has been a rewarding experience. Your mentorship has sharpened my research skills and opened doors to opportunities that have shaped my academic path. I am truly thankful for your guidance and the pivotal role you've played in my development.

I would also like to extend my gratitude to the other members of my supervisory committee, Dr. Ray Truant and Dr. Cecile Fradin. Your rigorous discussions and insightful feedback on my data have consistently provided me with new perspectives. I deeply appreciate the generous investment of your time, resources, and expertise in supporting my research. Each committee meeting has significantly advanced my progress, and I am truly grateful for your help.

I would like to express my heartfelt thanks to Dr. Anthony Tsikouras, Dr. Nehad Hirmiz, and Dr. Elizabeth Osterlund, for their patience and for taking the time to thoroughly explain the nuances of their research. Little did I realize that one day, I would inherit the culmination of their collective efforts. Without your dedication and hard work, there would have been no torch to carry forward.

A special thank you to my fellow students and lab mates, Andrea Buendia, Nikolina Malic, and Laura Polga, your confidence and encouragement were a source of consistent motivation through this adventure. I am fortunate to have worked alongside such talented and intelligent individuals, and I will cherish those memories. To all the unnamed members of the lab, your camaraderie and support have made this academic journey both enjoyable and fulfilling.

This thesis is the culmination of the collective efforts, encouragement, and support from each of you. Your contributions have been indispensable in shaping both my academic and personal growth, and I am deeply grateful to have had you as part of this significant milestone in my journey.

Table of Contents

Lay Abstract.....	iii
Abstract.....	iv
Acknowledgments.....	v
Table of Contents.....	vi
List of Abbreviations	viii
List of Figures.....	ix
List of Tables	xi
Declaration of Academic Achievement	xii
Chapter 1. Introduction.....	1
1.1 Motivation.....	1
1.2 Roadmap	2
1.3 Previous systems.....	3
1.4 Proposed solution.....	4
1.5 Thesis organization	6
1.6 Contributions.....	6
Chapter 2. Background	12
2.1 Fluorescence microscopy and its application	12
2.2 Methods of Confocal Measurement	19
2.3 Spectrally Resolved imaging	23
2.4 Temporal domain imaging (fluorescence lifetime)	25
2.5 Methods of multipoint time resolved confocal imaging	30
2.6 Multidimensional imaging	33
2.7 Discussion	35
Chapter 3. 4Hz Multipoint Confocal FLIM Microscope.....	42
Introduction to Paper I.....	43
Contents of Paper I.....	44
3.1 Introduction.....	44
3.2 Methods.....	46
3.3 Results and Discussion	51
3.4 Discussion and Conclusion.....	55

Chapter 4. Multispectral Multipoint Confocal FLIM Microscope	60
Introduction to paper II	61
Contents of Paper II	62
4.1 Introduction.....	63
4.2 Methods.....	64
4.3 Results and discussion	69
4.4 Discussions and Conclusion	74
Chapter 5. A 1Hz Multipoint Multispectral Confocal Microscope	79
Introduction to Paper III.....	80
Contents of Paper III.....	81
5.1 Introduction.....	82
5.2 Methods.....	83
5.3 Results.....	88
5.4 Discussion.....	89
Chapter 6. Conclusions and Future Work.....	92
6.1 Summary.....	92
6.2 Future Directions	94
6.3 Conclusion	97

List of Abbreviations

APD	Avalanche Photodiode
CCD	Charge-Coupled Device
CMOS	Complementary Metal Oxide Semiconductor
DAC	Digital to Analog Converter
DC	Direct Current
DNA	Deoxyribonucleic Acid
EMCCD	Electron Multiplied Charge Coupled Device
FDA	U.S. Food and Drug Administration
FLIM	Fluorescence Lifetime Imaging
FOV	Field of View
FRET	Förster Resonance Energy Transfer
FWHM	Full Width Half Maximum
GOI	Gated Optical Intensifier
GPU	Graphical Processing Unit
HCS	High Content Screening
ICCD	Intensified Charge Coupled Device
MCP	Micro Channel Plate
MFC	Microsoft Foundation Class
MLA	Microlens Array
MMOA	Molecular Method of Action
MW	Molecular Weight
NA	Numerical Aperture
NDA	New Drug Application
OEM	Original Equipment Manufacturer
PMT	Photo-Multiplier Tube
RGB	Red Green Blue color model
RLD	Rapid Lifetime Determination
RNA	RiboNucleic Acid
ROI	Region of Interest
SPAD	Single Photon Avalanche Photodiode
TCSPC	Time Correlated Single Photon Counting
UI	User Interface
USD	United States Dollars

List of Figures

- 2-1 a) A Jablonski diagram demonstrating the fluorescence process. B) An example of fluorescence absorption and emission profiles by wavelength
- 2-2 The drug discovery process and its associated costs and win rate from the discovery process through clinical trials. (Adapted from [17])
- 2-3 The process of high content screening process using high resolution imaging. a) Phenotype based screening process of cell painting detects changes in cell structure. b) Target based screening process using FRET to detect protein-protein binding.
- 2-4 An example of the optical geometry of a single-point confocal system.
- 2-5 A Nipkow disk confocal scanner with a single spiral.
- 2-6 Multipoint confocal scanning methods. a) Mirror-based, and b) Window-based scanning methods.
- 2-7 a) An example of a prism based spectrometer for parallel detection. b) An example of spectral filter based separation of multiple spectral channels.
- 2-8 Single photon counting devices. Diagrams of the internal geometry of a) a PMT (adapted from [55]) and b) a SPAD pixel (adapted from [56]).
- 2-9 A diagram of the gated optical intensifier.
- 2-10 A diagram of the principles of a streak camera's operation.
- 2-11 The window scanned multipoint confocal FLIM microscope using a streak camera and a 2D to 1D fiber converter. (Adapted from [60]). a) the optical system layout b) Output from the streak camera demonstrating FLIM decays with inward (left) or outward (right) spatial-temporal encoding directions.
- 2-12 Spinning disk confocal FLIM, using a GOI and an excitation wavelength selector. [61]
- 2-13 Window scanned multipoint confocal FLIM microscope using a SPAD array. (Adapted from [62])
- 2-14 Multidimensional Multiphoton microscope, using a polychromator and a 16 channel PMT to perform spectrally resolved multiphoton FLIM. (Adapted from [47])
- 2-15 Multidimensional Confocal Microscope using a spectrograph and a streak camera to perform spectrally resolved confocal FLIM. (Adapted from [64])

- 3-1 The optical system with a simplified optical path and custom pinhole array.
- 3-2 a) Frame rate and b) scanner velocity measurements of galvanometer scanners for identification of the highest reliable mechanical scanning rate.
- 3-3 Bi-directional raster scan artifacts from incorrect camera trigger delay. a) Delay correction as a function of pixel dwell times. b) Pre(top) and post(bottom) correction results on image quality.
- 3-4 Three gate windows response to convolution with 1 mM Coumarin6 fluorescence decay with 1000 ms pixel dwell times. Gates 1, 2, and 3 are plotted in red, blue, and green respectively. The internal software imposes a limit to the delay of the gates and that is shown in the graph as a red arrow.
- 3-5 Confocal FLIM image of the *Convallaria Majali*'s at 4 frames per second. A) confocal intensity, b) confocal FLIM, c) composite image. Scale bars are 20 μm
- 3-6 Figure 3-6. Fluorescence measurement limits. a) Fluorescence lifetime measured through changes in mean pixel photon count. b) fluorescence photon count against coumarin 6 dilution series for pixel dwell times of 250 μs , 500 μs , and 1000 μs .
- 3-7 a) Full field of view confocal lifetime images for Coumarin-6(top) and Fluorescein (bottom). B) Histograms for Coumarin-6 and Fluorescein.
- 3-8 a) Live cell measurements of cytosolic expression of the fluorescent proteins mCerulean3 and Venus, co-transfected in HEK293T cells, imaged with pixel dwell times of 250 μs and 1000 μs . Scalebars of 10 μm . b) Histograms of the fluorescent lifetimes for two regions labeled A and B, for each pixel dwell time.
- 3-9 Live cell FLIM-FRET experiment demonstrates full field of view images of HEK293T cells, transiently transfected with mCerulean3, Venus, mCerulean3 and Venus, and an mCerulean3-Venus linker protein that undergoes FRET. Scalebars of 20 μm . b) The normalized histograms of the four fields of view.
- 4-1 Schematic of Multipoint Multispectral Confocal FLIM. a) Optical path of the confocal scanning system attached to an inverted fluorescence microscope. Pulsed laser emission is frequency doubled (blue) and expanded to generate multiplexed excitation with a micro lens array. The excitation is raster scanned using windows scanners. The returned fluorescence emission (Yellow) is de-scanned before being spectrally separated with an imaging spectrometer (Red, Green, Blue overlap). The resulting spectrally encoded image is amplified using a gated optical intensifier for time resolved spectral imaging. b) The spectral calibration includes the isolation of the calibration signal from the background by threshold masking (left), segmenting of spectra using watershed segmentation (middle), and calibration by reference wavelength bands to generate dispersion curves (right).

- 4-2 Images show a fixed convallaria sample stained with acridine orange for simultaneous spectral and lifetime analysis. Spectral bands are 40 nm wide with 50 percent overlap, and pixel dwell time is 1 ms. a) A series of twelve spectrally separate time gated images (six displayed) reconstructed and combined to form a three-color image represented here in red, green and blue (300×300 pixels with an image size 125×125 μm). b) Three spectrally distinct ROI highlighted demonstrate variations in spectra and spectral lifetime curves for a sample with a single stain.
- 4-3 a) A series of lifetime images taken from a convallaria stained with safranin (550 nm) and fast green (650 nm). Inserts for each wavelength are the normalized histogram of the lifetime image. Spectral bands are 40 nm wide with 50 percent overlap, and pixel dwell time is 1 ms. b) Four spectrally distinct ROI highlighted demonstrate variations in spectra and spectral lifetime curves. Components in ROI2 and ROI3 are excluded by threshold rules and are not present in the lifetime analysis.
- 4-4 Fluorescence lifetime imaging of lifetime standards. a) Fluorescence lifetime images of Coumarin6 (C6) solution in ethanol, and Fluorescein (F1) in 0.1M NaOH, both samples at a concentration of [10 μM] at the 509 nm emission band. b) Sets of histograms of both lifetime images across the most intense spectral bands where both overlap, demonstrate the accuracy and precision of this method for capturing multispectral confocal lifetime images. Spectral bands are 40 nm wide with 50 percent overlap, and pixel dwell time is 1 ms, with an excitation power of 6 μW per focus.
- 4-5 Selected spectral lifetime images of HEK293T cells expressing (a) mCerulean3 fluorescent protein only at an emission wavelength of 471 nm (b) Venus fluorescent protein only at an emission wavelength of 554 nm (c) mCerulean3 and Venus transfected but unbound at an emission wavelength of 471 nm (d) and mCerulean3 tethered to Venus using a 13 amino-acids linker at an emission wavelength of 471 nm. e-f) Intensity and lifetime spectra of the samples over 5 fields of view with 1 ms pixel dwell time for a total exposure time of 1.8 seconds. Spectral bands are 40 nm wide with 50 percent overlap, and pixel dwell time is 1 ms, and excitation power is 2.5 μW per focus at 442 nm.
- 5-1 Diagram of the multispectral multipoint confocal microscope.
- 5-2 a) Example of pixel in the final image labeled by the readout frame they originated from. b) A depiction of the sweeping behavior to paint the spectral streak onto the sensor.
- 5-3 a) Full field of view for all 32x32 spectra generated with the pinhole array swept confocal spectrometer. Red ROI denotes the 4x4 region used for analysis. b) Spectral streaks with scanning off and on to demonstrate the sweeping concept. The red arrow denotes the full range of motion of the spectral streaks when undergoing displacement by the window scanner.

- 5-4 a) Isolated spectral streak with a red line identifying the placement of the cross-section highlighted. The cross-section of spectral streak for analysis of FWHM. b) Laser-generated spectral response using a 532 nm laser. A red line identifying the placement of the cross-section is highlighted. The cross-section of monochromatic spectral response for analysis of spectral FWHM.
- 5-5 Spectral calibration. a) Band streaks as imaged onto the sensor with streak scanning converted to a three-channel image that best represents their color. b) Cross section of laser generated monochromatic spot functions for a 532 nm and 640 nm laser. Red and green vertical lines are the estimated position of the spot peaks from the tri-band calibration.
- 5-6 a) False-color RGB image of convallaria Magali's stained with Fast Green and Safranin generated from 22 distinct spectral band measurements with three regions of interest are highlighted. b) Spectral emission curves of the three selected regions of interest.
- 5-7 a) False-color RGB image of Convallaria Majalis stained with Acridine Orange over 22 spectral bands. The insert is the principal component weight by spectral band. b) Images of the first and second principal components separated.

List of Tables

- 1-1 Outline of our previous multiplexing confocal FLIM microscopes and their performance.
- 6-1 A comparison of each instrument demonstrated in this thesis.

Declaration of Academic Achievement

The research work documented in this thesis includes three main modules:

- 1) A 32x32 point multiplexing confocal FLIM microscope that has a real time frame rate of 4 Hz was designed and constructed. Demonstration on live cell samples to demonstrate its performance in capturing FRET at 4 Hz.
- 2) A 10x10 point multispectral confocal FLIM microscope is designed and constructed. Demonstration on live cell samples to measure 12 spectral band multispectral FLIM-FRET validate its performance in capturing both donor and acceptor response to FRET. This project details the first multiplexed multispectral confocal FLIM microscope.
- 3) A 1 Hz multispectral confocal microscope was designed and constructed. This multipoint confocal microscope offers 22 distinct spectral bands captured simultaneously on a single detector.

The resulting fluorescence microscopy system design will be the foundation of the first fast multispectral confocal FLIM microscope for measuring fast dynamic processes within live cells.

Co-authored Publications

Qiyin Fang, Morgan Richards, Yiping Wang, “Sampling-Based Two-Dimensional Temporal Imaging,” In: Liang, J. (eds) “Coded Optical Imaging,” Springer, Cham. 2024, doi:10.1007/978-3-031-39062-3_24

*I co-authored this book chapter. My role was to assist in writing the core sections on multiplexed time resolved measurements and to generate figures for the work.

Peter, S., **Richards, M.**, Fang, Q., & Kitai, A. (2022). Enhanced red emission of glycothermally synthesized Ce: YAG nanophosphors via Mn²⁺ addition. *Materials Chemistry and Physics*, 277, 125497.

*Samuel and I built a direct pulse sampling system to measure the time-resolved fluorescence decay of a new material Samuel created. I was directly involved in the design and construction of the measurement system. I performed some of the data analysis and derived many core conclusions surrounding the interpretation of the fluorescence decay data. I also contributed to editing the manuscript.

Hirmiz, N., Tsikouras, A., Osterlund, E. J., **Richards, M.**, Andrews, D. W., & Fang, Q. (2020). Highly multiplexed confocal fluorescence lifetime microscope designed for screening applications. *IEEE Journal of Selected Topics in Quantum Electronics*, 27(5), 1-9.

*As an undergraduate student, I was responsible for writing the software that incorporated the SPC3 into the imaging system while being supervised by Dr. Anthony Tsikouras. I also contributed to editing the manuscript.

Hirmiz, N., Tsikouras, A., Osterlund, E. J., **Richards, M.**, Andrews, D. W., & Fang, Q. (2020). Multiplexed confocal microscope with a refraction window scanner and a single-photon avalanche photodiode array detector. *Optics Letters*, 45(1), 69-72.

*As an undergraduate student, I was responsible for writing the software that incorporated the SPC3 into the imaging system while being supervised by Dr. Anthony Tsikouras. I also contributed to editing the manuscript.

Hirmiz, N., Tsikouras, A., Osterlund, E. J., **Richards, M.**, Andrews, D. W., & Fang, Q. (2019). Cross-talk reduction in a multiplexed synchroscan streak camera with simultaneous calibration. *Optics express*, 27(16), 22602-22614.

*I worked with the graduate students (first three authors) to review and organized the results, as well as preparing for the manuscript. I also contributed to the editing of the manuscript.

Conference Publications

Richards, M., Shirakawa, Y., Badr, F., Kagawa, K., Kawahito, S., & Fang, Q. (2020). A multiplexed confocal FLIM microscope with 4-taps time-gated imager. In *Three-Dimensional and Multidimensional Microscopy: Image Acquisition and Processing XXVII* (Vol. 11245, pp. 61-65). SPIE.

*I designed and built a multipoint confocal FLIM microscope system using a 4-tap CMOS sensor while participating in the JSPS program. I presented the results of that research at SPIE.

Hirmiz, N., Tsikouras, A., Osterlund, E. J., **Richards, M.**, Kun, J., Andrews, D. W., & Fang, Q. (2019). Investigating Bcl-2 family protein-protein interactions using a high-speed multiplexing confocal FLIM microscope. In *European Conference on Biomedical Optics* (p. 11076_44). Optical Society of America.

*As an undergraduate student, I was responsible for writing the software that incorporated the SPC3 into the imaging system while being supervised by Dr. Anthony Tsikouras. I also contributed to editing the manuscript.

Project Contributions

This research project is the result of an interdisciplinary collaborative effort. This work has been prepared into three manuscripts with a few co-authors. At the time of this thesis defense, one (Chapter 4) has been accepted for publication, one (Chapter 3) has been submitted and been peer reviewed, and a third manuscript (Chapter 5) is in the process of finalization and submission. I am the lead author of all three studies. I conceptualized, implemented, and applied all methods of the multipoint multidimensional microscope for fast 4Hz confocal FLIM imaging, multispectral confocal FLIM, and a 1Hz multispectral confocal microscope.

Besides my supervisor, Dr. Qiyin Fang, the following collaborators have been contributed to both the research project and editing of the manuscripts where the corresponding thesis chapters are based on.

Dr. Elizabeth Osterlund devised the biological experiments for the dynamic FLIM imaging system (Chapter 3), and the multispectral confocal FLIM microscope (Chapter 4). She edited and revised the paper drafts of Chapter 3 and Chapter 4.

Dr. Ray Truant supported the research projects by providing material assistance and supervising biological experiments for the dynamic FLIM imaging system (Chapter 3), and the multispectral confocal FLIM microscope (Chapter 4). He edited and revised the paper drafts of Chapter 3 and Chapter 4.

Ms. Nikolina Malic conducted the biological experiments for the dynamic FLIM imaging system (Chapter 3), and the multispectral confocal FLIM microscope (Chapter 4), and assisted with the alignment of the 1Hz multispectral system (Chapter 5). She edited and revised all three paper drafts (Chapters 3-5).

Ms. Andrea Buendia assisted with the biological experiments for the dynamic FLIM imaging system (Chapter 3), and the multispectral confocal FLIM microscope (Chapter 4). She edited and revised the paper drafts of Chapter 3 and Chapter 4.

Ms. Laura Polga assisted with the calibration of the galvo scanners in the 4Hz FLIM system (Chapter 3). She edited and revised all three paper drafts (Chapters 3-5).

Chapter 1. Introduction

1.1 Motivation

The cell is the fundamental unit of life and the basis for understanding all living organisms. The cell's basic functions require a complex dynamic ecosystem of interactions within itself and with its environment. This complex and dynamic ecosystem is called the interactome, and it governs the biological function of the cell through an interconnected set of relationships [1]. Interactions occur between a mixture of nucleic acids, small molecules, and proteins. These interactions are difficult to measure using biochemical assays as they are transient and dynamic interactions by nature [2]. Understanding these interactions and being able to modulate their functions could lead to a new understanding of both basic function and the discovery of new novel medicines [3].

Fluorescence microscopy has been a critical technology in biology research and in the development of new drugs and treatments. These microscopy systems provide a method to measure the spatially resolved reaction of live cells to varying chemical or environmental factors [4,5]. Fluorescence labeling has created many highly specific tags that localize to organelles or are attached to proteins of interest [6,7]. These fluorescent labels allow the observation of dynamic behaviors with high contrast, while the spectral differences of labels can be used to distinguish labeled elements [8,9]. Spectrally labeling two objects of interest may not provide a precise method of identifying their interaction. An advanced fluorescence method known as Förster Resonance Energy Transfer (FRET) has introduced a new method to measure protein-protein interactions optically [10]. Due to the spectral overlap of fluorescence tags, which can prevent accurate FRET measurements, techniques such as fluorescence lifetime imaging (FLIM) have become gold standards for measuring FRET as the lifetime offers a precise quantifiable method of detecting binding [11–13].

The failure of a specific contrast method to identify complete descriptions of cellular behavior can be overcome by having additional contrasting methods. Typically, each contrast method has a unique method of measurement that may not be compatible with another. Methods also may not be compatible with simultaneous acquisition and can introduce issues such as photobleaching and phototoxicity when performed sequentially due to large irradiance of samples [14–17]. Such a method to measure multiple contrast mechanisms simultaneously is termed multidimensional microscopy. Measurement of spectral and lifetime contrasts simultaneously will allow the identification of multiple fluorescent labels when co-localized and distinguish co-localization from interaction through FLIM-derived FRET [18–20]. Spatially resolved measurement provides structural details of the cell's state, leading to morphological insights [21]. When measured in quick succession, these contrasts can describe the inner workings of the interactions and the interconnected relationships essential to building a new model of the cell's inner workings.

Currently, single-point confocal measurement is a well-implemented technology for multidimensional imaging. They offer superb temporal resolutions when coupled with pulsed lasers and time-correlated single photon counting detectors [22] or streak cameras [23], which offer temporal resolutions in the picoseconds and hundreds of femtoseconds, respectively. Due to their single-spot fluorescence return, they can be spectral separated using diffractive or prismatic devices and quite simply be imaged onto a linear sensor and often have spectral resolutions as small as 0.5 nm [23]. These technologies are

fundamentally limited and do not scale well for capturing large numbers of samples quickly as they are slow. They are slow as the single point acquisition is limited by the fluorescence emission and the fluorescence detection rate from the single spot [24].

The ideal instrument would combine the capabilities of current multidimensional single-point confocal instruments with the speed and gentle nature of multipoint confocal microscopes. Single-point confocal microscopy takes advantage of modern instrumentation and high laser powers to perform multidimensional imaging [18,19,25–27]. Multipoint confocal has demonstrated its speed and gentle nature by dividing a large field of view into smaller regions that can be acquired in parallel [28]. This technique lowers laser power requirements by relaxing pixel dwell times and leads to reduced photobleaching and phototoxicity. Current multipoint confocal microscopy technologies are incompatible with multidimensional imaging due to measurement methodology. An ideal instrument would be a multipoint confocal microscope able to capture spectrally resolved fluorescence lifetimes images at frame rates sufficient for measuring dynamic events in live cells.

1.2 Roadmap

The biological systems we wish to measure are large three-dimensional live cell models undergoing fast dynamic processes with highly labeled and overlapping spectral features that bind in known and sometimes unknown processes. Designing a microscope that can measure all these features simultaneously is a difficult task unsuited for any single technology. Fast multidimensional methods will be required to realize imaging of these biological models. Understanding technologies available today can provide a guide to the potential pathways to creating the next-generation microscopes.

Accomplishment of the fast multidimensional imaging microscope is dependent on innovation in 3 core directions. Spatial multiplexing for parallel measurement of the sample in the spatial domain. Capturing complete spectra of all spectral wavelengths simultaneously to prevent repeated scanning of the same spatial domain and reduce photobleaching and phototoxicity. Measuring complete time-resolved fluorescence decays for all spatial and spectral dimensions simultaneously to prevent repeated exposures that produce photobleaching that alters computed fluorescence lifetime when measured through sequential temporal gates.

Multipoint confocal has been accomplished through a series of steps to multiplex from a single-point measurement [29], to hundreds of points [30], and now is commonly implemented in the thousands of points [31,32]. Further increases are possible as few systems take advantage of the full field of view of the microscope. Beyond scaling the size of the multifocal array, a limitation in the spot density is necessary to prevent crosstalk between pinholes. Consideration must also be given to the illumination source as there are few technologies that are broadly affordable for multiwavelength high-power pulsed lasers required for the practical implementation of this technology.

Spectral measurements are difficult to perform on multiplexed confocal setups. In a single-point confocal microscope, there is sufficient spatial freedom to place very large footprint spectral streaks onto a sensor. Due to the confocal pinhole diameter being the limiting feature size of a monochromatic spectrum, the limiting spectral resolution requires a large footprint to be dispersed for high-resolution spectroscopy in the nanometers. multipoint confocal microscopes do not have room to spare on the

sensor as the two-dimensional nature of the spot array is captured fully by the image sensor. Currently, multipoint confocal microscopes are limited to 2-4 simultaneous spectral band measurements achieved through filtering schemes [33]. Further improvements are possible by utilizing the inter-focal space for spectral encoding. Depending on the diameter of the resulting monochromatic spot, the spectral streak can be rotated to accommodate upwards of 20 spectral channels.

Historically, two fast single photon sensitive detection technologies have been available for measurements of time-resolved fluorescence studies: the photomultiplier tube and the streak camera. These systems are traditionally only implemented in single-point confocal technologies. The combination of multipoint confocal methods with time-resolved fluorescence studies has employed the gated optical intensifier, although its poor spatial resolution limits the practical implementation in modern methodologies. The streak camera, which is the fastest two-dimensional sensor with a temporal resolution in the hundreds of femtoseconds, has successfully been implemented in multipoint confocal with the invention of the window scanner technology [34]. Single Photon Avalanche Diode (SPAD) array and multi-tap pixel technologies have made significant advancements within the last two decades, seeing both multiple temporal gate measurements and larger-than-one-megapixel architectures [35–38]. Scaling issues are present in all two-dimensional technologies as the designers struggle to balance the miniaturization of their technologies with the issues of electromagnetic interference and electronic crosstalk [39,40]. Future directions of these technologies may lead to upwards of 2000 by 2000 pixel format technologies, bringing them in line with current image sensor trends. These technologies will be natively compatible with current multipoint confocal measurement technologies.

By combining different aspects of each technology, the creation of a multipoint multispectral confocal FLIM microscope will be possible. Such a system potentially has one thousand or more focal point multiplexing, with 50 spectral bands for each focus at a spectral resolution of 10 nm or higher. Current technology is compatible with a demonstration of this multidimensional concept, however it would be insufficient for fast measurement. Growth of the SPAD array and multitap array technology is the limiting factor for scaling the multidimensional microscope, as the sensor size limits the total field of view captured.

1.3 Previous Systems

The multiplexing confocal is the heart of this thesis. Multiplexing refers to the parallel capture of fluorescence signals generated from multiple excitation points. The parallel excitation points are responsible for imaging a small, unique subregion of interest. There are 32x32 points of multiplexing in our current system, meaning 1024 unique subregions are created in each image. The subregions of interest are determined by the geometry of the excitation points, and for our systems, are a square grid that consists of 30x30 pixels. Thus, the final image resolution is a 960x960 image size. Before my thesis, there have been three distinct iterations of the multiplexing confocal microscope, each a significant advancement of the technology. These systems and their capabilities are detailed in Table 1-1.

Systems	Prototype I	Prototype II	Prototype III
Number of focal points	10×10	10×10	32×32
Detector	Streak Camera (Linear sweep)	Streak Camera (Sinusoidal sweep)	Time gated SPAD array
Scanning Mechanism	Stage Scanning	Window Scanning	Window Scanning
Laser pulse rate (MHz)	4	40	50
Image size (pixels)	400×400	300×300	960×960
Acquisition time (s)	800	90	3
Time sampling method	Full decay capture	Full decay capture	Sequential temporal gates

Table 1-1 Outline of our previous multiplexing confocal FLIM microscopes and their performance.

Each system has made an order of magnitude improvement upon its predecessor on one or more of the performance metrics. However, there exist limitations to the current design. Specifically, the third prototype is still not fast enough for its intended application. The high content screening was its targeted application. However, it failed to achieve the 1 Hz imaging rate benchmark for full FLIM images. Additionally, there are core issues with image quality, particularly there is an expansion of the pinhole diameter to allow increased light throughput, resulting in reduced confocal sectioning, and there is severe vignetting present that reduces the effective field of view to only the central region of the multiplexing array. Scanning with the Galvano scanners also was poorly coordinated and incapable of achieving the mechanically limited performance of the system. This left performance on the table for fast real-time imaging.

1.4 Proposed Solution

The core issues surrounding the image quality metrics of the system are centered on the efficiency of photon detection. The system uses a complicated series of imaging relays that each perform one specific job on the light. A dedicated image relay filters light, magnifies the image, and confocally rejects out-of-focus light. Passing through each lens in the relay, including the microlenses, reflects a small amount of light from the final image. Although each surface is coated with anti-reflective coefficients, the light reduction is a compounding effect that results in low photon counts.

The galvo scanners, although having sufficient torque to generate the required scanning behaviors, were not utilized to their full potential. Coordination of the galvo scanner was conducted with a microcontroller (Uno, Arduino). The microcontroller acted as a router between the controlling computer and both the galvo scanner and the camera. The system which requires 900 images from the camera, was configured to perform a burst of 30 images for a single row, the mechanical scanning of axis 1 (fast axis) would be triggered by the microcontroller, and once the axis ended its sweep the computer would transfer image data to its memory. The computer would send a serial message through the

microcontroller to the galvo scanner to move the next row (slow axis) of the image, this is the process of the raster scan. This process happens 30 times to generate a 30x30 image dataset (stored within 30 files). The process occurs twice as the sensor used in prototype three is unable to capture multiple time gates simultaneously. This process of repeated start and stop of the scanning fundamentally limits the overall speed of the imaging system.

The core issues of the multiplexed confocal microscopes were solved in a three-step approach. First, the optical path was redesigned around the use of a pinhole array as a means to achieve confocal rejection of out-of-focus light. This allowed me to reduce the number of elements in the optical path by half. The pinhole design provides superior confocal rejection and reduced crosstalk. The second step is to remove the microcontroller and replace it with an application specific circuit that is designed to coordinate scanner synchronization with camera and laser triggering. This is achieved with an integrated motor controller board that can store the scan path within its memory, which removes the start and stop behavior. The sensor had additional functionality added upon request by the SPAD array manufacturer Micro Photon Devices (MPD) to allow multiple burst image events to occur, allowing all 900 frames to be stored on the sensor simultaneously and read out at the end of each capture process. MPD also released a new sensor with three built-in time gates for each pixel, removing the need to rescan for each temporal data point. The software was redesigned to have a second image processing thread to allow simultaneous image capture and data processing. Characterizing each of these changes was a requirement to achieve high-speed and high-quality fluorescence lifetime images. The resulting system achieved FLIM images at a resolution of 960x960 pixels with a real time imaging frequency of 4Hz.

To achieve multispectral time-resolved fluorescence confocal microscopy, a new novel design was required, which used a low dispersion prism to spectrally separate the emission into the sparse spacing. This design takes advantage of both the sparse nature of multipoint acquisition and the stationary de-scanned fluorescence image. The resulting spectrally resolved fluorescence images were read out on a dense time-resolved detector, a gated optical intensifier coupled to an sCMOS sensor. Image process was developed to automate the spectral calibration procedure and image processing software to analyze multispectral time resolved datasets. The final system, utilizing a 10x10 point multiplexing geometry, captures 30x30 scans to generate a 300x300 pixel image. The system achieves this in 1800 ms with a 1ms pixel exposure for each position with two-time measurements being required. The final image time of the system was just under 2 minutes due to slow readout rate of the sCMOS sensor. The final spectral resolution was 40 nm, and 12 unique time-resolved spectral bands were acquired simultaneously.

Finally, a new novel multispectral multipoint confocal microscope was designed to decrease frame requirements from 900 images to just 30 images. This design uses a window scanner to sweep spectrally resolved streaks across an image sensor. The window galvoscaner, which previously was a start and step scanner that accepted one position at a time, needed to be converted from a digitally controlled input to an analog input. The analog input was connected to an amplified voltage output of a microcontroller's DAC. This allowed waveform generation on the DAC with sufficient speed to scan at the same rate as the cannon system. This design is novel in that it acquires 22 spectral band images simultaneously, each 20 nm wide at a real-time frequency of 1Hz. The final image dimension is 960x1920 pixels.

1.5 Thesis organization

The **Introduction** provides motivation and proposed solutions for developing a multipoint multidimensional confocal FLIM microscope.

Chapter 2 presents a relevant background on the pharmaceutical drug screening process and highlights the reasons why a multidimensional microscope is desired and could be an important development. Each dimension (spatial, spectral, dynamic (ns), dynamic (s)) is motivated by its necessity, and the supporting technology is examined. Finally, the state of current multidimensional imaging is presented.

Chapter 3 presents a newly designed optical system to improve the optical throughput of the multipoint confocal microscope. Emphasis was placed on reducing the total number of elements in the optical path to improve throughput, allowing faster imaging speeds in live cells while improving image quality. Thus, I have designed a 32x32 point multiplexing time-resolved confocal microscope that is capable of imaging at a real-time frequency of 4 Hz for measuring live cell dynamic processes. Using a pinhole array simplifies the optical system design, allowing improved optical efficiency for imaging lower fluorophore concentrations at faster frame rates. Its performance was demonstrated in fixed stained samples and imaging of FLIM-FRET in live cells.

Chapter 4 presents a new optical system that demonstrates multispectral imaging in parallel with fluorescence lifetime measurements. We were able to successfully spectrally separate time-resolved fluorescence signals onto a gated optical intensifier and measure multispectral time-resolved confocal fluorescence. This system uses a prism-based imaging spectrometer to separate a 10x10 array of confocal foci into their spectral components. This allows the sampling of the spectra by a time-resolved image sensor to produce a multispectral time-resolved data set used for generating multispectral lifetime images. This system captures 300x300 pixel fluorescence lifetime images containing 12 unique spectral bands covering a 450-700 nm spectral range in 1.8 seconds of exposure. Its performance was demonstrated in fixed stained samples and in multispectral imaging of FLIM-FRET in live cells.

Chapter 5 provides a novel optical system that spatially encodes the multipoint multispectral image onto a dense sensor to permit imaging at faster frame rates than the previous multispectral system could achieve. The system is the first of its kind to use single photon excitation to achieve swept multispectral multipoint confocal imaging. It can image a 32x32 point multiplexing at 1 Hz and provides 22 spectral bands of imaging over the 450 nm to 650 nm spectral range.

Chapter 6 concludes this thesis, providing a summary of the improvements to the multipoint confocal microscope, and future directions I believe will yield the most significant advancements to this project.

1.6 Contributions

This thesis is presented as three papers within chapters 3 to 5. I wrote the original drafts of each article and made revisions based on the feedback of the listed co-authors.

Chapter 3 describes a fast multifocal confocal microscope to achieve confocal FLIM at a frame rate of 4 Hz. The novelty of this work is the development of a sub-second imaging system for measuring dynamic processes. Compared to our previous work, the overall system design was revised by redesigning the

optical path using new optical elements such as the pinhole array and redesigning the scanning control systems, which led to significant improvement of FLIM imaging frame rate to 4 Hz (at 960x960 frame size), which is about 14 times faster compared to the state-of-the-art FLIM instrumentation such as is found in the Leica Stelara's Falcon and the Becker and Hickl DCS-120 with potential to scale with detector technology. Additionally, the pixel dwell time used in this technique is 250 μ s, which allows gentle excitation powers at 0.5 μ W per focus to capture sufficient photon counts for lifetime measurement on samples such as transfected live cell models.

This work is significant as this is the first implementation of the multiplexed confocal FLIM microscope that has a speed capable of measuring fast dynamic processes. The speed of this technology will only improve with more powerful lasers and faster scanners integrated into its design. This implementation marks an order of magnitude improvement to the previous design. This research has a broader significance to the scientific community as currently, there are many fast processes that are difficult to measure using current technology. Measurements such as cyclic cellular processes and triggered biological pathways have few devices capable of measuring their process with FLIM. This methodology demonstrates a new method to achieve high-speed confocal FLIM measurements.

This implementation captures much faster than the 1 Hz imaging speed required to be implemented in a screening application and can capture an entire well within 1 second given stage scanning equipment given 4 FOV per well. This marks a powerful commercialization potential as the implementation of a FLIM microscope in routine screening pipelines has been held back due to the speed of the technology.

Chapter 4 describes the first multipoint multispectral time-resolved confocal microscope. This system exploits the unique nature of the window scanning confocal microscopes' sparse sampling to capture multispectral information. There is currently no multipoint multispectral confocal FLIM microscope available for comparison. This system offers 12 unique simultaneous spectral band measurements, each with a spectral bandwidth of 40 nm evenly spaced from 450 nm to 700nm. This system captures images in 1.8 seconds of exposure (at 300x300 frame size). Additionally, the pixel dwell time used in this technique is 1 ms which allows gentle excitation powers as low as 2.5 μ W per focus to capture sufficient photon counts for lifetime measurement on samples such as transfected live cell models.

This work is a significant body of work as it is the first demonstration of a multipoint multispectral confocal FLIM microscope. The technique achieves true multidimensional imaging at an exposure time that demonstrates its potential to be used in high content screening assays. This multispectral FLIM microscope is a demonstration of the multiplexing potential using currently available technology, whereas the hope has been in the development of new technologies to create large array SPAD sensors.

Chapter 5 describes the creation of a multipoint multispectral confocal microscope. The system uses the window scanner technology to uniformly sweep multispectral streaks at the same position they are being sampled. This technology achieves a real time imaging rate of 1 Hz and captures 22 spectral bands simultaneously at 20 nm spectral resolution.

The significance of this work is that it bridges the powerful multispectral capabilities of single-point confocal microscopy and the speed and gentle imaging characteristics of multipoint confocal. This will be a powerful technique for acquiring full spectral datasets while preventing photobleaching and phototoxicity. This will enable multilabel measurements to be conducted using a single highly sensitive detector and carve a path to the integration of next-generation time-resolved sensors for multispectral multipoint confocal FLIM microscopy at 1Hz imaging rates.

The technology will also have a broader significance to the world as it will reduce the complexity and cost of high-speed multispectral confocal microscopy. Using only a single sensor for readout reduces the financial impact of adopting the technology, as traditional multispectral multipoint microscopy ties the number of spectral bands acquired to the number of sensors used.

References

- [1] Sanchez C, Lachaize C, Janody F, Bellon B, Roder L, Euzenat J, Rechenmann F and Jacq B 1999 Grasping at molecular interactions and genetic networks in *Drosophila melanogaster* using FlyNets, an Internet database *Nucleic Acids Res* **27** 89–94
- [2] Poluri K M, Gulati K, Tripathi D K and Nagar N 2023 Drug Design Methods to Regulate Protein–Protein Interactions *Protein-Protein Interactions* (Springer Nature Singapore) pp 265–341
- [3] Rapposelli S, Gaudio E, Bertozzi F and Gul S 2021 Editorial: Protein–Protein Interactions: Drug Discovery for the Future *Front Chem* **9** 1049
- [4] Combs C A and Shroff H 2017 Fluorescence Microscopy: A Concise Guide to Current Imaging Methods *Curr Protoc Neurosci* **79** 1–25
- [5] Balasubramanian H, Hobson C M, Chew T-L and Aaron J S 2023 Imagining the future of optical microscopy: everything, everywhere, all at once *Commun Biol* **6** 1096
- [6] Zorov D B, Kobrinsky E, Juhaszova M and Sollott S J 2004 Examining intracellular organelle function using fluorescent probes: From animalcules to quantum dots *Circ Res* **95** 239–52
- [7] Choi N-E, Lee J-Y, Park E-C, Lee J-H and Lee J 2021 Recent Advances in Organelle-Targeted Fluorescent Probes *Molecules* **26** 217
- [8] Garini Y, Young I T and McNamara G 2006 Spectral imaging: Principles and applications *Cytometry Part A* **69** 735–47
- [9] Zimmermann T, Rietdorf J and Pepperkok R 2003 Spectral imaging and its applications in live cell microscopy *FEBS Lett* **546** 87–92
- [10] Medintz I and Hildebrandt N 2013 *FRET – Förster Resonance Energy Transfer* (Wiley)
- [11] Preus S and Wilhelmsson L M 2012 Advances in Quantitative FRET-Based Methods for Studying Nucleic Acids *ChemBioChem* **13** 1990–2001
- [12] Kaufmann T, Herbert S, Hackl B, Besold J M, Schramek C, Gotzmann J, Elsayad K and Slade D 2020 Direct measurement of protein-protein interactions by FLIM-FRET at UV laser-induced DNA damage sites in living cells *Nucleic Acids Res* **48** E122–E122
- [13] Osterlund E and Andrews D 2015 The use of FLIM-FRET for the detection of mitochondria-associated protein interactions *Mitochondrial Medicine : Probing Mitochondrial Function* vol 1 pp 395–419
- [14] Anon 2018 Phototoxicity revisited *Nat Methods* **15** 751
- [15] Laissie P P, Alghamdi R A, Tomancak P, Reynaud E G and Shroff H 2017 Assessing phototoxicity in live fluorescence imaging *Nat Methods* **14** 657–61
- [16] Boudreau C, Wee T-L, Duh Y-R, Couto M P, Ardakani K H and Brown C M 2016 Excitation Light Dose Engineering to Reduce Photo-bleaching and Photo-toxicity *Sci Rep* **6** 30892

- [17] Knight M M, Roberts S R, Lee D A and Bader D L 2003 Live cell imaging using confocal microscopy induces intracellular calcium transients and cell death *American Journal of Physiology-Cell Physiology* **284** C1083–9
- [18] Scipioni L, Rossetta A, Tedeschi G and Gratton E 2021 Phasor S-FLIM: a new paradigm for fast and robust spectral fluorescence lifetime imaging *Nat Methods* **18** 542–50
- [19] Manning H B, Owen D M, Auksorius E, de Beule P A A, Oddos S, Talbot C B, Dunsby C, Munro I, Magee A I, Neil M A A and French P M W 2007 Applications of rapid time-gated hyperspectral FLIM: live cell imaging of membrane order and 6-D microscopy ed T Wilson and A Periasamy p 663019
- [20] Popleteeva M, Haas K T, Stoppa D, Pancheri L, Gasparini L, Kaminski C F, Cassidy L D, Venkitaraman A R and Esposito A 2015 Fast and simple spectral FLIM for biochemical and medical imaging *Opt Express* **23** 23511
- [21] Bickle M 2010 The beautiful cell: High-content screening in drug discovery *Anal Bioanal Chem* **398** 219–26
- [22] Becker W, Bergmann A and Biskup C 2007 Multispectral fluorescence lifetime imaging by TCSPC *Microscopy Research and Technique* vol 70 (Wiley-Liss Inc.) pp 403–9
- [23] Williams G O S, Williams E, Finlayson N, Erdogan A T, Wang Q, Fernandes S, Akram A R, Dhaliwal K, Henderson R K, Girkin J M and Bradley M 2021 Full spectrum fluorescence lifetime imaging with 0.5 nm spectral and 50 ps temporal resolution *Nat Commun* **12** 6616
- [24] Becker W 2017 *The bh TCSPC Handbook, Pile-Up* (Becker & Hickel)
- [25] Becker W, Bergmann A and Biskup C 2007 Multispectral fluorescence lifetime imaging by TCSPC *Microscopy Research and Technique* vol 70 (Wiley-Liss Inc.) pp 403–9
- [26] Lagarto J L, Villa F, Tisa S, Zappa F, Shcheslavskiy V, Pavone F S and Cicchi R 2020 Real-time multispectral fluorescence lifetime imaging using Single Photon Avalanche Diode arrays *Sci Rep* **10** 8116
- [27] Qu J, Liu L, Guo B, Lin Z, Hu T, Tian J, Wang S, Zhang J and Niu H 2005 Development of a multispectral multiphoton fluorescence lifetime imaging microscopy system using a streak camera *Optics in Health Care and Biomedical Optics: Diagnostics and Treatment II* vol 5630 (SPIE) p 510
- [28] Gräf R, Rietdorf J and Zimmermann T 2005 Live cell spinning disk microscopy *Adv Biochem Eng Biotechnol* **95** 57–75
- [29] Zimmermann T and O'Toole P 2014 *Confocal Microscopy* vol 1075, ed S W Paddock (New York, NY: Springer New York)
- [30] Tsikouras A, Berman R, Andrews D W and Fang Q 2015 High-speed multifocal array scanning using refractive window tilting *Biomed Opt Express* **6** 3737
- [31] Oreopoulos J, Berman R and Browne M 2014 Spinning-disk confocal microscopy *Methods in Cell Biology* vol 123 (Elsevier Inc.) pp 153–75

- [32] Hirmiz N, Tsikouras A, Osterlund E J, Richards M, Andrews D W and Fang Q 2020 Multiplexed confocal microscope with a refraction window scanner and a single-photon avalanche photodiode array detector *Opt Lett* **45** 69
- [33] Michael Stanley C 2008 Filters and mirrors for laser applications *Nat Methods* **5** an12–3
- [34] Hirmiz N, Tsikouras A, Osterlund E J, Richards M, Andrews D W and Fang Q 2019 Cross-talk reduction in a multiplexed synchroscan streak camera with simultaneous calibration *Opt Express* **27** 22602
- [35] Ulku A C, Bruschini C, Antolovic I M, Kuo Y, Ankri R, Weiss S, Michalet X and Charbon E 2019 A 512 × 512 SPAD Image Sensor With Integrated Gating for Widefield FLIM *IEEE Journal of Selected Topics in Quantum Electronics* **25** 1–12
- [36] Shirakawa Y, Seo M-W, Yasutomi K, Kagawa K, Teranishi N and Kawahito S 2017 Design of an 8-tap CMOS lock-in pixel with lateral electric field charge modulator for highly time-resolved imaging *Silicon Photonics XII* **10108** 101080N
- [37] Li Z, Kawahito S, Yasutomi K, Kagawa K, Ukon J, Hashimoto M and Niioka H 2012 A time-resolved CMOS image sensor with draining-only modulation pixels for fluorescence lifetime imaging *IEEE Trans Electron Devices* **59** 2715–22
- [38] Wayne M, Ulku A, Ardelean A, Mos P, Bruschini C and Charbon E 2022 A 500 × 500 Dual-Gate SPAD Imager with 100% Temporal Aperture and 1 ns Minimum Gate Length for FLIM and Phasor Imaging Applications *IEEE Trans Electron Devices* **69** 2865–72
- [39] Qian X, Jiang W, Elsharabasy A and Deen M J 2023 Modeling for Single-Photon Avalanche Diodes: State-of-the-Art and Research Challenges *Sensors* **23** 3412
- [40] Seo M-W, Shirakawa Y, Kagawa K, Yasutomi K and Kawahito S 2017 A high performance multi-tap CMOS lock-in pixel image sensor for biomedical applications *High-Speed Biomedical Imaging and Spectroscopy: Toward Big Data Instrumentation and Management II* **10076** 100760V

Chapter 2. Background

2.1 – Fluorescence microscopy and its applications

Microscopy first allowed scientists to view the microscopic world of biology. Coupled with the camera, scientific measurements of the interactions of cells with biologically active reagents began and have since been a powerful method of discovering entities with the potential to become drugs. Fluorescence has long been a studied phenomenon but was first accurately described by G.G. Stokes and has revolutionized the microscopes capability [1]. Fluorescent molecules have been used to measure microscopic processes by enhancing the signal contrast of stained subcellular compartments and organelles. The discovery of green fluorescent proteins extracted from the jellyfish *Aequorea Victoria* by O. Shimomura began a new era of fluorescence microscopy where the fluorescence molecules could originate from cellular origins, greatly enhancing their utility as an indicator of biological action in live cells [2]. These fluorescent proteins have proliferated into numerous spectrally distinct labels as scientists have altered their structure to create new molecules with different spectral properties. Individually, they are quite useful, but with multiple simultaneously labeled features, the entire cell becomes visible, and the dynamic nature of life is measurable.

Fluorescence is a luminescence phenomenon in which a fluorophore can emit light following optical excitation. It is characterized by absorption and emission of a photon, with the absorbed photon being of higher energy. The fluorescence phenomenon can be described quantum mechanically by the transition of an electron between two energy levels, as illustrated in Figure 2-1a. Electrons exist in discrete energy levels in molecules, each with its own vibrational energy levels, and when stimulated by a photon, they can absorb its energy and transition to a higher energy state, such as the transition from S_0 to S_1 . If the excited electron absorbed more than enough energy between its state and the lowest vibrational state in the excited level, it would undergo non-radiative relaxations to the lowest vibrational state. At this point, the electron will give up its energy as a photon and relax back to the lower energy state. The transitions to and from the excited state have differences in energy, resulting in spectral differences between the two photons, as illustrated in Figure 2-1b. The difference in energy is called the Stokes shift of the fluorescent protein and is the key feature that distinguishes absorption from emission. The excitation and emission are complex phenomena with distinct spectral curves. The shape of these

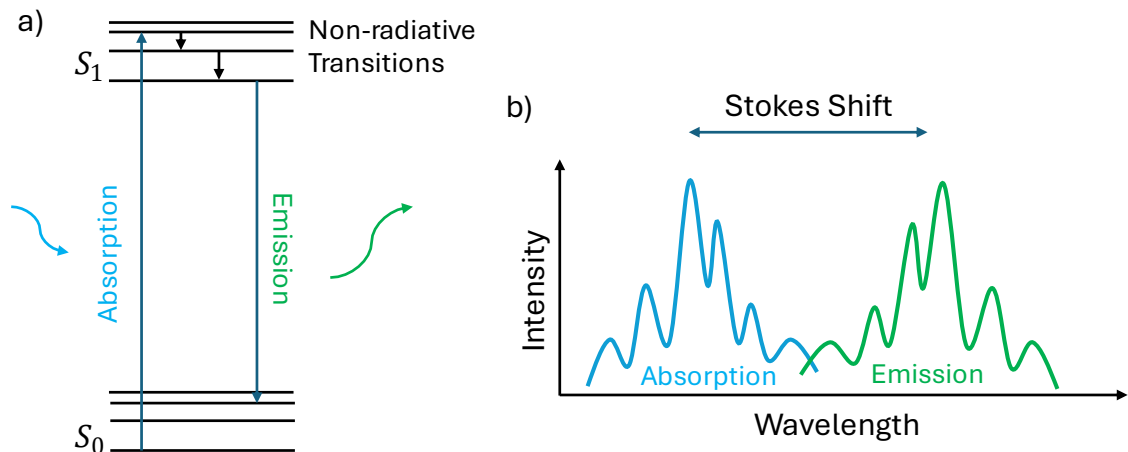


Figure 2-1. a)A Jablonski diagram demonstrating the fluorescence process. B)An example of fluorescence absorption and emission profiles by wavelength

curves is described by the Frank-Condon principle, which governs the transition probabilities between excited and emission states and results in unique spectra for each fluorescence protein [3].

There are many fluorescent probes available for use in fluorescence microscopy. These labels are divided into two classes, dyes and proteins [4]. Fluorescent dyes are typically added to the cells being imaged and then washed out. These dyes have a functional chemical component that reacts with some biological target or process to fix the dye in location, allowing the remaining dye to be removed and the labeled regions to be identified. Many fluorescent dyes change brightness upon binding to the specific target resulting in a large difference in signal that reduces noise from non bound dye. This differs from fluorescent proteins, where the fluorescent modification is through genetic modification of the cells. Fluorescent proteins are inserted into the cell as genetic information, such as during transfection. The protein is fabricated within the cell based on the genetic information and that protein is created on the structure or messaging protein of interest.

The spectral width of a fluorophore's emission profile is highly specific but is commonly around 40nm and asymmetric. They are characterized by their spectral profiles as well as the extinction coefficient and the quantum yield, which are indicators that describe how well the label absorbs excitation light and how much energy is converted to fluorescence emission, respectively [3,4]. The range of fluorescence emission currently available ranges from the UV to the IR but largely resides within 400-650 nm. Due to how broad the spectral profiles are, it is common for fluorescence signals to overlap spectrally, requiring a process to separate two or more species. Separation of features is straightforward due to the additive properties of fluorescence emission. Techniques such as linear unmixing can separate features so long as the number of fluorophores is not greater than the number of spectral channels [5]. Imaging a multilabel experiment's entire range can be difficult, especially if high-resolution spectral features are required. Spectral features are lost when imaging at spectral bandwidths higher than 0.5 nm; however, spectral distinction using spectral decomposition is possible with much larger bandwidths, provided the [3]. Resolving fluorophores requires a spectral bandwidth sufficient to observe the features that distinguish the labels. The resolutions are typically linked to the imaging method and can vary from as low as 1.5 nm to as large as 40nm [6,7].

2.1.1 Fluorescence Dynamics

Transitions between states and energy levels occur over fast time scales, with non-radiative transitions occurring at times of $\sim 10^{-12}$ seconds and fluorescence decays occurring around $\sim 10^{-9}$ seconds. These fluorescence processes happen randomly, with fluorescence decay of an excited population being modeled by an exponential process.

$$N(t) = N e^{-k_r t} \quad (1)$$

Where k_r is the radiative fluorescence decay rate of the protein. These temporal decays are measurable and provide a highly stable contrast method. Using fluorescence lifetimes allows the separation of two fluorescent proteins with overlapping spectral emission. The measurement of the decay is characterized by the fluorescence lifetime which is the reciprocal of the decay rate.

$$\tau = \frac{1}{k_r} \quad (2)$$

The fluorescence lifetime as a contrast method in imaging is referred to as fluorescence lifetime imaging (FLIM). It is a powerful technique commonly used to measure spatial changes in the decay rate of the population and distinguish fluorescent species by their molecular structure. When designing

experiments, labels must be selected such that the difference in lifetime expected is greater than the minimum lifetime resolution of the imaging system. The lifetime range and resolution a microscope can measure are highly specific to the instrument, with temporal resolutions as low as 50 ps for measuring extremely fast fluorescence decay phenomena [8]. A high resolution is important as most dynamic processes will measure multiple fluorescence species simultaneously, resulting in a need to extract multiple exponential components from the decay profile. Typical fluorescence probes have lifetimes in the range of 1 ns to 10 ns. Distinction of lifetimes below +/- 0.5 ns required in most circumstances as selected probes typically differ by 1 ns in lifetime by experimental design.

Careful planning of experiments is required for the successful use of fluorescent proteins in microscopy. Factors such as environmental effects and photobleaching can affect fluorescence probe brightness and longevity. Environmental factors can induce fluorescence quenching, and excessive laser powers can produce photobleaching, both of which reduce fluorescence intensity. Fluorescence quenching occurs through two processes, collisional and static routes. Collisional quenching occurs when an excited fluorophore collides with another protein resulting in the loss of the excited state. It introduces a new pathway for fluorescence energy to leave the system as a nonradiative pathway, which results in a reduction in lifetime.

$$\tau = \frac{1}{k_{nr} + k_r} \quad (3)$$

Where k_{nr} is the non-radiative decay rate from the excited state. Static quenching occurs when a complex forms between the fluorophore and another molecule which inhibits the fluorophore from entering the excited state, thereby preventing fluorescence entirely. As the fluorophore does not enter the excited state, there is no potential for fluorescence, and the lifetime measurements of the population are not altered. Such changes are observed instead by measuring changes to the absorption spectrum. Careful control of environmental conditions such as temperature and pressure affect quenching rates.

Photobleaching represents a loss in the fluorescence intensity of a fluorophore resulting from the fluorescence cycle producing largely irreversible changes to the molecular structure. This change in structure prevents the protein from undergoing its normal excitation and emission cycle and reduces the population's fluorescence intensity. The rate of the fluorescence reduction depends on the excitation intensity and is highly dependent on the fluorescent molecule [9,10]. Fluorescence photobleaching does not contribute to changes in lifetime changes. Photobleaching is a serious issue in fluorescence microscopy, and instrumentation is designed to have the highest sensitivities to fluorescence emission so that the minimum amount of excitation energy is required.

2.1.2 – FRET

All biological processes are controlled by molecular interactions. Cells are governed by a complex network of proteins (DNA / RNA), and protein-protein interactions (PPIs). These molecules form an interconnected network known as an interactome which governs the biological function of the organism [11]. A tool to measure PPIs is Förster Resonance Energy Transfer (FRET), which tags two proteins of interest with fluorescent probes that interact only when the probes are in proximity (proteins are bound), and in the correct rotational orientation. FRET is a non-radiative process, meaning it does not involve the absorption and re-emission of a photon [12,13]. Transfer occurs when the oscillations of an optically induced excited state in a donor resonate with the energy gap of an acceptor. The energy gaps of a fluorophore are given by the excitation and emission spectra, and this provides an easy method

to understand if, theoretically, two fluorophores are compatible with this technique. For FRET to occur, the donor's emission spectra must overlap with the acceptor's excitation spectra. As FRET provides a new mechanism of energy movement in a system, the efficiency of that energy movement can be described by a ratio of the total rate of the FRET process and the rate of fluorescence and all other energy loss paths:

$$E_{FRET} = \frac{k_{nr-FRET}}{k_r + k_{nr} + k_{nr-FRET}} \quad (1)$$

Where $k_{nr-FRET}$, describes the rate of non-radiative decay due to Förster Resonance Energy Transfer, and k_{nr} would describe the rate of non-radiative decay due to other factors. This efficiency is an important metric as it allows us to measure the quantum yield of this specific transition process, i.e. the energy transition probability given an excited donor fluorophore. The efficiency of the energy transfer is given by dipole interactions:

$$E_{FRET} = \frac{1}{1 + \left(\frac{r}{R_0}\right)^6} \quad (2)$$

Where r is the separation of the donor and acceptor pair, and R_0 is the critical radius or the radius in which the energy transfer is 50% efficient. Typical FRET distances occur in the nanometers as given by the critical radius:

$$R_0^6 = \frac{2.07}{128\pi^5 N_A} \frac{\kappa^2 Q_D}{n^4} J(\lambda) \quad (3)$$

Where Q_D is the donor quantum yield in the absence of the acceptor, κ^2 is the dipole orientation factor, n is the refractive index of the medium, N_A is Avogadro constant, and $J(\lambda)$ is the spectral overlap integral. Due to the small separation and the specific orientation an acceptor/donor pair must be to transfer energy via FRET, we know that the two molecules they are attached to must be bound in a specific configuration as it is extremely unlikely, they will be within the critical radius and hold that specific orientation. Thus, FRET is a method of measuring how well two proteins are bound based on the energy transfer efficiency, and we can assess how well some external modulation of the protein-protein interaction is performing. Traditionally, FRET is measured through changes in the donor's fluorescence intensity. The calculation of FRET efficiency is most commonly determined using the ratio of the fluorescence intensities:

$$E = 1 - \frac{F'_D}{F_D} \quad (4)$$

Where F'_D , and F_D , are the fluorescence intensities of the donor with and without the energy transfer to an acceptor.

When measuring FRET using the traditional fluorescence intensity ratio, great care must be taken to ensure the donor's fluorescence is measured without contamination of the acceptor's fluorescence. This is difficult as most fluorescence spectral curves are quite broad, and for fluorophores that are of similar spectra, there may inevitably be some overlap. Fluorescence intensity also poses a problem as measurements of intensities may be different between control and test samples naturally, intensities may be different due to uneven localization of fluorescent proteins.

Instead, since an additional pathway for de-excitation has been provided to the fluorophore undergoing FRET, the energy loss rate will be faster on average. This represents an increase in the rate of non-radiative transitions and is directly measurable by the fluorescence lifetime. The fluorescence lifetime is a measure of the exponential decay of the excited state for a fluorophore, and its duration can be determined as the inverse of the sum of transition rates,

$$\tau = \frac{1}{k_r + k_{nr}} \quad (5)$$

Fluorescence lifetime measurements are an excellent method to measure the changes introduced by FRET as the addition of non-radiative pathways will reduce the fluorescence lifetime. Fluorescence lifetime imaging of FRET (FLIM-FRET) then allows subcellular measurements of lifetime changes without the issues of relative concentration differences of fluorophores, their brightness, photobleaching, and careful selection of spectral filters allows rejection of acceptor fluorescence. The FRET efficiency can be directly calculated through the fluorescence lifetime as:

$$E = 1 - \frac{\tau_{DA}}{\tau_D} \quad (6).$$

Where τ_D is the fluorescence lifetime decay of a donor without the presence of an acceptor, and τ_{DA} is the fluorescence lifetime of the donor undergoing FRET with an acceptor. The selection of FLIM-FRET compatible probes is similar to the selection of FRET pairs, with the additional requirement that lifetime changes induced by FRET are measurable by the FLIM instrument. Lifetime imaging is then aided by high-resolution measurements, such as in confocal microscopy, as rejection of out-of-focus elements prevents natural endogenous fluorophores from altering the measured fluorescence lifetime.

2.1.3 – Multi-dimensional and dynamic imaging

Fluorescence is analyzed through multiple dimensions, as each has its own distinct advantage. To capture multiple fluorescence modalities as spatially resolved images simultaneously is called multidimensional imaging. In our work, we will refer to multispectral, time-resolved, spatially resolved, and dynamic imaging as multidimensional imaging. Multispectral imaging is the process of acquiring multiple spectral measurements of a sample and constructing a spatial and spectral relationship [14–16]. This technique enables multilabel experiments by utilizing spectral separation algorithms to distinguish between multiple entities with different spectral signatures [17–19]. Spatial images of time-resolved fluorescence called FLIM offer contrast where traditional methods like multispectral imaging fail, as it can differentiate between species with identical emission spectra or resolve processes occurring below optical resolution limits, such as protein interactions and conformational changes. Unlike intensity-based techniques, fluorescence lifetime measurements remain unaffected by variations in brightness or concentration, making them especially valuable in challenging imaging conditions. Both time-resolved fluorescence measurements and multispectral imaging are significantly enhanced when integrated with high-resolution imaging techniques, such as confocal microscopy. The use of confocal imaging improves emitter localization and specificity, leading to valuable morphological insights [20,21]. Measurements of these imaging dimensions in quick succession allow the dynamic behavior of the organism from multiple perspectives to be measured, permitting a comprehensive understanding of its function as well as the role of each labeled feature in that function. Imaging rates as fast as four frames per second would be required to accurately measure the cyclic process of cells such as cardiomyocytes used in the study of cardiovascular disease and the

generation of new models for studying fibrillation, or neurons and their interactions with microglia to study the regulation of neural activity [22,23].

Although imaging in multiple dimensions offers distinct advantages, it is uncommon to find multidimensional imaging systems in current high-resolution imaging platforms suitable for fast, live-cell imaging. Integrating fluorescence lifetime imaging microscopy and multispectral imaging into such platforms could provide a comprehensive understanding of cellular processes, creating a powerful tool for biological research across many disciplines. Furthermore, a multipoint multidimensional imaging system would serve as a highly promising technique for drug discovery, which is a complicated process burdened by unsustainable costs and a need for significant improvements in efficiency and efficacy. The continuous rise in costs of operation, along with the inevitable loss of monopoly due to patent expirations, necessitates a decrease in drug development costs to create a sustainable and thriving market. To achieve this, it is essential to develop new technologies that can quantify subcellular processes and enhance our understanding of molecular actions [24–26]. This would accelerate the understanding of drug-target interactions and provide crucial phenotypic insights.

2.1.4 – The state of drug discovery

Drug discovery is a complex multistage process, with each stage having its own costs and risks for failure. Basic research initiates the drug discovery process with the identification of bioactive compounds that is followed by preclinical testing in vitro using various assays and in vivo using animal models. Following discovery, these compounds go through years of additional testing during clinical trials before having the chance to be approved for commercial sale as a drug or biological product [24]. Figure 2-2 details the stages, costs, probabilities of success in each stage, and the time to complete each stage. A 2016 study estimated the total capitalized cost of an approved drug to be ~1.8 billion dollars (USD), with an average time to market of 97 months from the start of clinical trials to FDA approval [27]. Approximately 24.3 submitted compounds are required for one successful launch.

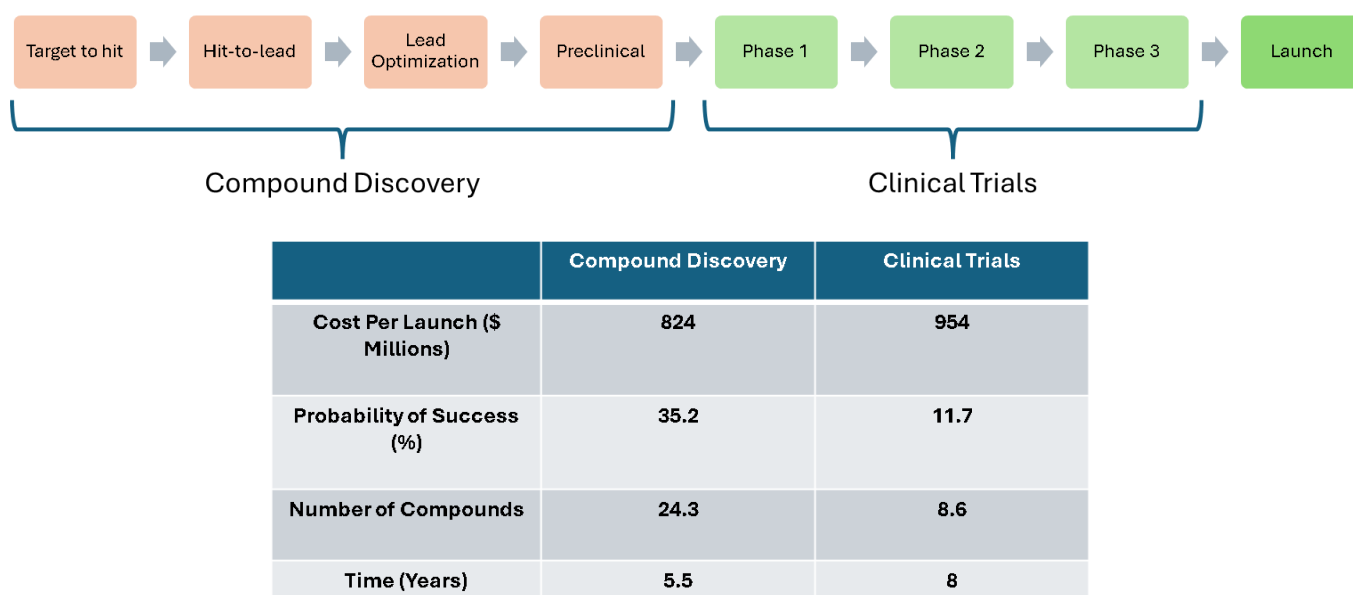


Figure 2-2. The drug discovery process and its associated costs and success rate from the discovery process through clinical trials. (Adapted from [24])

Productive and successful discovery programs not only need to identify large numbers of candidates early on but also need to quickly identify failures to prevent costly clinical trial failures. The final cost of taking a drug to market is not just calculated as the cost of the individual compound's success, but it combines the opportunity cost of all failed drugs in a submission. At a 95% attrition rate, there is a large demand for innovation in models that are physiologically relevant to humans [28]. A discovery program is designed to generate large numbers of candidates which induce a desired biological response. As a result, several technologies, such as bioengineered tissue models, organoids, and organs on chips, have emerged as potential models to complement 2D cell cultures with improved relevance of the physiological response.

Many new models require different imaging techniques to capture the subcellular response to environmental changes or biologically active compounds. Physiological responses vary by many factors, such as cell type, rate of chemical reaction, and diffusion of molecules [29,30]. New methods in coculturing bring the promise of engineered models that undergo dynamic processes and may be better models for areas of research that study cardiovascular or neurological conditions [22,23]. Measurement of dynamic processes is difficult as noise from out-of-focus fluorescence and spectral crosstalk leads to reduced specificity of signal fluctuations. The applications of caged compounds and triggered biological pathways, or in cyclic cardiovascular and neurological models, both require sub-second timescale measurements [31–34]. Multidimensional imaging technologies offer new methods to improve the specificity of the cellular response. Currently, there are few systems capable of measuring multiple contrast dimensions simultaneously at a frame rate fast enough to temporally measure the dynamic fluctuations in these methods.

2.1.5 – High-Content Screening

Measurements in complex models commonly use advanced high-resolution imaging platforms for fast and non-invasive measurements of cellular response. High-resolution systems have a particular advantage when compared to conventional widefield microscopy, as they provide images with improved optical clarity and allow better quantification of sub-cellular features by rejection of-focus light, thereby increasing signal-to-noise, especially in multilayer samples [21,35]. The large volumes of data from image-based microscopy can require significant human effort to derive actionable insights from cellular features within the images. Recently, advances in artificial intelligence, and specifically deep learning, have demonstrated an ability to transform the way we interact with these datasets generated in imaged-based drug discovery [36]. Figure 2-3a depicts an example of an image-based screen that derives experimental insights from relationships among morphological features. Such a screen that identifies a relationship between spatial features within the cell can be described as a phenotypic screen. Another type of tool depicted in Figure 2-3b demonstrates a target-based screen where two molecules are tagged with a fluorescent protein, and the binding of the molecules determines if fluorescence energy is transferred through the fluorescence proteins in a process known as Förster Resonance Energy Transfer (FRET). This energy transfer can only happen when the proteins are bound and is an excellent indicator of positive target interaction.

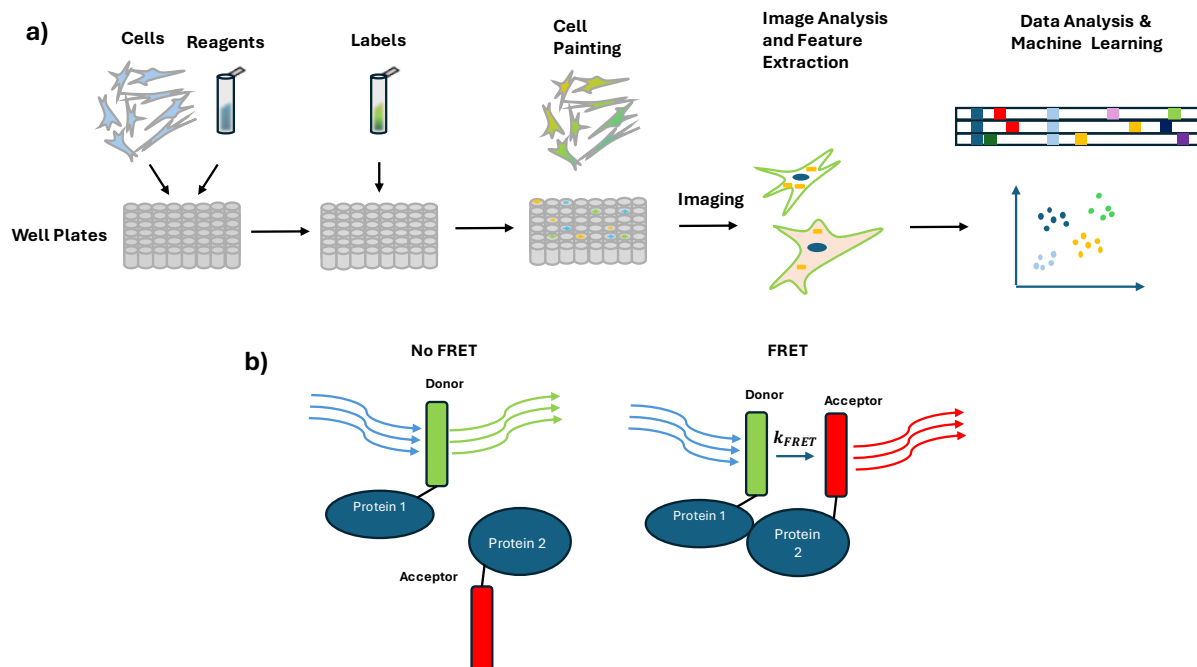


Figure 2-3. The process of high content screening process using high resolution imaging. a) Phenotype based screening process of cell painting detects changes in cell structure. b) Target based screening process using FRET to detect protein-protein binding.

Two major classes of drug discovery are phenotypic drug discovery and target-based drug discovery [26]. Target-based drug discovery consists of hypothesis-driven approaches and applying molecular and chemical knowledge to investigate specific mechanisms of action. Target-based approaches, however, may be formed on an incorrect hypothesis and or may not have a high therapeutic effect. Phenotypic approaches do not require a specific understanding of the biological mechanism of action, and activity in such assays might be translated into a therapeutic impact in a disease state more effectively than in target-based assays. Phenotypic assays, however, are a challenge to optimize as the molecular properties of the candidate drug as well as knowledge of its mechanism of action is unknown. Both techniques have advantages and disadvantages, and both are extensively used to discover new molecular entities.

2.2 Methods of Confocal Measurement

The fundamental theory of confocal measurements is outlined in the following sections. The text discusses systems for achieving confocal measurements using both single-point and multipoint geometry. It also compares the advantages and limitations based on various attributes.

2.2.1- Confocal imaging and common Single Point confocal

Confocal imaging provides a relatively non-invasive method of slicing a three-dimensional sample. It improves contrast by rejecting light originating outside of a diffraction-limited focal volume. Figure 2-4 illustrates the fundamental optical path of a single-point confocal scanner. It typically achieves this by placing a pinhole corresponding to one airy disc in diameter within a conjugate image

plane. The light that originates from the diffraction-limited volume will be imaged through the pinhole by a lens or series of lenses, whereas light from outside that volume, both laterally and axially, will not pass efficiently through the center of the pinhole [37].

The most common confocal system produces a single focus and scans it across the sample in a pattern known as a raster scan. This means to sweep across the sample building an image row by row. Optical signals are filtered by wavelength to remove reflected excitation and recorded using some highly sensitive detector such as a photomultiplier tube (PMT) or an avalanche photodiode (APD). Selection of the pinhole diameter is crucial for accurate measurements in thick samples. The focal volume is a diffraction-limited volume with diameter given by the first zero of the Airy diffraction pattern:

$$D_{limit} = 1.22 \frac{\lambda}{N.A.} \quad (7)$$

Where λ is the wavelength of light and $N.A.$ is the numerical aperture of the lens you use to focus the light onto the sample. The laws of physics restrict the measurable spatial frequency of information in your sample to this size for conventional microscopy. The diameter of the pinhole is chosen to capture all the light within the first zero and must account for the magnification of the optical system:

$$D_{pinhole} = 1.22 \frac{\lambda}{N.A.} M_{sys} \quad (8)$$

Where M_{sys} , is the magnification provided by the optical system.

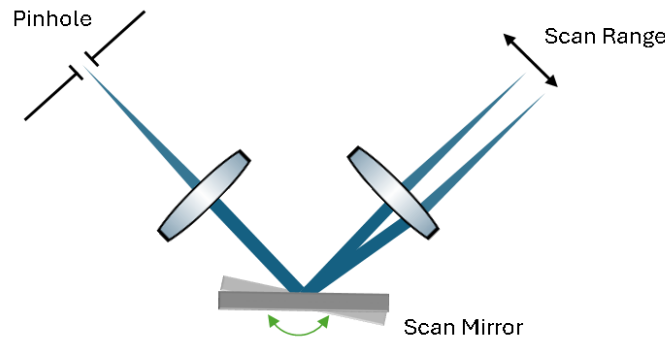


Figure 2-4. An example of the optical geometry of a single-point confocal system.

2.2.2 - Multipoint Confocal

Multipoint confocal is the extension of single point confocal theory that has its own advantages and disadvantages. Multipoint confocal offers a gentle method to quickly image large fields of view compared to single point confocal. Multipoint confocal systems all divide some field of view into a set of regions that can be imaged with confocal optics simultaneously. The simultaneous imaging allows the same area to be imaged faster by the multiplexing factor if all imaging characteristics, such as pixel dwell time and detector sensitivity, remain the same. Reduced requirements on operating speeds also provide the ability to relax the optical excitation intensity and increase pixel dwell times. This is advantageous for live biological specimens where multiple images may be needed either for long duration imaging of a dynamic process or for building a three-dimensional optically sectioned

measurement of a thick specimen, as intense optical signals have the potential to photobleach fluorescent labels and induce photochemical toxicity.

Multipoint confocal, however, is not without its disadvantages. Multipoint confocal requires additional confocal pinholes. Additional pinholes within the spatial filter provide new potential pathways for noise signals to leak through the wrong pinhole and produce noise on the sensor. This is not an insignificant issue, especially for thick samples, as the rejection of out-of-focus light is the key performance metric of confocal microscopy. As a result of the reduced background signal rejection, multipoint confocal imaging cannot achieve as high an imaging quality for specimens above a 50 μm sample thickness when compared to single point confocal microscopy [38].

2.2.2.1 - Spinning Disk Confocal

Multipoint confocal technology has been dominated by an optical scanning mechanism known as the Nipkow disk [39]. The Nipkow disk has a series of pinholes wrapped around its center (the point of rotation) at even spacing such that each point increases its radial distance by a magnified airy disk diameter. As illustrated in Figure 2-5, for a disk with a single spiral, a scan of a sample is completed by one full rotation of the disk, each pinhole painting a radial zone of the image onto an imaging sensor. Modern Nipkow disks are typically composed of multiple pinhole spirals allowing several full images to be formed by one full disk rotation. The intrinsic speed of the Nipkow disk as a scanning technique is that its output is directly coupled to modern high speed image sensors. The image sensor has pixel density and sensitivity requirements, and the EMCCD has been the traditional detector of choice with sCMOS detectors more recently becoming the popular choice. The traditional Nipkow spinning disk confocal is limited by its ability to couple excitation light into the pinholes. Modern versions of the spinning disk confocal differentiate themselves with the addition of a second disk with small lenses known as micro-lenses placed in identical spirals such that they can focus excitation light efficiently through the pinhole disk.

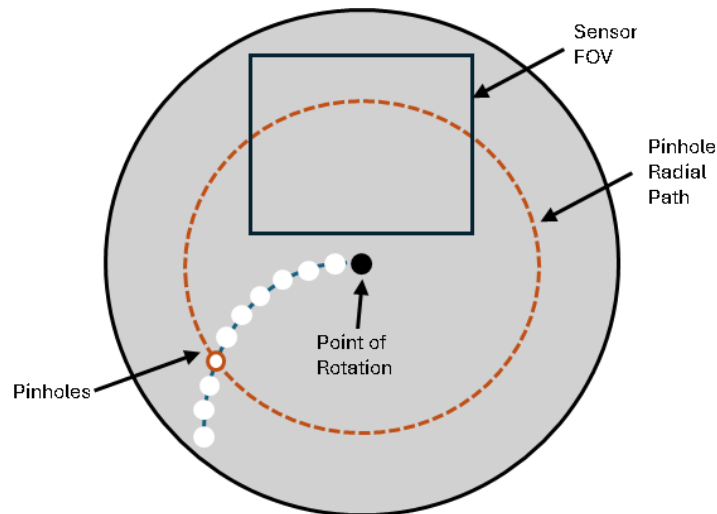


Figure 2-5. A Nipkow disk confocal scanner with a single spiral.

2.2.2.2 - Window Scanning Confocal

Multipoint confocal scanning has had challenges to implement due to the uniform scanning requirements for each point. A uniform mapping of the spots needs to occur such that each spatial position on the sample is scanned exactly once to prevent non-uniform illumination, which leads to excessive photobleaching and phototoxicity. Single point confocal scanning uses mirror-based scanning to introduce angular changes into the optical trajectory of the excitation beam. When the point of rotation is placed directly in the focal point of an ideal lens, the angular change is collimated into a displacement of the beam. Fluorescence will return through the same optical path and be de-scanned onto a stationary single point detector. For single point applications, this technique has no flaws, as fast scanning can occur with powerful scanning motors. Unfortunately, mirror-based scanning of the uniform array of points results in non-uniform displacement of the points in multipoint scanning. The displacement of a mirror scanning based beam displacement is a function of the incident angle of the beam. To scan the multiple points simultaneously, a pair of lenses is used in a 4F scanning relay, with the mirror scanner placed in the common focus of the lenses. This means that for an array of points imaged by a 4F telecentric scanning system, as illustrated in Figure 2-6.a, the marginal image points have a different angular displacement than image points passed through the center of the image relay. The displacement of the image points is given by,

$$\Delta d = f \tan \left(\tan^{-1} \frac{d_{in}}{f} + 2\phi \right) - d_{in} \sim 2f\phi. \quad (9)$$

Where f is the common focal length of the lenses in the relay, d_{in} is the initial distance from the optical axis of the relay, and ϕ is the angular displacement of the mirror rotation between the initial and final position.

Window scanners are a new and innovative method of scanning that utilizes a transparent window and its refractive properties to uniformly shift an image of excitation spots across a sample. This window is made of transparent glass with a refractive index different from air [40]. When tilted, the window produces refraction at the air-glass boundary, creating a refractive angle that generates displacement over the thickness of the glass. This refractive angle is removed when the image exits the glass at the glass-air boundary. Though the displacement is small, it is well suited for high-resolution stepping, allowing for very large images to be uniformly displaced. These are excellent characteristics for multipoint confocal imaging, as the multi-point sampling array is displaced at a distance typically no larger than the pitch of the spots. In window scanning, the window size and the resulting mass of the window tend to be the limiting factor for the largest window size and, thus, the largest field of view. Figure 2-6.b demonstrates the concept of the window scanner to displace an array of beams uniformly. The displacement of the window scanners is given by,

$$\Delta d = T \left(\tan(\phi) - \tan \left(\sin^{-1} \left(\frac{\sin(\phi)}{n} \right) \right) \right) \cos(\phi) \cong T\phi \left(\frac{n-1}{n} \right). \quad (10)$$

Where T is the thickness of the window, ϕ is the angular displacement of the window, and n is the refractive index of the material that forms the window. Note that there is no dependence on the distance from the optical axis with the window scanner displacement. Window scanners are an excellent option for scanning large images uniformly. However, they are slow compared to mirror scanners as the

thickness of the window is what gives it the power to displace images, whereas, for mirror scanners, the mirror only needs a thin depth to reflect the scanning beam.

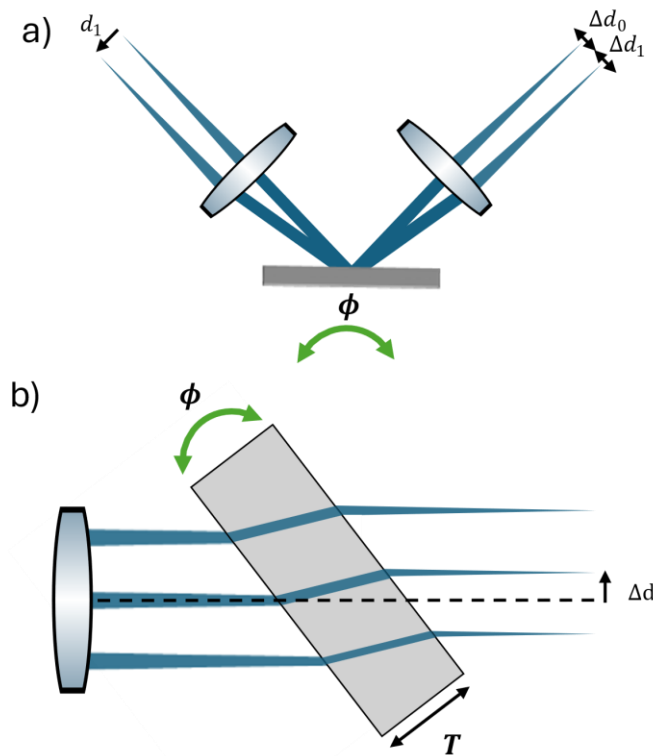


Figure 2-6. Multipoint confocal scanning methods. a) Mirror-based, and b) Window-based scanning methods.

2.3 Spectrally resolved imaging

Spectrally resolved imaging provides unique fingerprints of emissive or absorbing materials. There exist two commonly employed imaging philosophies for multispectral imaging: sequential spectral acquisition and parallel spectral acquisition [15,16]. Sequential spectral acquisition typically involves exciting the sample with a single wavelength of light and then collecting the emission in a single wavelength band. This approach acquires images for each spectral channel one at a time. The primary advantage of sequential acquisition is its ability to minimize channel crosstalk. This is achieved by strategically selecting excitation wavelengths that reduce the overlap between the emission spectra of different fluorophores, ensuring that each fluorophore is excited in isolation as much as possible. This change in excitation can occur at a slow temporal frequency, where entire images have different spectral excitation levels, or at a fast temporal frequency, where laser pulse trains have a phase difference in the excitation frequency, and fluorescence captured corresponds to the fluorescence decay of a single species [15,41,42]. As a result, the collected emission signals are cleaner, with reduced interference from other labels in the sample. A series of spectral images are acquired at a single position, and their images are combined to provide a multispectral data cube. The process of sequential spectral acquisition can be time-consuming, as it requires multiple scans of the same area to collect all the necessary spectral information. However, the benefit of reduced crosstalk often outweighs this drawback, especially in

applications where the accuracy and clarity of the spectral data are paramount. By carefully designing the excitation and emission settings, researchers can obtain high-quality multispectral images that offer valuable insights into the molecular composition and interactions within the sample. Parallel spectral acquisition such as demonstrated in Figure 2-7.a, alternatively, consists of collecting all spectral information simultaneously, either by separating spectral channels onto different detectors or by some spectrally encoded aperture that allows multiwavelength detection on one sensor [16,43–46]. Parallel spectral image acquisition such as in Figure 2-7.b, has become possible due to developments in designing highly customizable spectral filters that allow parallel excitation and emission collection [47]. These filters allow fluorescence emission to be collected between excitation wavelengths and separated so that there is minimal excitation bleed through to spectral images.

2.3.1- Single point multispectral confocal scanning

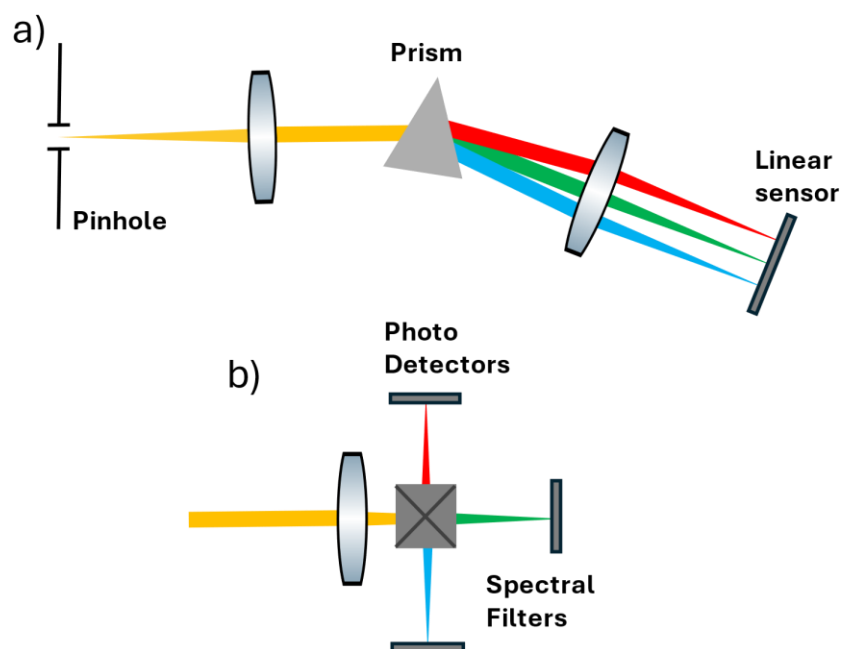


Figure 2-7. a) An example of a prism based spectrometer for parallel detection. b) An example of spectral filter based separation of multiple spectral channels.

Currently, single point multispectral confocal microscopy has the largest number of optical instruments that can be used to perform spectral separation [6,8,48–53]. This is because the spectrally resolving device can paint the spectral information onto unique spatial coordinates of a sensor without concern for spatial crosstalk between spatial readouts. This can only occur as the sensor is only ever measuring the fluorescence of a single point at a time. Common instruments to separate spectral data in single point microscopy include a prism or a diffraction grating based polychromator. These instruments offer the highest spectral resolution for correlating spectral changes to biological events.

2.3.1- Multipoint multispectral confocal imaging

Optical systems are designed with specific functionality in mind. Single point confocal microscopy methods are unparalleled in their confocal sectioning. They have undergone multiple generations of upgrades to extend their functionality and sensitivity and are outfitted with each new contrast method discovered. They suffer from one significant limitation in that they are limited to measuring a single point, which limits the rate at which they can process large samples. Multipoint confocal, such as the spinning disk confocal, has solved this issue by offering a method to quickly acquire large samples [54,55]. Unfortunately, spinning disk confocal imaging systems must separate spectral channels into unique detectors due to the methodology of scanning. The spiral pattern of sampling points that progressively paint an image onto a detector completely fills the sensor with the rotation of their pattern. As a result, traditional spectrally resolving methods such as prisms or diffraction gratings, which are used in single-point microscopy, are not compatible with this technique. Color cameras that use Bayer filters are common, however, they are uncommon on spinning disk confocal platforms. Multispectral Filter based imaging techniques they will result in lower image resolution due to each spectral channel being a quarter of half the available pixel density. For single-point detection systems such as conventional confocal microscopy, parallel spectral detection is common, with the use of AOTFs being commonly employed for highly flexible spectral single and multi-channel detection [6,56].

2.4 Temporal domain imaging (fluorescence lifetime)

2.4.1 - Bandwidth

Spatial information is not the only tool that can be used to provide a measurable contrast of two different species. Many fluorescent species have unique transient characteristics in nanosecond or shorter time scales which are inaccessible to conventional image sensor technology and require specialized electronics to investigate.

The most straightforward method of measuring a time-varying signal is the temporal sampling technique, where changes in the input signal amplitude over time are measured or sampled multiple times by a single detector. To accurately characterize these dynamics the sampling speed should be at least twice the speed of the fastest process to be accurately measured, as specified by the Shannon-Nyquist theorem.

Signal speeds are measured by their frequency, and the fastest signal that is accurately measurable for a given system is referred to as its bandwidth frequency. A very slow signal with a frequency near 0 Hz, has an almost perfect measurable change, however, as a signal frequency increases the system will measure the amplitude of the change with decreasing accuracy. The bandwidth is commonly selected to be the frequency that is attenuated by 3 dB (~30%), according to the IEEE 1057 standard, and is designed to at least satisfy the Shannon Nyquist criteria.

2.4.2 – Rise Time

To measure the rapid decay of the excited state of a fluorescent molecule, we must use an intense optical pulse capable of creating sufficient signal fluorescence. An ideal optical pulse would be an instantaneous event with a temporal profile of a delta function. However, this is unachievable due to practical limitations in the frequency range of a laser cavity and or the electronics that ultimately drive the lasing process. At best, optical pulses have a duration in the femtosecond regime, such as those commonly found in mode-locked solid-state lasers with optical pulses of ~140 fs, such as in the popular

but expensive Chameleon Ultra (Coherent). Due to advancements in cheaper semiconductor diode lasers, optical pulses in the ~ 500 ps range are common with devices such as the Picoquant LDH series; however, these lasers, when driven to their extremes, have significantly worse optical pulse properties as a slow second pulse occurs after the primary fast pulse. As such, being able to measure the influence of the non-ideal excitation function requires a system with a fast rise time. Rise time is defined as the time between the output signal increase from 10% to 90% of its maximum amplitude of an ideal delta input pulse (e.g., the rising edge of a step function). It is the resultant property of the entire system frequency response. Ultimately, the overall temporal resolution of a measurement system is limited by the slowest module. For example, the analog bandwidth of a temporal sensing system can be calculated from the rise time of each individual component:

$$\text{Bandwidth} \cdot \text{Rise Time} = 0.35 \quad (9)$$

$$\text{Risetime}_{\text{system}}^2 = \text{Risetime}_{\text{detector}}^2 + \text{Risetime}_{\text{amplifier}}^2 + \text{Risetime}_{\text{digitizer}}^2 \quad (10)$$

2.4.3 - Single point detectors for time fluorescence measurements

Single-pixel photodetectors currently under development can reach bandwidths as high as 100 GHz. In comparison, real-time high-speed digitizers on the market, such as the Keysight UXR1104A Infiniium, can reach bandwidths up to 110 GHz with a rise time of 5.6 ps (10%-90%) and a sampling rate of 256 GSa/s. Without an additional amplifier, the highest achievable bandwidth for a sampling system is about 70 GHz, corresponding to a rise time of 10 ps, which meets most fast optical measurement needs. However, a preamplifier may be required for weak signals if the detector does not have enough intrinsic amplification, commercial preamplifiers for time-resolved fluorescence detectors generally operate in the low GHz range, significantly reducing the system's temporal performance.

Similarly, researchers use time-correlated single photon counting (TCSPC) in time-domain measurements, including imaging applications [57]. The single photon counting technique is inherently slower than the pulse sampling technique because it needs to acquire signals over many repetitive events (ranging from hundreds of thousands to a few million). Although it does not provide single-shot or real-time imaging capabilities, it can achieve temporal resolutions in the tens of picoseconds with relatively inexpensive instrumentation for suitable applications. Over the past two decades (2000–2023), TCSPC has become the predominant time-domain measurement technique in bioimaging, owing to advances in high repetition rate picosecond pulsed diode lasers.

Two detection technologies that are commonly used to take measurements at these speeds are the photo-multiplier tube (PMT), and the single-photon avalanche photodiode (SPAD). Both detectors boast high sensitivity, speed, and gain for detecting single photon events. Both are compatible with TCSPC technology and are extensively used in time-resolved fluorescence instrumentation.

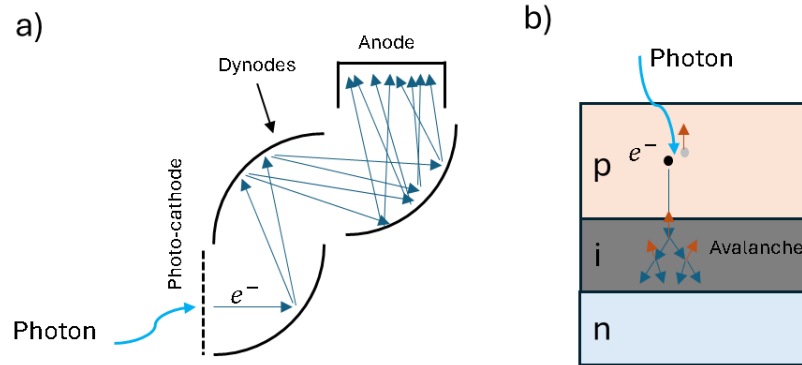


Figure 2-8. Single photon counting devices. Diagrams of the internal geometry of a) a PMT and b) a SPAD pixel.

The structure of a PMT is demonstrated in Figure 2-8.a . The PMT operates through an initial photon-to-electron conversion, and a series of multiplication stages to amplify the signal of a single photon enough to be measured by external electronics [58]. The core components of the PMT are the photocathode, a focusing electrode, a series of dynodes, and an anode. The photocathode is responsible for the conversion of incident photons into free electrons within the vacuum tube. These electrons are called photo-electrons due to the nature they are generated. The photo-electrons are drawn into the PMT by a voltage between the photocathode and the focusing electrode, so they are efficiently drawn into the electron multiplication region. Photo-electrons that impact a dynode with enough kinetic energy generate secondary electrons. Secondary electrons continue to the next dynode and repeat the multiplication process at each successive dynode, producing a gain of signal. Those amplified electrons are finally collected by an anode and read out by external electronics. The PMT then can generate large signals based on single photon events. The spread in the timing of the electrons is carefully designed through numerical methods to optimize electron flow paths, reduce the temporal spread of electrons, and prevent space charge effects. While the amplification of a photon trigger is happening, it is difficult to separate the signal of a second photon event, and thus most electronics will wait until the full multiplication event has ended. This time during which the electronics cannot distinguish a successive photon event is known as *deadtime* or a period of inactivity that limits the total count rate of the device.

The structure of a SPAD pixel is demonstrated in Figure 2-8.b . At its core, a SPAD pixel is an avalanche photodiode reverse-biased above its breakdown voltage such that it operates in what is known as *Geiger mode* [59]. In Geiger mode, the high voltage across the pixel accelerates photoelectrons generated in the absorption region through the semiconductor to a kinetic energy sufficient to produce impact ionization within the amplification region. The amplification of the photoelectron generates a sufficient current for detection by external electronics. Unlike traditional photodetectors, the photocurrent response of a SPAD is large and requires a process known as *quenching* to stop the avalanche process before damage to the pixel occurs. The total duration from the beginning of the avalanche process to its quenching is known as *deadtime* of the detector and is a period where photon detection does not occur and limits the total count rate.

The high sensitivity of this detector allows measurements of single photon events, and the short and consistent pulse width allows precise timing of photon arrival time relative to the incident laser pulse. Specialized electronics will measure repeated photon timing events relative to laser pulse arrival and build up a histogram of arrival times for fitting fluorescence lifetime. The inherent *deadtime* in each detection methodology presents an issue as the arrival of two photons will be counted as a single event,

a process known as photon-pileup. Deadtimes for current TCSPC SPAD detectors can range from 80 to 250 nanoseconds. This limitation, combined with the frequency of excitation pulses used in FLIM experiments, which typically range from 10-80 MHz (12.5-100 nanoseconds period), establishes the "TCSPC limit". This limit ultimately restricts the acquisition speed in FLIM imaging [60].

2.4.4 – Multipoint detectors for time resolved fluorescence

2.4.4.1- Gated Optical Intensifier

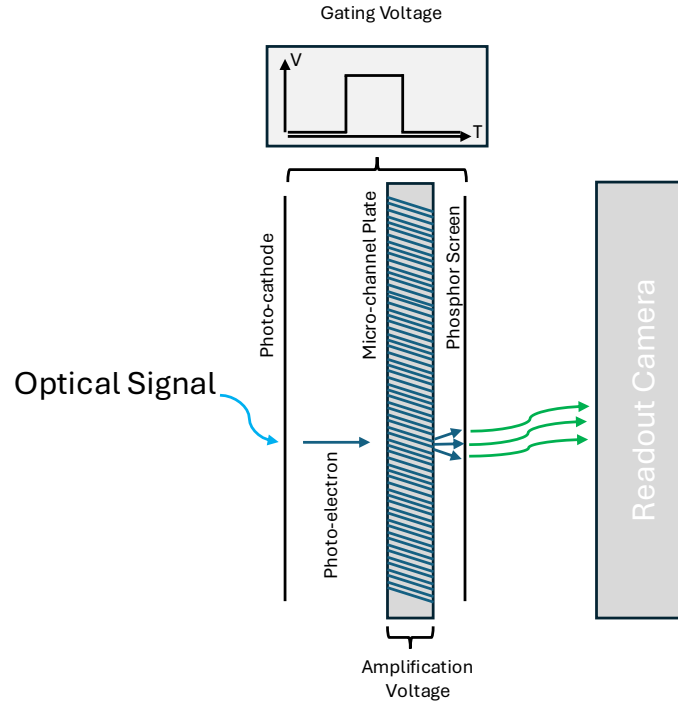


Figure 2-9. A diagram of the gated optical intensifier.

Parallel acquisition of spatial positions is a powerful technique for achieving a higher imaging frame rate. An approach to develop fast gated image intensification uses an image intensifier and a photo-electron shutter that opens and closes within a few nanoseconds or even sub-nanosecond [61]. As shown in Figure 2-9, incoming light is first converted into photoelectrons when it hits the photocathode. The resulting photoelectrons are then accelerated across a vacuum towards the microchannel plate (MCP). When the voltage is on, the electrons flow across the gap, and when the voltage is off, the electrons do not flow. When a high-voltage DC electrical field is applied across the MCP, the electrons that reach it are pulled through the channels of the MCP. While the microchannels are millimeters long (i.e., the thickness of the MCP), the diameter of each channel is only a few micrometers, and the channel itself is tilted, resulting in the inevitable impact of the photoelectrons on the surface of the channel. This impact has enough energy to produce secondary electrons which escape the channel's surface back into the channel. As the photoelectrons are generated with isotropic moving directions, they will bounce multiple times on the channel surface before exiting the anode. By the time they move across the microchannel, a single photoelectron can be amplified millions of times depending on the length of the MCP. Then the

amplified electrons will hit a phosphor screen right after the MCP and become a light signal again. The microchannels in the MCP allow the spatial distribution of the photons incident onto the device to be maintained when showing up on the phosphor screen. A conventional camera (e.g., CCD or CMOS) will “read out” the phosphorescence image.

2.4.4.2- Streak Camera

The streak camera is another time resolved fluorescence detector. Although the word camera is used, the streak camera is line scanning detector that encodes the temporal information of a single spatial line across the face of a detector as a streak. The streak camera is shown below in Figure 2-10. The streak camera converts a line of light into photoelectrons by a photocathode. The photoelectrons are accelerated down a channel towards a phosphor screen that can convert the photoelectrons back into light. While the photoelectrons travel through the channel, a time-varying voltage is applied to a pair of deflector plates that create a time-varying electric field to spatially deviate the trajectory of the photoelectrons. The synchronization of optical pulses with the time-varying deviation of trajectory allows precise displacement of electron trajectory, resulting in excellent temporal resolution of less than 0.2 ps. The technique essentially spatially encodes the temporal delay of the photoelectrons into unique spatial positions. As this happens with an entire spatial streak a 2D image is generated, one dimension is the spatial position, the second being the temporal profile. The Streak camera uses a MCP to amplify the time encoded photoelectrons, thereby amplifying the optical signal with high timing characteristics being maintained before being readout by a camera.

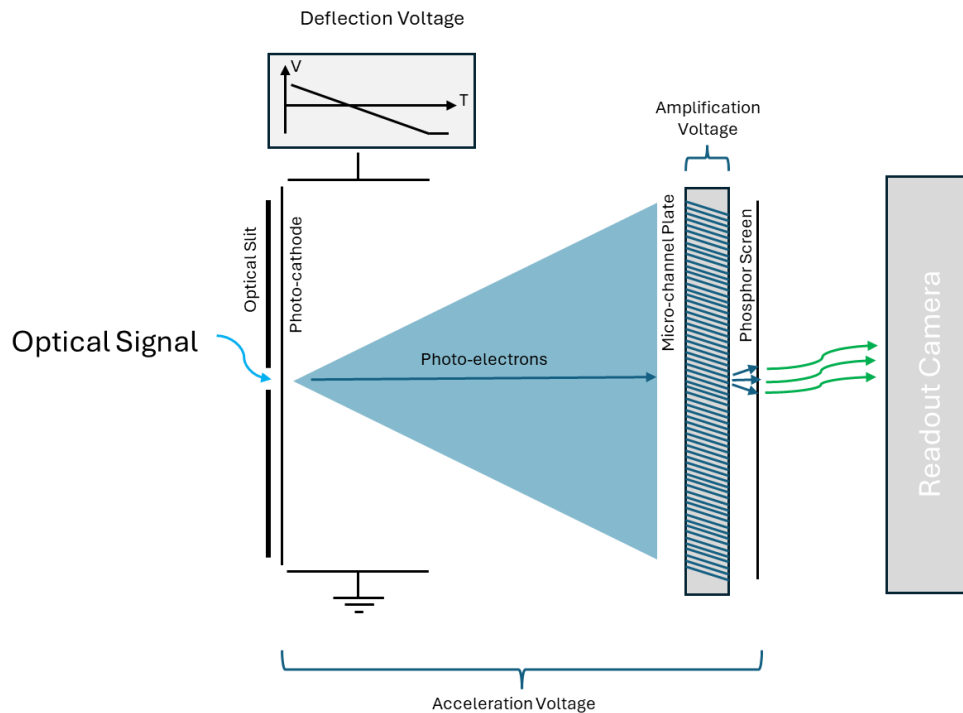


Figure 2-10. A diagram of the principles of a streak camera's operation.

2.4.4.3- SPAD Arrays

The miniaturization of CMOS technology and the maturation of SPAD has enabled the fabrication of SPAD arrays. SPAD arrays operate in the same manner that their single pixel designs do, with timing measurement, recharge, and readout electronics being required for each individual pixel[62]. This results

in a large total area of the pixel, and by extension the entire sensor, that is insensitive to light and is referred to as a low fill factor. This large unused space on the sensor face results in poor photon detection efficiency for conventional imaging applications such as widefield imaging, which needs small pixel areas to capture high-resolution spatial features. The use of microlens arrays placed directly on top of the sensor reduces the poor fill factor as the lens over each pixel helps redirect some light into the pixels active sensing area, measurement limitation.

Miniaturization of elements helps with large pixel size directly but presents issues with crosstalk of pixels. Further miniaturization of the pixel technology is possible, and even moving some on-pixel electronics out of the main sensing area to the borders is possible to a certain extent with in-column and on-chip architecture. This type of miniaturization comes with trade-offs such as electrical/optical crosstalk and readout bandwidth limitations that should be considered.

2.5 Methods of multipoint time resolved confocal imaging

2.5.1 Streak system for multipoint confocal FLIM

A novel implementation of a multipoint confocal FLIM microscope uses the streak camera as the main detector with the aid of a 2D to 1D fiber array to reshape the input from a microlens array. The speed of light changes in optical fiber ($n \sim 1.5$), which allows flexibility in tuning the delay not only in length but also in fiber materials. In a free-space delay line setup, it is relatively easy to change the delay time by varying the relative distances between components. Although the delay time in fiber delay lines cannot be changed after being cut to a predefined length, they can be precisely controlled or standardized with a fixed length.

Figure 2-11 shows an example of this design for time-resolved fluorescence measurement using a multipoint confocal microscope [63]. A microlens array is used to generate 10×10 multipoint excitation on the specimen. A 2D image of excited fluorescence spots generated by the emission microlens arrays and is projected to the 2D end of the fiber bundle with 100 fibers configured in a 10×10 format [45, 53]. These fibers are rearranged into a 1D format at the opposite end of the fiber and coupled to the input slit of a streak camera. The temporal shape of the signal in each pixel of the 2D image is then measured though as a line (1D). The streak camera will output “streak” images of each input channel (i.e., pixel) as its temporal shape. A computer program will process the resulting streaks into fluorescence lifetimes for each pixel and reconstruct the 2D image based on the correlations between the 2D-1D fiber bundle arrangement. So far, this is a simple 2D to 1D rearrangement or encoding. Streak camera suffers from poor spatial resolution similar to the ICCD since it uses the same type of photocathode at the front end. This issue led to significant cross-talk between the adjacent input fiber channels. To reduce this crosstalk between the channels, the fibers in the bundle are separated into two groups with two different lengths. Then they are rearranged to alternate between the two different lengths at the 1D end. Since the streak camera measures the photon arriving time at the photocathode, the optical signal carried by the shorter fibers will arrive at the photocathode first, resulting in 50 input channels (group A, half of the 100 fibers) being active with an inactive fiber (from group B) placed between each channel. The light carried by the longer fibers will arrive at a later time, which is a different starting point in the streak camera’s spatial sweep. In the case of fluorescence lifetime imaging of biological samples, the fluorescence probe lifetime is short enough to have the signal from the shorter fibers (group A) decay to a negligible level before the long fiber (group B) photons arrive at the photocathode. As a result, both groups will have an extra “buffer” input channel that can effectively minimize crosstalk. The basic principle of using fiber

delay to selectively group and treat different inputs can certainly be applied to more than just two groups.

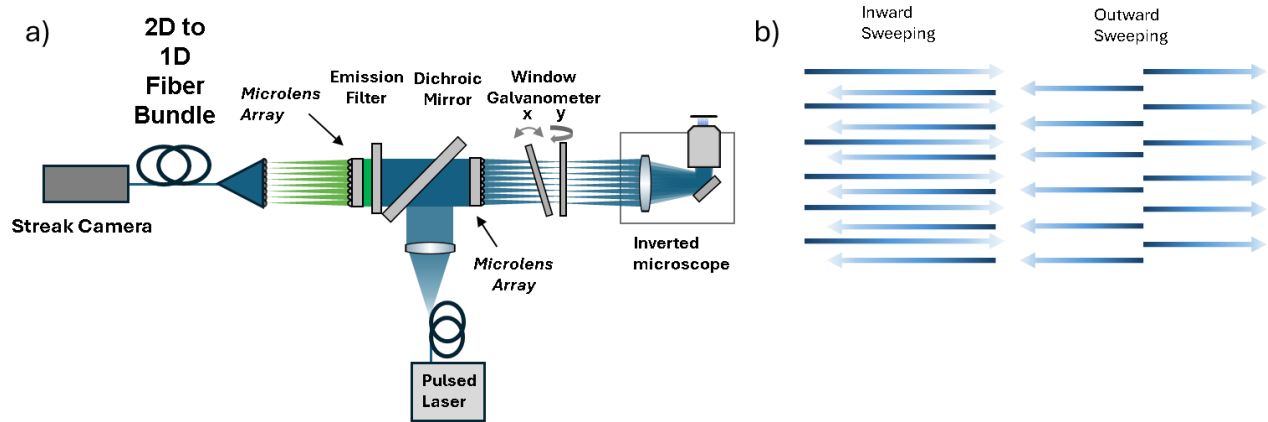


Figure 2-11. The window scanned multipoint confocal FLIM microscope using a streak camera and a 2D to 1D fiber converter. (Adapted from[63]). a) the optical system layout b) Output from the streak camera demonstrating FLIM decays with inward(left) or outward(right) spatial-temporal encoding directions.

2.5.2 Gated Optical Intensifier for Multipoint Confocal FLIM

Multipoint confocal FLIM is possible in a straight forward implementation due to the design of the spinning disk that allows direct coupling of time resolved image sensors to its output. The confocal Nipkow pinhole disk highly rejects out-of-focus light, and spinning of the disk allows a full confocal image to be formed on integration. The setup in Figure 2-12 is a demonstration with a custom prism-based wavelength selector designed to allow rapid selection of the excitation wavelength that is coupled into an optical fiber[64]. The spinning disk confocal system was a CSU10 Nipkow disk (Yokogawa) scan head, using a gated optical intensifier (Kentech Instruments, model number HRI). The output image of the phosphor screen that converts the amplified and gated optical signal, is relayed by a pair of imaging lenses onto a cooled CCD (Hamamatsu ORCA-ER) for readout. This method generates time gated images of the confocal section that can be sequentially taken at appropriate timing delays to build a fluorescence decay profile. In this paper the author chose to use two gates and the rapid lifetime determination (RLD) method. The spinning disk implementation was able to achieve full field of view FLIM at an impressive frame rate of ten frames per second at 336x256 pixels. The disadvantages of this technique lie in the reduced spatial resolution due to the gated optical intensifiers limiting spatial resolution. In this example, the sample is axially sectioned quite well but the resulting lateral spatial resolution of the image is poor.

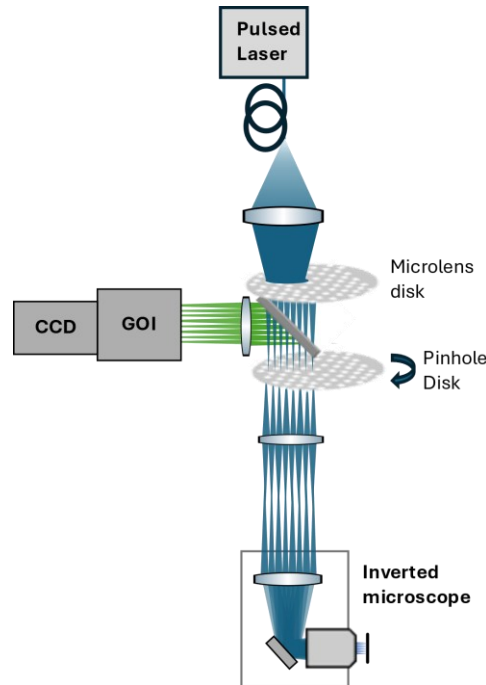


Figure 2-12. Spinning disk confocal FLIM, using a GOI (Adapted from [64])

2.5.3 Multipoint confocal FLIM using SPAD ARRAY

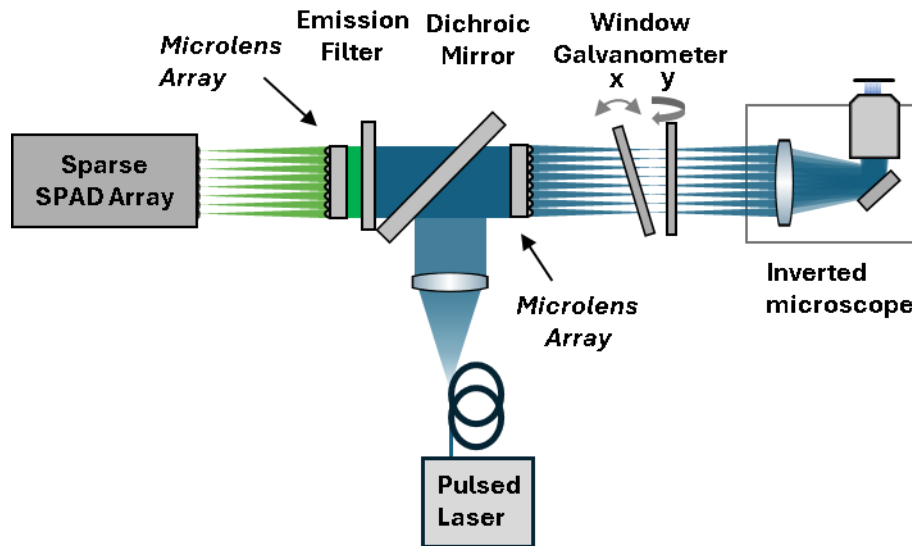


Figure 2-13. Window scanned multipoint confocal FLIM microscope using a SPAD array. (Adapted from [65])

A new implementation of multipoint confocal FLIM is illustrated in Figure 2-13, where the streak camera is replaced with a SPAD array [65]. Due to the window scanners uniformly scanning a large image, it is possible to implement a 32x32 point multiplexing confocal scanner and directly couple the output fluorescence to an SPAD array image (SPC3, MPD). The SPAD array as an image sensor has very poor spatial resolution due to the low pixel count and poor fill factor. The large pixel pitch and poor

fill factor can be matched with integration onto a microlens based confocal scanner as the pixel pitch can be matched to the microlens pitch with some magnifying optical relay. The window scanner allows precision placement of the confocal volume array and fine stepping between MLA pitch distances thus allowing a high-resolution time resolved fluorescence image to be generated from sparse array of points. In this implementation a time-gated detector is used rather than a TCSPC detector, as the reduced data size offers faster lifetime fitting through rapid lifetime determination. Currently, this implementation of confocal scanner takes 1.5 seconds to collect a single gated image and must collect two gated images to generate a FLIM image, thus taking 3.0 seconds for a FLIM image.

2.6 Multidimensional imaging

2.6.1 - Existing methods in multidimensional imaging

Multidimensional imaging is the process of collecting several contrast methods simultaneously. Four powerful contrast methods in optical microscopy are spatial, spectral, temporal, and dynamic contrasts which all offer a unique perspective into cellular processes. Spatial contrast involves the capture of three dimension or structural information. This powerful contrast mode allows the correlation of changes to a samples structure to a drug or biologic of interest, which can offer relationships between drugs and pathology. Spectrally resolved imaging distinguishes fluorescent labels by their unique spectral signature and can identify co-localization. This technique can separate features and identify chemical reactions within the subcellular environment. Temporally resolved fluorescence imaging occurs on the order of nanoseconds and is a more recent addition as detector technology has struggled to make these fast measurements. The fluorescence lifetime offers unique quantum mechanical contrast that indicates changes to the fluorescent molecule, either through changes to the molecule's structure or its energy dynamics.

Multidimensional imaging captures previously hidden events by offering multiple perspectives that potentially capture “blind spots” from each contrast agent. These contrasts are rarely found together due to the unique requirements of each methodology. These techniques, in their current state, have a slow total throughput when combined. Dynamic measurements, which correspond to a high rate of successive images (movies), are critical to many applications because it allow us to connect the initial and final state of a system through a sequence of steps. Dynamic measurements directly provide us the order of events, and with the other contrast agents, can help us build models to better understand a complicated process.

Sequentially measuring lifetime decay across spectral bands is possible but presents significant challenges that prevent practical implementation. This approach is highly inefficient because most emitted photons are discarded by the spectrally resolving instrumentation, requiring long exposure times to achieve an adequate signal-to-noise ratio for lifetime fitting. This, in turn, increases the risk of photobleaching, which compromises both spectral and lifetime data. Photobleaching permanently alters the fluorophore, preventing fluorescence and increasing nonradiative decay pathways that alter the lifetime. To avoid these issues, it is preferable to collect all emission wavelengths simultaneously with sufficient resolution to perform spectral decomposition. In this section we will discuss some of the solutions for multidimensional (spectral, and lifetime) confocal microscopy.

2.6.2- Becker and Hickle multiwavelength tcspc system

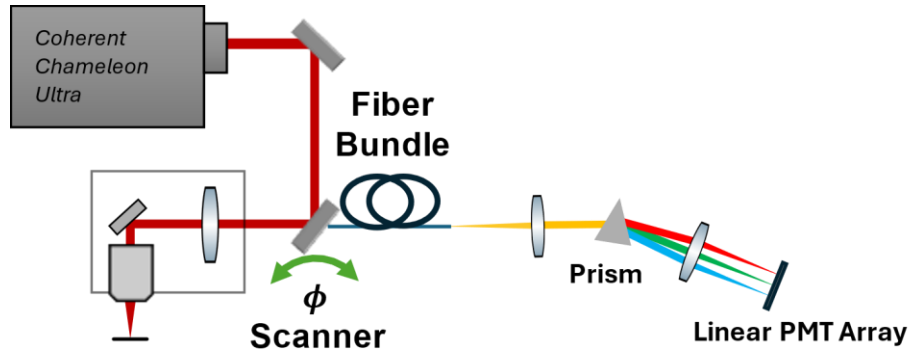


Figure 2-14. Multidimensional Multiphoton microscope, using a polychromator and a 16 channel PMT to perform spectrally resolved multiphoton FLIM. (Adapted from [51])

One of the earliest examples of a multidimensional system is given by Becker et al [66], and is illustrated in Figure 2-14. (2002), where a multi-anode photomultiplier tube (PMT) is used to collect multispectral and time-resolved fluorescence data from a confocal microscope. In this system, the fluorescence emission from a single-point multiphoton microscope is coupled into a fiber array bundle. This bundle is then transformed from a 2D configuration into a 1D array, which is subsequently spectrally separated by a polychromator. The polychromator disperses the light into its component wavelengths, resulting in a 2D spectral image of the single focal volume. The multispectral image is captured by a 16-channel PMT array, which converts the time-tagged photon events into a series of 64-time windows, each indicating the photon's arrival time relative to the initial laser pulse. Through this process, a comprehensive spectral and temporal decay profile is built up for each position measured by the confocal scanner. The system can produce images at a resolution of 256x256 pixels within 20 seconds, while maintaining full spectral resolution. With recent developments in SPAD technology, the PMT array is commonly exchanged for SPAD arrays [8,48–50,52].

2.6.2- Single point multidimensional imaging with the streak camera

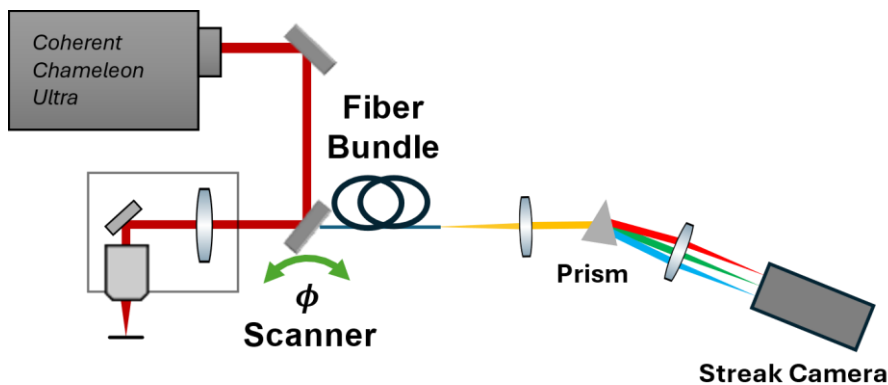


Figure 2-15. Multidimensional Confocal Microscope using a spectrograph and a streak camera to perform spectrally resolved confocal FLIM. (Adapted from [67])

A demonstration of multidimensional confocal microscopy using a streak camera is illustrated in Figure 2-14.a, where it is employed to provide high-resolution spectral lifetime images from a point-scanning confocal microscope [67]. In this system, a single-point scanning microscope utilizes a polychromator

(250is, Chromex) to spectrally separate the emission originating from a Zeiss laser scanning confocal microscope (LSM-510, Zeiss). The spectrally separated confocal emission is then temporally measured by a streak camera, which generates a spectral temporal image for each point in the two-dimensional scan.

One significant drawback is the poor optical efficiency of the streak camera due to the low efficiency of its photocathode. This can result in lower signal intensities, potentially affecting the quality of the fluorescence lifetime measurements. Additionally, the slow readout speed of the image sensor creates a bottleneck in reading out streak camera results, limiting the overall speed at which full scans can be acquired and processed. Despite these limitations, the multidimensional confocal system demonstrated by Biskup et al. represents a powerful tool for high-resolution spectral lifetime imaging, capable of providing detailed insights into the temporal and spectral characteristics of fluorescent samples.

2.7 Discussion

Developing a fast multispectral confocal FLIM microscope presents several challenges in live cell imaging. Conventional fast imaging platforms, such as spinning disc confocal and light sheet microscopy, are typically limited to capturing a single spectral channel per image and face optical resolution constraints when paired with current high-resolution widefield time-resolved image sensors. While single-point multispectral confocal FLIM platforms are available, they often operate with photon count rate-limited exposure times to generate sufficient signals for accurate decay fitting. Consequently, these platforms may not be suitable for tasks that require high frame rates, long durations, and imaging of samples with low fluorescence intensity unless high-power lasers are employed.

In contrast, spatially parallelized confocal multispectral FLIM imaging could offer the capability to conduct spectrally complex or multilabel lifetime experiments with higher frame rates, thanks to its spatial and spectral multiplexing factors. This imaging approach holds significant potential for multi-time point or multi-depth (z-stack) experiments. By parallelizing the spatial scanning, it reduces the photon count rate requirement, enabling the use of laser powers compatible with live cell imaging and providing enhanced contrast in challenging imaging situations.

Spectral measurements in multipoint confocal systems are crucial for accurately distinguishing between multiple fluorophores within a sample. This process involves using advanced spectral filters or new detection techniques to capture and separate emissions from different fluorophores, enabling detailed spectral deconvolution. To achieve a fast system, a parallel detection configuration is desirable. However, this has not been successful with the spinning disk confocal platform due to its optical geometry fully utilizing the image plane during operation. Instead, a window scanner-based multiplexing optical geometry is ideal for parallel multispectral measurements, as window scanners can both scan and de-scan large fields of view uniformly, rendering emission images stationary. These emission images of the focal array have unused image plane space that can host additional information, such as spectral streaks.

For combining time-resolved fluorescence measurements with simultaneous parallel multispectral imaging, the detector must have the required temporal imaging bandwidth and spatial pixel density. This ensures precise measurement of both the temporal and spectral profiles. While there are currently few detectors that can provide high spatial and temporal resolution, emerging technologies are expected to modernize high-speed imaging. To be commercially attractive, the system must avoid bottlenecks in the

workflow and keep pace with the demands of its intended application. A typical high-content screening (HCS) microscope images 100,000 samples per day, requiring roughly one sample image per second. Subcellular imaging must also be done at high resolution to produce meaningful insights, necessitating confocal resolution imaging or better.

The goal of this project is to design a multipoint confocal system with a window optical scanner that uses a time-resolved fluorescence camera to collect many spectrally resolved fluorescence decays simultaneously with a frame rate that is compatible with high content screening and dynamic imaging. The system is being designed to connect as a module to existing HCS microscope platforms, offering a turnkey solution for drug screening laboratories.

References

- [1] Stokes G 1852 XXX. On the change of refrangibility of light *Philos Trans R Soc Lond* **142** 463–562
- [2] Shimomura O, Johnson F H and Saiga Y 1962 Extraction, Purification and Properties of Aequorin, a Bioluminescent Protein from the Luminous Hydromedusan, *Aequorea J Cell Comp Physiol* **59** 223–39
- [3] Lakowicz J R 2006 *Principles of Fluorescence Spectroscopy* ed J R Lakowicz (Boston, MA: Springer US)
- [4] Specht E A, Braselmann E and Palmer A E 2017 A Critical and Comparative Review of Fluorescent Tools for Live-Cell Imaging *Annu Rev Physiol* **79** 93–117
- [5] Zimmermann T 2005 Spectral imaging and linear unmixing in light microscopy *Adv Biochem Eng Biotechnol* **95** 245–65
- [6] Frank J H, Elder A D, Swartling J, Venkitaraman A R, Jeyasekharan A D and Kaminski C F 2007 A white light confocal microscope for spectrally resolved multidimensional imaging *J Microsc* **227** 203–15
- [7] McRae T D, Oleksyn D, Miller J and Gao Y-R 2019 Robust blind spectral unmixing for fluorescence microscopy using unsupervised learning ed M van Zandvoort *PLoS One* **14** e0225410
- [8] Williams G O S, Williams E, Finlayson N, Erdogan A T, sWang Q, Fernandes S, Akram A R, Dhaliwal K, Henderson R K, Girkin J M and Bradley M 2021 Full spectrum fluorescence lifetime imaging with 0.5 nm spectral and 50 ps temporal resolution *Nat Commun* **12** 6616
- [9] Sarkar P, Koushik S V, Vogel S S, Gryczynski I and Gryczynski Z 2009 Photophysical properties of Cerulean and Venus fluorescent proteins | Browse - Journal of Biomedical Optics *J Biomed Opt* **14** 034047
- [10] Zhang X F, Zhang J and Liu L 2014 Fluorescence properties of twenty fluorescein derivatives: Lifetime, quantum yield, absorption and emission spectra *J Fluoresc* **24** 819–26
- [11] Sanchez C, Lachaize C, Janody F, Bellon B, Roder L, Euzenat J, Rechenmann F and Jacq B 1999 Grasping at molecular interactions and genetic networks in *Drosophila melanogaster* using FlyNets, an Internet database *Nucleic Acids Res* **27** 89–94

- [12] Medintz I and Hildebrandt N 2013 *FRET – Förster Resonance Energy Transfer* (Wiley)
- [13] Piston D W and Kremers G J 2007 Fluorescent protein FRET: the good, the bad and the ugly *Trends Biochem Sci* **32** 407–14
- [14] Hiraoka Y, Shimi T and Haraguchi T 2002 Multispectral Imaging Fluorescence Microscopy for Living Cells. *Cell Struct Funct* **27** 367–74
- [15] Garini Y, Young I T and McNamara G 2006 Spectral imaging: Principles and applications *Cytometry Part A* **69** 735–47
- [16] Hagen N and Kudenov M W 2013 Review of snapshot spectral imaging technologies *Optical Engineering* **52** 090901
- [17] Skala M C, Riching K M, Gendron-Fitzpatrick A, Eickhoff J, Eliceiri K W, White J G and Ramanujam N 2007 In vivo multiphoton microscopy of NADH and FAD redox states, fluorescence lifetimes, and cellular morphology in precancerous epithelia *Proc Natl Acad Sci U S A* **104** 19494–9
- [18] Digman M A, Caiolfa V R, Zamai M and Gratton E 2008 The phasor approach to fluorescence lifetime imaging analysis *Biophys J* **94** L14–6
- [19] Becker W, Bergmann A, Hink M A, König K, Benndorf K and Biskup C 2004 Fluorescence Lifetime Imaging by Time-Correlated Single-Photon Counting *Microsc Res Tech* **63** 58–66
- [20] James B. Pawley 2006 *Handbook Of Biological Confocal Microscopy* ed J B Pawley (Boston, MA: Springer US)
- [21] Jonkman J, Brown C M, Wright G D, Anderson K I and North A J 2020 Tutorial: guidance for quantitative confocal microscopy *Nat Protoc* **15** 1585–611
- [22] Brown G E, Han Y D, Michell A R, Ly O T, Vanoye C G, Spanghero E, George A L, Darbar D and Khetani S R 2024 Engineered cocultures of iPSC-derived atrial cardiomyocytes and atrial fibroblasts for modeling atrial fibrillation *Sci Adv* **10** 1222
- [23] Badimon A, Strasburger H J, Ayata P, Chen X, Nair A, Ikegami A, Hwang P, Chan A T, Graves S M, Uweru J O, Ledderose C, Kutlu M G, Wheeler M A, Kahan A, Ishikawa M, Wang Y-C, Loh Y-H E, Jiang J X, Surmeier D J, Robson S C, Junger W G, Sebra R, Calipari E S, Kenny P J, Eyo U B, Colonna M, Quintana F J, Wake H, Gradinaru V and Schaefer A 2020 Negative feedback control of neuronal activity by microglia *Nature* **586** 417–23
- [24] Paul S M, Mytelka D S, Dunwiddie C T, Persinger C C, Munos B H, Lindborg S R and Schacht A L 2010 How to improve RD productivity: The pharmaceutical industry’s grand challenge *Nat Rev Drug Discov* **9** 203–14
- [25] Mullard A 2024 2023 FDA approvals *Nat Rev Drug Discov* **23** 88–95
- [26] Swinney D C and Anthony J 2011 How were new medicines discovered? *Nat Rev Drug Discov* **10** 507–19

- [27] DiMasi J A, Grabowski H G and Hansen R W 2016 Innovation in the pharmaceutical industry: New estimates of R&D costs *J Health Econ* **47** 20–33
- [28] Loewa A, Feng J J and Hedtrich S 2023 Human disease models in drug development *Nature Reviews Bioengineering* **1** 545–59
- [29] Biju T S, Priya V V and Francis A P 2023 Role of three-dimensional cell culture in therapeutics and diagnostics: an updated review *Drug Deliv Transl Res* **13** 2239–53
- [30] Habanjar O, Diab-Assaf M, Caldefie-Chezet F and Delort L 2021 3D Cell Culture Systems: Tumor Application, Advantages, and Disadvantages *Int J Mol Sci* **22** 12200
- [31] Ellis-Davies G C R 2007 Caged compounds: Photorelease technology for control of cellular chemistry and physiology *Nat Methods* **4** 619–28
- [32] Pasti L, Volterra A, Pozzan T and Carmignoto G 1997 Intracellular Calcium Oscillations in Astrocytes: A Highly Plastic, Bidirectional Form of Communication between Neurons and Astrocytes *In Situ The Journal of Neuroscience* **17** 7817–30
- [33] Chang Y-F, Broyles C N, Brook F A, Davies M J, Turtle C W, Nagai T and Daniels M J 2017 Non-invasive phenotyping and drug testing in single cardiomyocytes or beta-cells by calcium imaging and optogenetics ed J Rajasingh *PLoS One* **12** e0174181
- [34] Kaufmann T, Herbert S, Hackl B, Besold J M, Schramek C, Gotzmann J, Elsayad K and Slade D 2020 Direct measurement of protein-protein interactions by FLIM-FRET at UV laser-induced DNA damage sites in living cells *Nucleic Acids Res* **48** E122–E122
- [35] Zanella F, Lorens J B and Link W 2010 High content screening: Seeing is believing *Trends Biotechnol* **28** 237–45
- [36] Kraus O Z and Frey B J 2016 Computer vision for high content screening *Crit Rev Biochem Mol Biol* **51** 102–9
- [37] Zimmermann T and O’Toole P 2014 *Confocal Microscopy* vol 1075, ed S W Paddock (New York, NY: Springer New York)
- [38] Wang E, Babbey C M and Dunn K W 2005 Performance comparison between the high-speed Yokogawa spinning disc confocal system and single-point scanning confocal systems *J Microsc* **218** 148–59
- [39] Oreopoulos J, Berman R and Browne M 2014 Spinning-disk confocal microscopy *Methods in Cell Biology* vol 123 (Elsevier Inc.) pp 153–75
- [40] Tsikouras A, Berman R, Andrews D W and Fang Q 2015 High-speed multifocal array scanning using refractive window tilting *Biomed Opt Express* **6** 3737
- [41] Hendrix J, Schimpf W, Höller M and Lamb D C 2013 Pulsed interleaved excitation fluctuation imaging *Biophys J* **105** 848–61
- [42] Wiseman P W 2013 Fluctuation imaging spiced up with a piece of PIE *Biophys J* **105** 831

- [43] Bird D K, Eliceiri K W, Fan C-H and White J G 2004 Simultaneous two-photon spectral and lifetime fluorescence microscopy *Appl Opt* **43** 5173
- [44] Cha J W, Tzeranis D, Subramanian J, Yannas I V., Nedivi E and So P T C 2014 Spectral-resolved multifocal multiphoton microscopy with multianode photomultiplier tubes *Opt Express* **22** 21368
- [45] Pian Q, Yao R, Sinsuebphon N and Intes X 2017 Compressive hyperspectral time-resolved wide-field fluorescence lifetime imaging *Nat Photonics* **11** 411–4
- [46] Carver G E, Locknar S A, Morrison W A, Krishnan Ramanujan V and Farkas D L 2014 High-speed multispectral confocal biomedical imaging *J Biomed Opt* **19** 036016
- [47] Michael Stanley C 2008 Filters and mirrors for laser applications *Nat Methods* **5** an12–3
- [48] Scipioni L, Rossetta A, Tedeschi G and Gratton E 2021 Phasor S-FLIM: a new paradigm for fast and robust spectral fluorescence lifetime imaging *Nat Methods* **18** 542–50
- [49] Popleteeva M, Haas K T, Stoppa D, Pancheri L, Gasparini L, Kaminski C F, Cassidy L D, Venkitaraman A R and Esposito A 2015 Fast and simple spectral FLIM for biochemical and medical imaging *Opt Express* **23** 23511
- [50] Esposito A and Venkitaraman A R 2019 Enhancing Biochemical Resolution by Hyperdimensional Imaging Microscopy *Biophys J* **116** 1815–22
- [51] Becker W, Bergmann A and Biskup C 2007 Multispectral fluorescence lifetime imaging by TCSPC *Microscopy Research and Technique* vol 70 (Wiley-Liss Inc.) pp 403–9
- [52] Qu J, Liu L, Guo B, Lin Z, Hu T, Tian J, Wang S, Zhang J and Niu H 2005 Development of a multispectral multiphoton fluorescence lifetime imaging microscopy system using a streak camera *Optics in Health Care and Biomedical Optics: Diagnostics and Treatment II* vol 5630 (SPIE) p 510
- [53] Biskup C U, Kelbauskas L, Zimmer T, Dietrich S, Benndorf K, Becker W, Bergmann A and Klocker N 2005 Spectrally resolved fluorescence lifetime and FRET measurements *Multiphoton Microscopy in the Biomedical Sciences V* vol 5700 (SPIE) p 188
- [54] Oreopoulos J, Berman R and Browne M 2014 Spinning-disk confocal microscopy *Methods in Cell Biology* vol 123 (Elsevier Inc.) pp 153–75
- [55] Gräf R, Rietdorf J and Zimmermann T 2005 Live cell spinning disk microscopy *Adv Biochem Eng Biotechnol* **95** 57–75
- [56] Velten A, White J G, Mackie T R and Eliceiri K W 2013 Hyperspectral Multi-Point Confocal Microscope *CLEO: 2013* vol 180 (Washington, D.C.: OSA) p AW11.2
- [57] Becker W, Bergmann A, Biskup C, Kelbauskas L, Zimmer T, Klocker N and Benndorf K 2003 High resolution TCSPC lifetime imaging ed A Periasamy and P T C So p 175
- [58] Anon *Photomultiplier Tubes: Basics and Applications* (Hamamatsu Photonics K.K.)

- [59] Qian X, Jiang W, Elsharabasy A and Deen M J 2023 Modeling for Single-Photon Avalanche Diodes: State-of-the-Art and Research Challenges *Sensors* **23** 3412
- [60] Katsoulidou V, Bergmann A and Becker W 2007 How fast can TCSPC FLIM be made? *Advanced Photon Counting Techniques II* vol 6771 (SPIE) p 67710B
- [61] van Geest L K and Bosch L A 1989 Gated Image Intensifiers And Applications ed I P Csorba p 19
- [62] Bruschini C, Homulle H, Antolovic I M, Burri S and Charbon E 2019 Single-photon avalanche diode imagers in biophotonics: review and outlook *Light Sci Appl* **8** 87
- [63] Hirmiz N, Tsikouras A, Osterlund E J, Richards M, Andrews D W and Fang Q 2019 Cross-talk reduction in a multiplexed synchroscan streak camera with simultaneous calibration *Opt Express* **27** 22602
- [64] Grant D M, McGinty J, McGhee E J, Bunney T D, Owen D M, Talbot C B, Zhang W, Kumar S, Munro I, Lanigan P M, Kennedy G T, Dunsby C, Magee A I, Courtney P, Katan M, Neil M A A and French P M W 2007 High speed optically sectioned fluorescence lifetime imaging permits study of live cell signaling events *Opt Express* **15** 15656
- [65] Hirmiz N, Tsikouras A, Osterlund E J, Richards M, Andrews D W and Fang Q 2020 Multiplexed confocal microscope with a refraction window scanner and a single-photon avalanche photodiode array detector *Opt Lett* **45** 69
- [66] Becker W, Bergmann A and Biskup C 2007 Multispectral fluorescence lifetime imaging by TCSPC *Microscopy Research and Technique* vol 70 (Wiley-Liss Inc.) pp 403–9
- [67] Biskup C, Hoffmann B, Kelbauskas L, Zimmer T, Klöcker N, Becker W and Benndorf K 2008 Multi-dimensional fluorescence lifetime measurements *Multiphoton Microscopy in the Biomedical Sciences VIII* vol 6860 (SPIE) p 68601I

Chapter 3. 4Hz Multipoint Confocal FLIM Microscope

Paper I – Multiplexed Confocal FLIM for Dynamic Molecular Imaging in Live Cells

MORGAN RICHARDS¹, NIKOLINA MALIC², ELIZABETH J. OSTERLUND³, ANDREA BUENDIA², LAURA POLGA¹, RAY TRUANT³, QIYIN FANG^{1,2,*}

¹McMaster University Department of Engineering Physics, Hamilton, ON, L8S 4L8, Canada

²McMaster University School of Biomedical Engineering, Hamilton, ON, L8S 4L8, Canadas

³McMaster University Department of Biochemistry and Biomedical Sciences, Hamilton, ON, L8S 4L8, Canada

Submitted to

Springer Nature: Discover Imaging

Introduction to Paper I

This chapter describes the development and implementation of a pinhole array based multipoint confocal FLIM microscope as a method of achieving sub one second per frame confocal FLIM measurements. The ability to measure sub-second dynamic lifetime changes is important to many applications, such as cardiovascular medicine, due to the cyclic nature of the sample.

In this chapter, we demonstrate how rapid confocal FLIM imaging can be achieved using a pinhole array based 32x32 point multipoint confocal microscope. This new design has achieved imaging at 4 Hz real-time frame rates owing to the improved optical system design. Calibration of the window scanners achieves consistent operation without loss of spatial synchronization at the limiting mechanical velocity. Standard fluorescent dyes were used to optimize the temporal acquisition parameters and determine the system's temporal resolution and detection limit for measuring fluorescence lifetimes. We used a fixed *Convallaria* sample to demonstrate the optical imaging quality and resolution of the pinhole based confocal images (960x960 pixels) at 4 fps. We imaged HEK293T cells expressing tethered and untethered mCerulean3 and Venus fluorescent proteins and demonstrated sustainable performance.

This work shows the effectiveness of the multipoint confocal FLIM microscope as a solution for imaging dynamic molecular processes in live cells. The targeted audience for this paper includes researchers in any application using confocal FLIM to measure dynamic fluorescence lifetime processes that occur at a time scale slower than 2 Hz.

Morgan Richards and Qiyin Fang were responsible for the conception of the microscope. Morgan Richards was responsible for the construction, and development of the microscope setup and all software. Morgan Richards and Laura Polga performed scanner calibration experiments. All authors contributed to the cell imaging validation experiment design. Nikolina Malic, Elizabeth Osterlund, and Andrea Buendia prepared biological samples. Morgan Richards, N.M., and A.B. performed the biological imaging experiments, and Morgan Richards analyzed the data. The first of the manuscript draft was prepared by Morgan Richards and all authors contributed to the editing.

Contents of Paper I

Abstract:

Quantitative measurements of the dynamics of biomolecular interactions allow biologists to develop a better understanding of biological processes that are critical to new diagnostic tools, drug discovery, and personalized treatments of diseases. Such measurements require multidimensional (spatial, spectral, and temporal) imaging with a high frame rate. Conventional single point confocal microscopy can produce 3D images at video rate but faces difficulties in accurately measuring fluorescence lifetime while maintaining low excitation power to avoid phototoxicity and photobleaching in live cells. Multipoint confocal fluorescence lifetime imaging offers access to microscopic dynamics at the subcellular resolution. We have designed a 32x32 point multiplexing time-resolved confocal microscope to address these problems and demonstrated the power of this system to measure live cell FLIM-FRET. The use of a pinhole array simplifies the optical system design, allowing improved optical efficiency for imaging lower concentrations at faster frame rates with a temporally calibrated single photon avalanche detector (SPAD) array. These efficiency improvements are leveraged by a redesign of the optomechanical system and software processing to achieve a frame rate 12 times faster than previously demonstrated. Its performance is demonstrated with fixed stained samples and FLIM-FRET constructs in live cells at a maximum imaging rate of 4 Hz at a picture resolution of 960x960.

3.1 Introduction

Accurately observing how cellular states evolve in response to molecular interactions is crucial for advancing our understanding of biological systems and the development of new novel medicine [1,2]. Real-time monitoring of these changes, particularly in live cells, requires multi-dimensional imaging techniques that can capture spatial, spectral, and temporal dynamics with high precision. Such capabilities are indispensable for revealing how perturbations at the molecular level influence the broader cellular environment [3].

Optical microscopy is a vital technique for conducting minimally invasive measurements of dynamic cellular processes. Fluorescence microscopy has become increasingly valuable due to its high target specificity, which is also driven by advancements in fluorescent probe design [4–6]. This technique enables spatially resolved measurements of subcellular processes and, when coupled with dynamic, or time-resolved, imaging, provides unique insights into molecular mechanisms of action, potentially leading to new understandings of drug or biological activity. Although widefield intensity imaging with sequential spectral band measurements is common, it encounters limitations in complex environments such as thick and multispecies samples. The thickness of a sample can result in poor image quality and reduced specificity due to the influence of out-of-focus light, while spectral crosstalk complicates the identification of multiple species [7,8].

Time-resolved fluorescence microscopy offers a novel approach by providing high specificity for fluorescence signals [9]. Confocal resolution further enhances this capability, particularly in crowded environments or when imaging thicker samples with dense spatial labeling and inevitable spectral overlap, by rejecting out-of-focus light. This ensures that only species within the diffraction-limited focal volume affect the measurement [10–12]. Techniques such as Förster Resonance Energy Transfer (FRET), which facilitates the indirect observation of molecular interactions, benefit significantly from fluorescence lifetime imaging microscopy (FLIM) as it is more robust than traditional intensity-based measurements [13]. FRET is the non-radiative transfer of energy from an excited donor fluorophore to an acceptor fluorophore, and its process is reflected in a reduction in the donor's lifetime due to additional non-radiative decay pathways. This process requires the donor and acceptor fluorophores to be within approximately 10 nm, providing quantitative measurements of protein binding and conformational change when the FRET fluorophores are attached to proteins of interest [14,15].

Live-cell imaging with confocal FLIM is inherently a slow process, primarily because image acquisition occurs one pixel at a time due to the absence of commercial multipoint confocal FLIM systems. This poses an obstacle to effectively using FLIM in pharmacological research because many biological signaling events and molecular interactions occur within the sub-second timescale. To avoid photobleaching and phototoxicity, the lowest possible excitation powers are used [16,17]. This results in photon count rate-limited pixel dwell times that determine the overall frame rate needed for accurate measurement of fluorescence decay [18]. A proliferation of techniques have been developed to push the boundary of FLIM imaging to higher speeds due to the abundance of promising applications [19].

Promising alternatives to single point confocal are multiplexed confocal imaging, which enables the parallel acquisition of multiple pixels, thereby significantly increasing the photon count rate in comparison to single-point confocal imaging. By allowing parallel spatial scanning, this method not only permits the use of laser powers that are compatible with live-cell imaging but also enhances contrast under challenging imaging conditions, all without compromising the frame rate [20]. Many multipoint techniques however use multiphoton imaging which is limited by the total laser power a sample can sustain before photothermal damage occurs, and typically have limited multiplexing factors due to the quadratic dependence of two-photon fluorescence on excitation laser intensities and limited optical efficiency of beam shaping optics [21,22].

We have previously demonstrated a proof-of-concept multiplexed confocal FLIM system capable of acquiring time-gated FLIM images in 3 seconds, proving its suitability for FLIM-FRET screening applications [23]. In this study, we present an improved optical system designed to enable high-speed imaging in a dynamic process that requires high frame rate measurements such as, the applications of caged compounds and triggered biological pathways, or in cyclic cardiovascular and neurological models both which require sub-second timescale measurements [24–27]. The system demonstrates improved optoelectronic synchronization, capable of generating three time-gated images for a real-time FLIM

capture frequency of 4 Hz at 960x960 pixel resolution, enabling dynamic FLIM measurements in live cells.

3.2 Methods

In the following sections, we demonstrate the optical system design, beginning with the optimization of the scanner to achieve the highest mechanical scanning rate. Next, we address the calibration of scanner synchronization with the detector to eliminate scanning artifacts. We also present a method for calibrating the multiple temporal gates of a single photon avalanche detector (SPAD) array, ensuring accurate lifetime fitting. This includes a detailed calibration procedure using fluorescent solutions to establish the lower photon count limit for precise lifetime measurements. Finally, we demonstrate the system's performance using both fixed, fluorescently stained samples and live samples expressing a transient FRET construct.

3.2.1 Optical System Design

The simplified optical system is shown in Figure 3-1. The system uses a pulsed diode laser (LDH-440M, Picoquant) that produces 440 nm laser pulses with pulse widths of ~ 1 ns at a pulse repetition rate of 50 MHz. The output beam is coupled to a multimode fiber to improve the uniformity of the output excitation beam. The divergent fiber output is collimated using a 300 mm lens (Thorlabs AC508-300-A) into a 1.4 cm beam to provide a large and collimated illumination wavefront. The system uses a 300 μm pitch, 32x32 MLA (18-1453-100-000, SUSS MicroOptics), for 1024-point multiplexing to enable fast acquisition times. The MLA excitation image is transmitted through a pair of achromatic doublets (Thorlabs AC508-200-A) placed to form a telecentric relay, $M=1$, and reflected off a 442 nm long-pass dichroic (Di03-R442-t1-25x36, Semrock), onto a custom designed pinhole array (Walthy Precision Co) to match the MLA excitation image footprint. The pinhole array has a square array of 25 μm pinholes at 300 μm pitch for optimal confocal imaging with a 60x objective. Together with a pair of galvanometer window scanners (GM-1000, Cannon) for raster scanning in X and Y [28], the system generates clean diffraction limited excitation spots that pass through the camera port of a Nikon Ti equipped with a 60x/1.40 NA objective (Plan Apo 60xA/1.40 Oil, Nikon). The fluorescence emission, once de-scanned, passes through the pinhole array and is relayed through an $M=0.5$ (Thorlabs AC508-100-A) telecentric relay, the 442 nm long pass dichroic, and a 488 nm/40 nm band pass emission filter (FF01-483-25, Semrock). Finally, the signal image is collected by a SPAD array detector (SPC3, Micro Photon Devices). Software improvements were made to increase real time imaging and image processing speed.

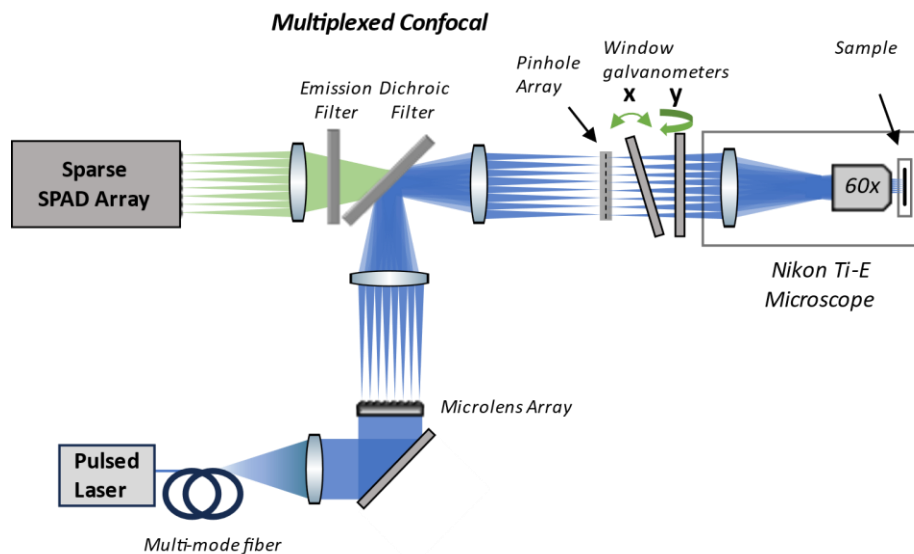


Figure. 3-1. The optical system with a simplified optical path and custom pinhole array.

3.2.2 Window Scanner Mechanical Limitations

A detailed calibration and characterization of the confocal system was performed to ensure consistently high-quality image generation at high frame rates. The scanner calibration involved measuring the scanner waveforms from the galvanometer drivers to determine the total scan duration and confirm the ranges of motion. Figure 3-2 provides measurements of the total scan duration and maximum scanner velocity, as a function of the pixel dwell time. Figure 3-2a shows that the updated scanning system achieves frame durations as low as 0.1 ms for a full frame. At 200 μs pixel dwell time, the expected full frame duration is 0.24 s, resulting in the system's highest mechanical frame rate of 4.1 fps. As indicated by Figure 3-2b, however, the scanner velocity diverges from the expected behavior at a pixel dwell time of less than 200 μs . There is an additional 64 ms per frame that corresponds to the time required to move data from the camera to the computer at the end of the imaging period, reset its memory in preparation for the next acquisition, and reset the position of the galvo scanners to their start position. This reset period is an order of magnitude faster than previously demonstrated [23]. Due to the lost imaging time from the reset period, a decision was made to use a pixel dwell time of 250 μs for live cells corresponding to a total scan duration of 0.28 s, as the gains in imaging rate are marginal when compared to the signal loss after this pixel dwell time. Thus, all dye standards and live cell images in this publication are imaged with a real time frequency of 3.7 Hz.

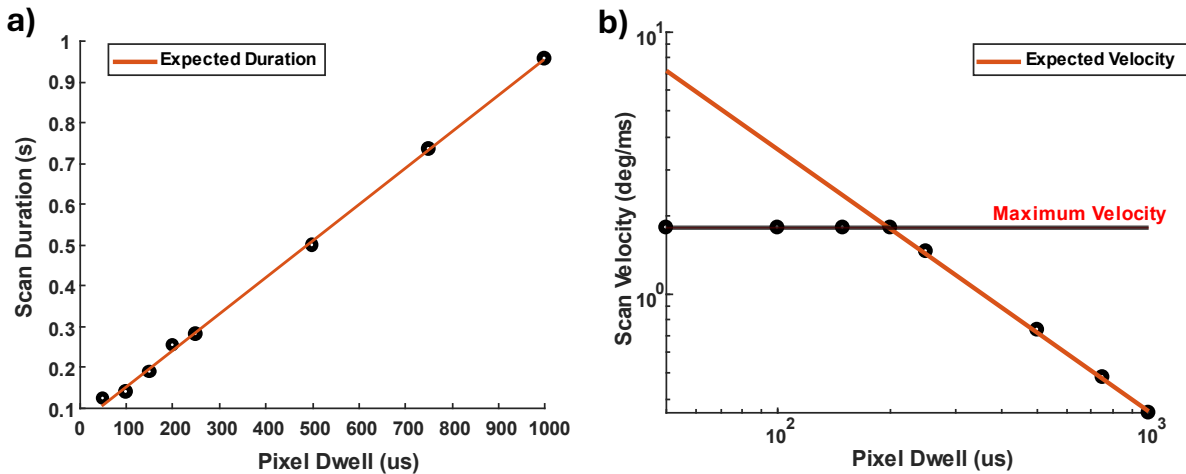


Figure 3-2. a) Frame rate and b) scanner velocity measurements of galvanometer scanners for identification of the highest reliable mechanical scanning rate.

3.2.3 Synchronization and Artefact Calibration

At higher frame rates significant artifacts became apparent in the fluorescence images. A difference in the scanner position during the bidirectional raster scan forms and increases at scan rates faster than 0.7 frames per second. This scanner-derived artifact was calibrated out by adjusting the scan start delay for each pixel dwell. This was accomplished by measuring the difference in the position of two adjoining rows and tracking the difference across a series of increasing scan start delays. Figure 3-S1 demonstrates the pixels that are threshold out of an image for both rows, where red and blue denote row 1 and row 2 respectively. The rows represent a change in the set trigger delay, and the columns represent their relative position. As the delay increases, a change in the relative position of the feature in the image occurs and forms a clear intersection illustrated by a black point where the delay is set correctly. Figure 3-3.a demonstrates the results of the calibration and the change in optimal trigger delay as a function of the pixel dwell time. The results have a linear trend when the pixel dwell time is less than 1.4 ms (1.3 s scan duration). This linear trend is stored within the software to allow adjustments to the scanner trigger delay dynamically as the user changes imaging parameters. Figure 3-3.b demonstrates the effects on image quality before (top) and after (bottom) calibration, respectively, during 4 Hz imaging of a fixed convallaria specimen.

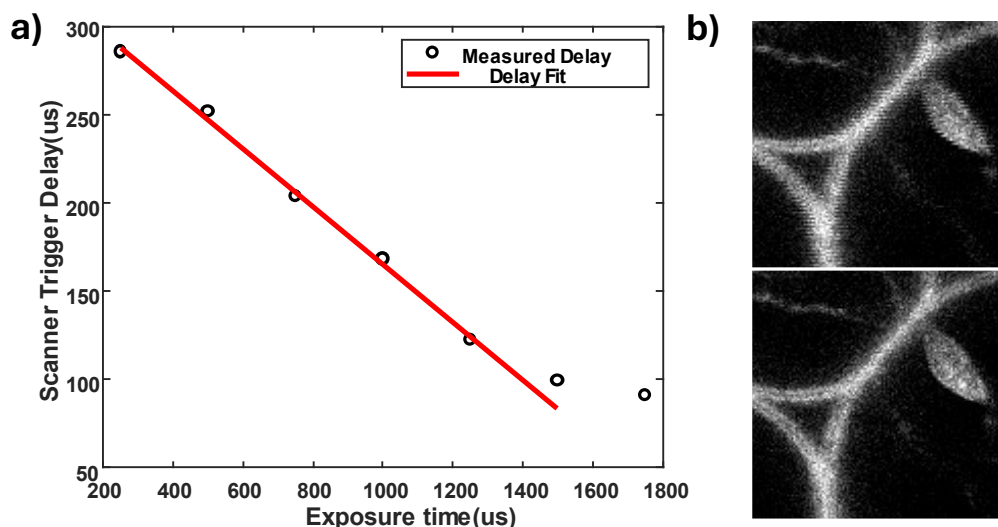


Figure 3-3. Bi-directional raster scan artifacts from incorrect camera trigger delay. a) Delay correction as a function of pixel dwell times. b) Pre (top) and post (bottom) correction results on image quality.

3.2.4 Calibration of the multiple temporal windows for lifetime measurement

To calibrate the windows scanners a 1 μM solution of Coumarin6 was used as a standardized sample. The 3 temporal gate windows were each convolved across the temporal profile of the laser-induced fluorescence decay. From the three temporal waveforms of the fluorescence decay, the positions relative to one another were measured. The positions were logged and used when calculating the fluorescence lifetime at a single fixed gate width of 3 ns. To calculate the lifetime of a sample, the method of rapid lifetime determination (RLD) is used [29]:

$$\tau_{RLD} = -\frac{\Delta t}{\ln\left(\frac{G_2}{G_1}\right)}.$$

RLD is a fast and efficient algorithm that is compatible with real time visualization for lifetime features and is useful for our 3-gate camera. The two gates that are selected for lifetime determination are gate 1 and gate 2. Gate 3 is used to collect the remaining fluorescence decay photons to allow higher photon counts in the intensity images.

The temporal windows of the three temporal gates are shown in Figure 3-4. Gates 1-3 are illustrated in red, blue, and green, and the camera software limits to gate delay selection are shown by the red horizontal arrow. Each gate shows a mono-exponential decay which is ideal for the RLD fitting method. The results of these measurements show the appropriate temporal width between gate 1 and gate 2 is 2.6 ns for the software-selected gate width of 3 ns. This gate separation was used throughout all experiments to maintain lifetime consistency.

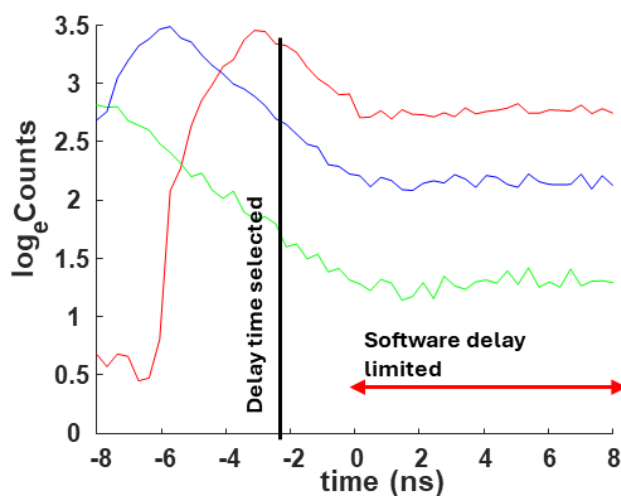


Figure 3-4. Three gate windows response to convolution with 1 μM Coumarin6 fluorescence decay with 1000 μs pixel dwell times. Gates 1, 2, and 3 are plotted in red, blue, and green respectively. The internal software imposes a limit to the delay of the gates and that is shown in the graph as a red arrow.

3.2.5 Dilution series measurements for lifetime precision and accuracy

To measure improvements in lifetime estimation at high frame rates a dilution series was performed. This allows us to measure the changes to the field of view and changes to the accuracy and precision of lifetime estimation. It also allows us to set appropriate threshold values for noise rejection in lifetime images. Care was taken to only reduce the influence of noise signal without adversely affecting the large field of view establishing a limit of measurement for all samples.

3.2.6 Sample Preparation

For a system that contains a spatially varying lifetime, the *Convallaria Rhizome* (Boston Electronics) was used. Stained with both Safranin and Fast-Green, the *convallaria* is imaged with an excitation wavelength of 442 nm at approximately 0.5 mW at the back focal plane of the objective corresponding to 0.5 μW power per focus, with emission wavelength being set to 520/40 nm. A 5x5 pixel spatial filter was applied to gate images to reduce photon count noise effects for lifetime calculation. Intensity images as well, as the alpha mask used to weigh the intensity of the lifetime images, have no spatial filter or modification. The image frame rate was 4Hz, temporal gates were 3 ns wide and placed with no separation such that the second gate begins where the first ends.

A dilution series of Fluorescein was created by dissolving 100 mg of fluorescein (Sigma 46955, MW = 332.31 g/mol) in 60.2 mL of phosphate buffered saline (PBS) and mixed thoroughly to create a 5 mM stock solution. 10 mL of the 5 mM stock solution was transferred into a falcon tube containing 40 mL

PBS to create a 1 mM solution. The 1 mM solution was labeled as the first tube, from which a series of 10x dilutions were performed. 200 μL of 1 mM fluorescein in PBS was pipetted into 1.8 mL of PBS to form 2 mL of 100 μM fluorescein. The 10x dilution was repeated three times to yield 10 μM , 1 μM , and 100 nM. Fluorescein stocks were stored at 4°C and protected from light. To make the Coumarin dilution series, 37mg of Coumarin-6 (Sigma 46955, MW = 350.43 g/mol) was dissolved in 50.1 mL of ethanol and mixed thoroughly to create a 2 mM stock solution. 0.5 mL of the 2 mM stock solution was transferred into a falcon tube containing 0.5 mL of ethanol to create a 1 mM solution. A series of 10x dilutions were then performed by pipetting 0.1 mL of Coumarin-6 into 0.9 mL of Ethanol. 100 μL from each of the Coumarin-6 and Fluorescein solutions were pipetted into separate wells on a 384-well plate. The solutions were stored at 4°C and protected from light. The image frame rate was 3.7Hz, temporal gates were 3 ns wide and placed with no separation such that the second gate begins where the first ends.

HEK293T cells (*H. sapiens*) were obtained from ATCC CRL-3216. Cells were routinely checked for mycoplasma contamination quarterly using the LookOut® Mycoplasma PCR Detection Kit (MP0035-1KT, Millipore Sigma). HEK293T cells were cultured in complete DMEM media, which is Dulbecco's Modified Eagle's Medium (DMEM) base media (11955-092, Gibco), supplemented with 10% FBS (Cat 098450, Wisent), 1mM sodium pyruvate (11360-070, Gibco) and 1x MEM non-essential amino acids (11140-050, Gibco). HEK293T cells were maintained at 37°C, 5% CO₂, 8% O₂ and were split (1 in 20) every 2-3 days. Extra care was taken when changing media on these cells in sample plates as they easily lift off the plate, even without trypsinization. We use phenol red-free media to reduce background autofluorescence signal in imaging. Thus, samples were prepared in Phenol Red Free Complete DMEM, which is Phenol Red Free DMEM F12 (319-080-CL, Wisent) supplemented with 10% FBS, 1 mM sodium pyruvate and 1x MEM non-essential amino acids (11140-050, Gibco). The transfection protocol was adapted from previously published methods [23]. The image frame rate was 3.7 Hz, temporal gates were 3 ns wide and placed with no separation such that the second gate begins where the first ends.

3.3. Results and Discussion

3.3.1 Convallaria

Figure 3-5 demonstrates the confocal FLIM of the Convallaria at 4 Hz. The confocal intensity and confocal FLIM are demonstrated separately in Figure 3-5 a-b) and the composite where the intensity is used as an alpha mask on the confocal FLIM image is demonstrated in Figure 3-5c. The convallaria demonstrates an excellent sample to investigate lifetime differences with as lifetime changes are associated with the differences in environment of the stain. Acridine orange is known to have a change in wavelength due to the type of nucleic acid it binds to as well as the pH of the environment [30], and these different regions can be identified with our confocal FLIM.

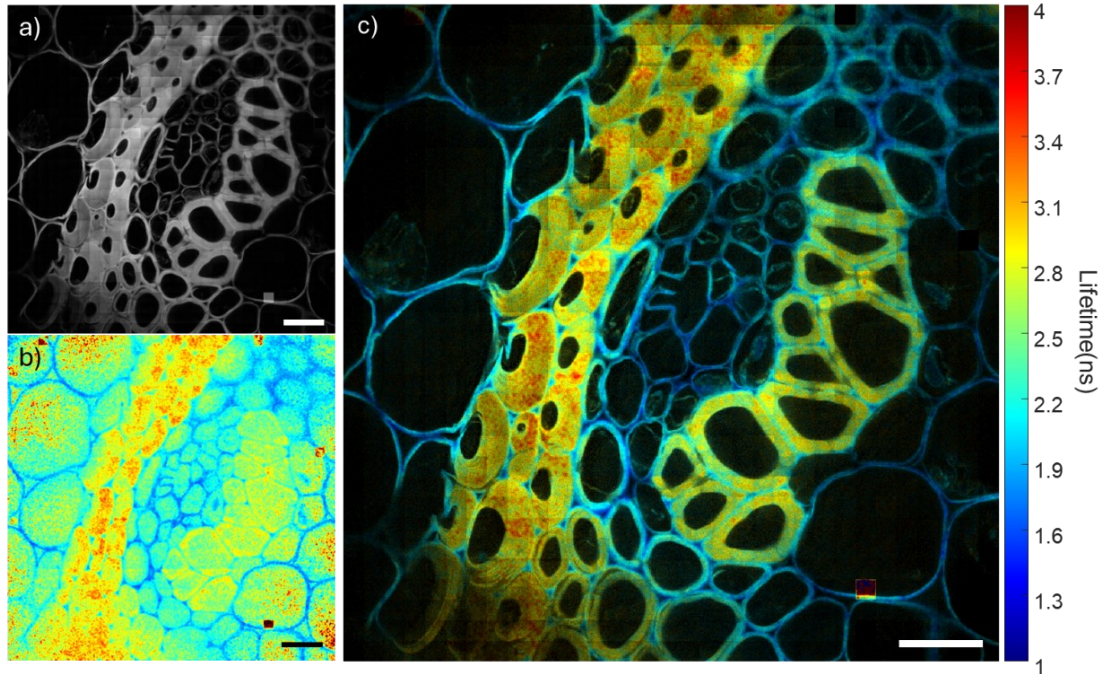


Figure 3-5. Confocal FLIM image of the *Convallaria Majali's* at 4 frames per second. A) confocal intensity, b) confocal FLIM, c) composite image. Scale bars are 20 μm .

3.3.2 Coumarin-6 dilution series for lifetime error, precision, intensity and threshold selection

The measurements from the dilution series and the associated accuracy and error analysis, as shown in Figure 3-6a, highlight the importance of maintaining a threshold of 25 photons to provide accurate lifetime estimation using RLD. This photon count allows for imaging 10 μM concentrations of Coumarin-6 with a pixel dwell time of 250 μs . At this threshold, 99% of the field of view is preserved, with only minimal losses occurring in the corners where excitation power is lowest. Figure 3-6b illustrates the system's sensitivity as a function of the Coumarin-6 concentration and demonstrates the results of the improved optical system by maintaining sufficient signal to measure accurate lifetimes at concentrations as low as 1 μM , with pixel dwell times of 500 μs and 1000 μs , corresponding to 2 Hz and 1 Hz imaging, respectively.

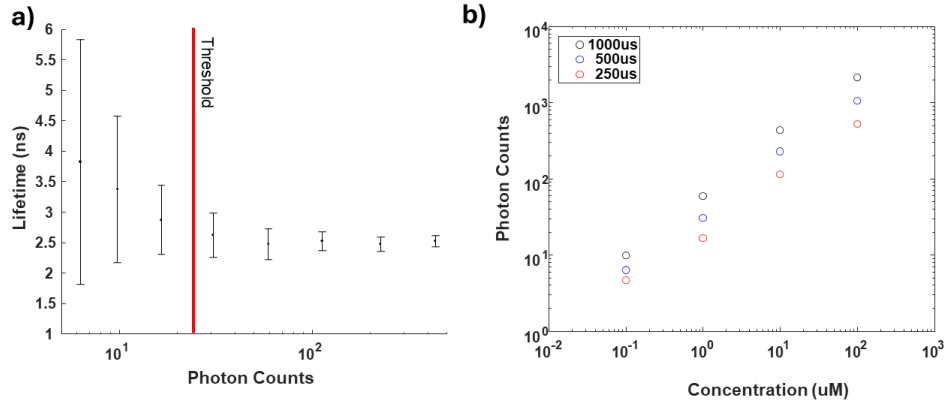


Figure 3-6. Fluorescence measurement limits. a) Fluorescence lifetime measured through changes in mean pixel photon count. b) fluorescence photon count against coumarin 6 dilution series for pixel dwell times of 250 μs , 500 μs , and 1000 μs .

Measurements of the full field of view for Coumarin-6 and Fluorescein are presented in Figure 3-7. Figure 3-7a demonstrates that at 250 μs dwell times, the system accurately measures 10 μM concentration solutions while maintaining an excellent field of view, allowing the full multiplexing factor during confocal FLIM imaging. In Figure 3-7b, the histograms of Coumarin-6 and Fluorescein are presented, which were measured as 2.5 ± 0.2 ns and 4.1 ± 0.7 ns, respectively. Additionally, Figure 6a reveals the presence of hot pixels, which appear as square mosaic regions with higher-than-average lifetimes, or darker-than-average regions due to threshold removal. These regions are due to sensor fabrication artifacts, not illumination issues, however, the corners of the Fluorescein image in Figure 3-7a (bottom) show increased error rates due to non-uniform illumination from the multimode fiber output. Together, these figures demonstrate the system's high accuracy and precision in measuring fluorescence lifetimes, particularly for Coumarin-6 and Fluorescein, which are regarded as gold standard samples due to their exceptionally stable lifetimes.

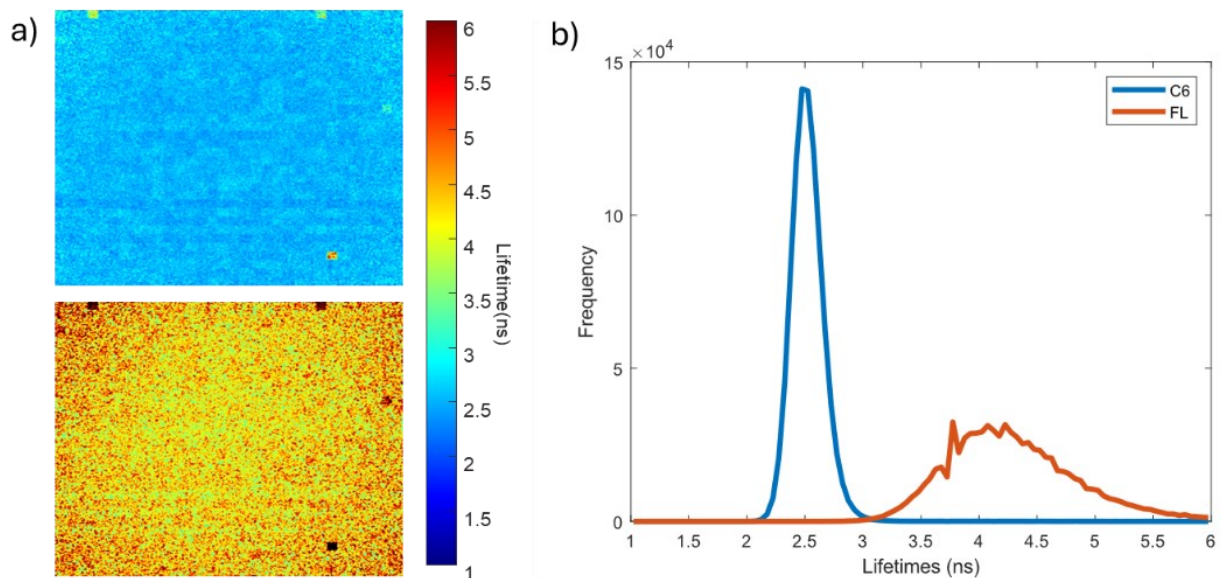


Figure 3-7. a) Full field of view confocal lifetime images for Coumarin-6(top) and Fluorescein (bottom). B) Histograms for Coumarin-6 and Fluorescein.

3.3.3 Live cell accuracy and precision analysis at high frame rates

Live cell FLIM measurements are a better demonstration of accuracy and precision at high frame rates in live cells. In Figure 3-8a, we demonstrate the confocal lifetime images of two cells with different lifetimes. The two subcellular regions of interest in Figure 3-8 are selected from cells transfected with both mCerulean3 and Venus, and show different ratios of expression of the two fluorescent proteins. Figure 3-8b demonstrates the histograms of the two 10x10 ROI labeled A and B from each field of view in Figure 3-8a. Lifetimes for each field of view for regions A and B are 3.7 ± 0.2 ns and 3.4 ± 0.1 ns for a pixel dwell time of $1000 \mu\text{s}$, and are 3.8 ± 0.3 ns, and 3.5 ± 0.2 ns for a pixel dwell time of $250 \mu\text{s}$.

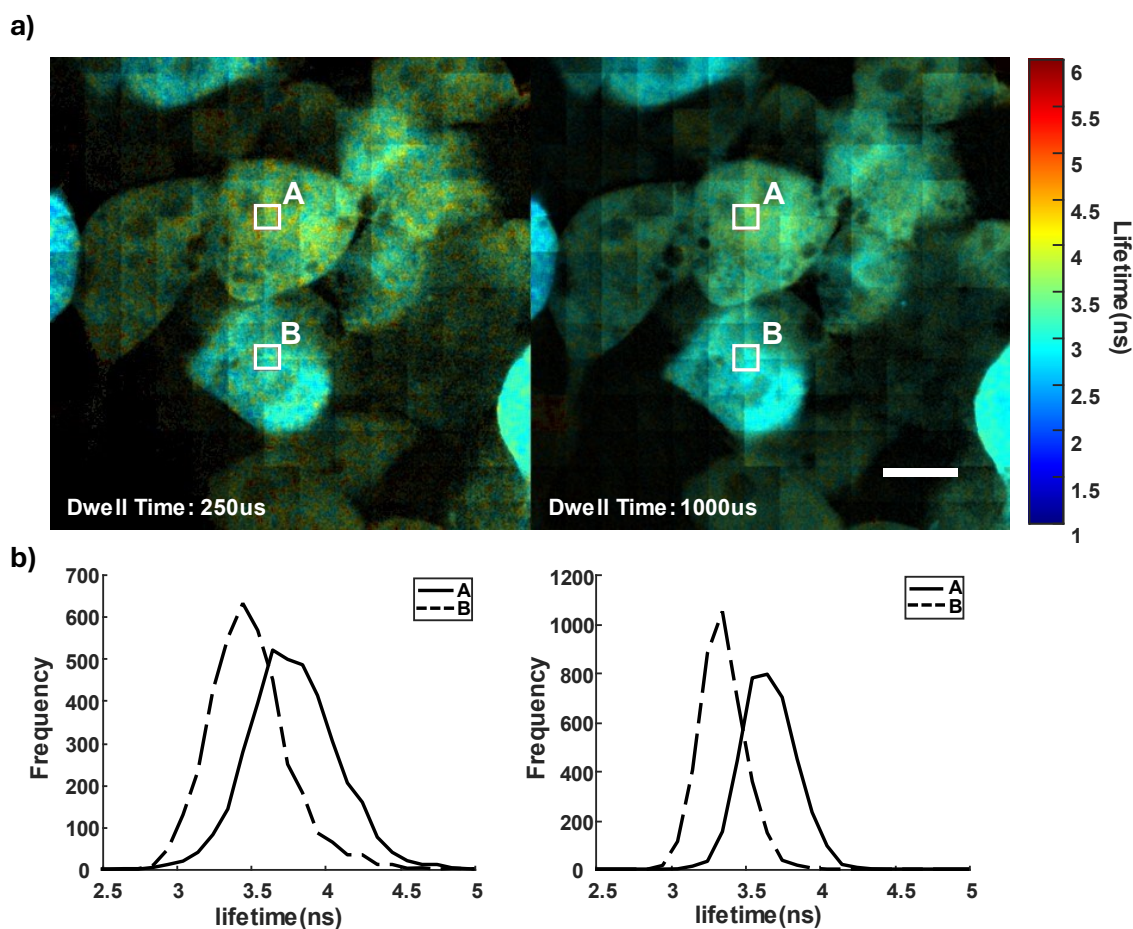


Figure 3-8. a) Live cell measurements of cytosolic expression of the fluorescent proteins mCerulean3 and Venus, co-transfected in HEK293T cells, imaged with pixel dwell times of $250 \mu\text{s}$ and $1000 \mu\text{s}$. Scalebars of $10 \mu\text{m}$. b) Histograms of the fluorescent lifetimes for two regions labeled A and B, for each pixel dwell time.

3.3.4 Live Cell Measurements for lifetime changes over FRET constructs

A live cell FLIM-FRET experiment was conducted to demonstrate the potential of our system to measure FRET in an assay format. Figure 3-9 demonstrates the results of the transfection of HEK293T with mCerulean3, Venus, mCerulean3, and Venus co-transfected, and a construct where mCerulean3 and Venus are linked and undergo FRET. Figure 3-9a demonstrates the full field of view measurements of the transfected cells, and demonstrates the differences between the single protein transfected cells and the co-transfected mCerulean3+Venus cells. Figure 3-9b demonstrates the normalized fluorescence lifetimes of the same fields of view. The histograms alone show a small change in the average lifetime as a result of the cotransfection, however with the confocal FLIM images, we can see the specific cells that are affecting the lifetime distribution. Our assay demonstrates excellent agreement with previously published lifetime values of 3.8 ns \pm 0.5 ns, 3.5 \pm 0.6 ns, 2.9 \pm 0.4 ns, and 2.3 \pm 0.3 ns, for mCerulean3, Mcerulean3+Venus, Venus, and the mCerulean3-Venus FRET construct.

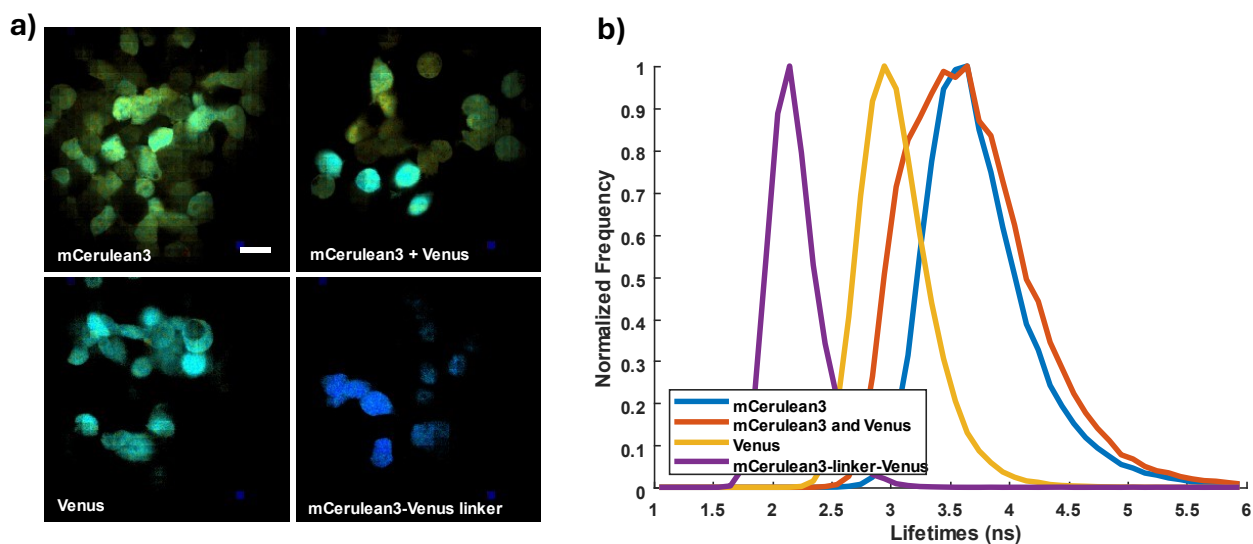


Figure 3-9. Live cell FLIM-FRET experiment demonstrates full field of view images of HEK293T cells, transiently transfected with mCerulean3, Venus, mCerulean3 and Venus, and an mCerulean3-Venus linker protein that undergoes FRET. Scalebars of 20 μ m. b) The normalized histograms of the four fields of view.

3.4 Discussion and Conclusion

We developed a fast multiplexed multipoint confocal FLIM with substantially improved sensitivity and speed for imaging live cell dynamic events at subcellular resolutions. This system obtains 960x960 pixel fluorescence lifetime images at a real time imaging frequency of 4 Hz. This system features a fully redesigned optical path that maintains the full field of view while increasing the image and optical quality of resulting confocal FLIM images. Improvements to software structure permit simultaneous image processing and acquisition.

Pinhole array based confocal imaging is not a new technology, as demonstrated in technologies such as the CSU series spinning disk confocal (Yokogawa) and the VT-Infinity4 confocal system (VisiTech International). These technologies will use methods such as pinhole rotation, or pinhole sweeping, to achieve high-resolution imaging with the sparse array. In each method, a pinhole is responsible for imaging one smooth arc or line through the sample [11]. This technology is unique in its use of the window scanner as a means of uniformly displacing large images to achieve scanning. The window scanner as demonstrated in (Tsikouras, 2015), achieves image displacement by utilizing the refractive properties of the window to impart uniform displacement. This is a perfect match for large field-of-view scanning when compared to mirror-based scanners which suffer from distortion during large image scanning and as a result, are incompatible with pinhole array-based confocal. The window scanners are responsible for performing a bidirectional raster scan between the pinhole spacings, covering a two-dimensional subarea.

Measurements of the fluorescent lifetime standards, Coumarin6 and Fluorescein, demonstrate lifetimes in agreement with literature reported values [31,32]. The lifetime precision of Fluorescein is significantly lower compared to Coumarin6, which can be attributed to the mismatch in excitation wavelengths. Fluorescein, with an excitation peak at 498 nm, is suboptimal for excitation using our 442 nm laser wavelength. Improvements should be made to the signal processing as the fluorescence decay curves in Figure 3-3, demonstrate an exponential decay that permits fitting with higher precision algorithms than RLD permits. Changes to the signal processing might best be explored by replacing the gated SPAD array with a TCSPC detector such as the PF32(PF32, Photon Force).

The frame rate of the system is now limited by the fastest mechanical scanning time of the window scanners rather than the optical design. This is due to the improved optical throughput because of the reduction in the number of surfaces in the emission optical path when using the pinhole array for confocal imaging. Traditional TCSPC systems are limited to a maximum of 0.1 photons per excitation pulse [33]. With a 50 MHz laser this limits the photon count rate to 5 Mcps. Under identical imaging conditions and the same photon count rate limitations, the multipoint confocal samples 32x32 points simultaneously meaning a maximum theoretical count rate of 1024 Mcps. Improvements to the system's maximum imaging frequency will depend on new optomechanical designs such as resonant galvanometric scanners, which may allow the technology to reach the tens of Hz [34].

This system serves as one step forward towards the design of a fast multipoint multidimensional confocal microscope. Future improvements to the system include hyperspectral and multiphoton image modalities. This technology has the potential to impact various fields including drug discovery by providing dynamic multidimensional imaging that can identify spatial and lifetime changes of labels in live cells.

Acknowledgments. This project is supported in part by the Natural Science and Engineering Research Council (NSERC) of Canada through a Discovery Grant, a John R. Evans Leaders Fund grant from the Canadian Foundation of Innovation and Ontario Research Fund-Research Infrastructure, and a MITACS Accelerate grant.

Conflict of Interest. M. Richards, and Q. Fang declares financial interests in McFocal Bioimaging.

Author contributions.

M.R. and Q.F. were responsible for conception of the microscope. M.R. was responsible for construction, and development of the microscope setup and all software, M.R and L.P. performed scanner calibration experiments. All authors contributed to the cell imaging validation experiment design. N.M., E.O., and A.B., and, prepared biological samples. M.R., N.M. and A.B. performed the biological imaging experiments, and M.R analysed the data. All authors contributed to the writing of the manuscript.

Data availability. Data underlying the results presented in this paper are not publicly available at this time but may be obtained from the authors upon reasonable request.

References.

- [1] Henzler-Wildman K and Kern D 2007 Dynamic personalities of proteins *Nature* **450** 964–72
- [2] Rapposelli S, Gaudio E, Bertozzi F and Gul S 2021 Editorial: Protein–Protein Interactions: Drug Discovery for the Future *Front Chem* **9** 1049
- [3] Nam K and Wolf-Watz M 2023 Protein dynamics: The future is bright and complicated! *Structural Dynamics* **10** 014301
- [4] Zhu H, Fan J, Du J and Peng X 2016 Fluorescent Probes for Sensing and Imaging within Specific Cellular Organelles *Acc Chem Res* **49** 2115–26
- [5] Choi N-E, Lee J-Y, Park E-C, Lee J-H and Lee J 2021 Recent Advances in Organelle-Targeted Fluorescent Probes *Molecules* **26** 217
- [6] Zorov D B, Kobrin sky E, Juhaszova M and Sollott S J 2004 Examining intracellular organelle function using fluorescent probes: From animalcules to quantum dots *Circ Res* **95** 239–52
- [7] Balasubramanian H, Hobson C M, Chew T-L and Aaron J S 2023 Imagining the future of optical microscopy: everything, everywhere, all at once *Commun Biol* **6** 1096
- [8] Combs C A and Shroff H 2017 Fluorescence Microscopy: A Concise Guide to Current Imaging Methods *Curr Protoc Neurosci* **79** 1–25
- [9] Berezin M Y and Achilefu S 2010 Fluorescence lifetime measurements and biological imaging *Chem Rev* **110** 2641–84
- [10] Jonkman J, Brown C M, Wright G D, Anderson K I and North A J 2020 Tutorial: guidance for quantitative confocal microscopy *Nat Protoc* **15** 1585–611
- [11] Jonkman J and Brown C M 2015 Any way you slice it—A comparison of confocal microscopy techniques *Journal of Biomolecular Techniques* **26** 54–65
- [12] Wang E, Babbey C M and Dunn K W 2005 Performance comparison between the high-speed Yokogawa spinning disc confocal system and single-point scanning confocal systems *J Microsc* **218** 148–59

- [13] Suhling K, French P M W and Phillips D 2005 Time-resolved fluorescence microscopy *Photochemical and Photobiological Sciences* **4** 13–22
- [14] Piston D W and Kremers G J 2007 Fluorescent protein FRET: the good, the bad and the ugly *Trends Biochem Sci* **32** 407–14
- [15] Medintz I and Hildebrandt N 2013 *FRET – Förster Resonance Energy Transfer* (Wiley)
- [16] Anon 2018 Phototoxicity revisited *Nat Methods* **15** 751
- [17] Laissue P P, Alghamdi R A, Tomancak P, Reynaud E G and Shroff H 2017 Assessing phototoxicity in live fluorescence imaging *Nat Methods* **14** 657–61
- [18] Katsoulidou V, Bergmann A and Becker W 2007 How fast can TCSPC FLIM be made? *Advanced Photon Counting Techniques II* vol 6771 (SPIE) p 67710B
- [19] Datta R, Heaster T M, Sharick J T, Gillette A A and Skala M C 2020 Fluorescence lifetime imaging microscopy: fundamentals and advances in instrumentation, analysis, and applications *J Biomed Opt* **25** 1
- [20] Liu X, Lin D, Becker W, Niu J, Yu B, Liu L and Qu J 2019 Fast fluorescence lifetime imaging techniques: A review on challenge and development *J Innov Opt Health Sci* **12** 1930003
- [21] Coelho S, Poland S, Krstajic N, Li D, Monypenny J, Walker R, Tyndall D, Ng T, Henderson R and Ameer-Beg S 2013 Multifocal multiphoton microscopy with adaptive optical correction *Multiphoton Microscopy in the Biomedical Sciences XIII* **8588** 858817
- [22] James B. Pawley 2006 *Handbook Of Biological Confocal Microscopy* ed J B Pawley (Boston, MA: Springer US)
- [23] Hirmiz N, Tsikouras A, Osterlund E J, Richards M, Andrews D W and Fang Q 2021 Highly Multiplexed Confocal Fluorescence Lifetime Microscope Designed for Screening Applications *IEEE Journal of Selected Topics in Quantum Electronics* **27** 1–9
- [24] Ellis-Davies G C R 2007 Caged compounds: Photorelease technology for control of cellular chemistry and physiology *Nat Methods* **4** 619–28
- [25] Pasti L, Volterra A, Pozzan T and Carmignoto G 1997 Intracellular Calcium Oscillations in Astrocytes: A Highly Plastic, Bidirectional Form of Communication between Neurons and Astrocytes *In Situ The Journal of Neuroscience* **17** 7817–30
- [26] Chang Y-F, Broyles C N, Brook F A, Davies M J, Turtle C W, Nagai T and Daniels M J 2017 Non-invasive phenotyping and drug testing in single cardiomyocytes or beta-cells by calcium imaging and optogenetics ed J Rajasingh *PLoS One* **12** e0174181
- [27] Kaufmann T, Herbert S, Hackl B, Besold J M, Schramek C, Gotzmann J, Elsayad K and Slade D 2020 Direct measurement of protein-protein interactions by FLIM-FRET at UV laser-induced DNA damage sites in living cells *Nucleic Acids Res* **48** E122–E122

- [28] Tsikouras A, Berman R, Andrews D W and Fang Q 2015 High-speed multifocal array scanning using refractive window tilting *Biomed Opt Express* **6** 3737
- [29] Woods R J, Scypinski Stephen and Love L J Cline 1984 Transient digitizer for the determination of microsecond luminescence lifetimes *Anal Chem* **56** 1395–400
- [30] Yektaeian N, Mehrabani D, Sepaskhah M, Zare S, Jamhiri I and Hatam G 2019 Lipophilic tracer Dil and fluorescence labeling of acridine orange used for Leishmania major tracing in the fibroblast cells *Heliyon* **5** e03073
- [31] Sun Y, Day R N and Periasamy A 2011 Investigating protein-protein interactions in living cells using fluorescence lifetime imaging microscopy *Nat Protoc* **6** 1324–40
- [32] Magde D, Rojas G E and Seybold P G 1999 Solvent dependence of the fluorescence lifetimes of xanthene dyes *Photochem Photobiol* **70** 737–44
- [33] Becker W 2017 *The bh TCSPC Handbook, Pile-Up* (Becker & Hickler)
- [34] Wu Y, Wu X, Lu R, Zhang J, Toro L and Stefani E 2015 Resonant Scanning with Large Field of View Reduces Photobleaching and Enhances Fluorescence Yield in STED Microscopy *Sci Rep* **5** 14766

Chapter 4. Multispectral Multipoint Confocal FLIM Microscope

Paper II – Multispectral multiplexed confocal FLIM for live cell imaging

**MORGAN RICHARDS¹, ELIZABETH J. OSTERLUND², ANDREA BUENDIA³, NIKOLINA MALIC³, RAY
TRUANT², QIYIN FANG^{1,3,*}**

¹McMaster University Department of Engineering Physics, Hamilton, ON, L8S 4L8, Canada

*²McMaster University Department of Biochemistry and Biomedical Sciences, Hamilton, ON, L8S 4L8,
Canada*

³McMaster University School of Biomedical Engineering, Hamilton, ON, L8S 4L8, Canada

Submitted to

Journal of Physics : Optics

Introduction to paper II

This chapter describes the development and implementation of a multispectral multipoint confocal FLIM microscope as a means of achieving simultaneous time-resolved multi-spectral images. The ability to measure spectral lifetime changes is important to many fields such as FLIM-FRET where identifying positive FRET is crucial to the study of protein-protein interactions.

In this chapter, we demonstrated how multispectral FLIM imaging can be achieved using a pinhole array based 10x10 point confocal microscope. This new design has achieved imaging 12 simultaneous spectral bands onto a gated optical intensifier. We used a fixed *Convallaria* sample to demonstrate the spectral and lifetime contrast that both imaging dimensions can separate. We measured the spectral independence of fluorescence lifetime in the lifetime standards Coumarin-6 and Fluorescein. We imaged HEK293T cells expressing tethered and untethered mCerulean3 and Venus fluorescent proteins. Through the time-resolved spectra, we demonstrated the ability to differentiate co-transfection from positive FRET cells.

This work demonstrates a time-resolved multi-spectral multipoint confocal microscopes as a solution for multispectral time resolved confocal imaging. The targeted audience for this paper includes researchers in any application using confocal FLIM to measure FRET or using lifetimes as a contrast dimension to isolate unique species. This manuscript was prepared by me and revised by the coauthors.

Contents of Paper II

Abstract: Spectrally resolved fluorescence lifetime imaging with high spatial precision offers comprehensive information on species localization and behavior. It is challenging to resolve weak fluorescence signals in multiple dimensions (spatial, spectral, and temporal) at high frame rates, especially in dynamic live cell processes, as photobleaching and phototoxicity limit acceptable photon count rates. We developed a multiplexed confocal FLIM technique, which uses a prism-based imaging spectrometer to separate a 10x10 array of confocal foci into their spectral components. This allows the sampling of the spectra by a time-resolved image sensor to produce a multispectral time-resolved data set used for generating multispectral lifetime images. This system captures 300x300 pixel fluorescence lifetime images containing 12 unique spectral bands covering a 450-700 nm spectral range in 1.8 seconds of exposure. Its performance was demonstrated in fixed stained samples and in multispectral imaging of FLIM-FRET in live cells.

4.1 Introduction

Fluorescence microscopy is a powerful tool widely used in biological research and drug discovery, enabling researchers to visualize and quantify biological processes in real-time. Conventional fluorescence microscopy measures the intensity of emitted fluorescence to infer the presence and quantity of specific molecules [1]. However, such intensity-based imaging typically employs bandpass filters for spectral selection and sequential measurements to avoid issues of spectral overlap and poor signal specificity, which can prevent accurate localization and analysis. Techniques have been developed to provide alternative imaging modalities providing new contrasts in temporal [2,3] and spectral domains [4,5]. As each new contrast mechanism is added, however, the weak fluorescence signal is further divided and reduced. Subsequent increases in exposure duration and/or excitation intensity present new challenges in measuring dynamic processes in live samples, particularly concerning photobleaching and phototoxicity [6,7].

Multispectral imaging enables the execution of multilabel experiments by leveraging spectral unmixing algorithms to separate multiple cellular components [8,9]. Time resolved fluorescence is a powerful tool that provides insights where traditional contrast techniques fail, as it can separate two species that have identical emission spectra, or where the process is below the optical resolution limits, such as protein interaction, or conformational changes [10,11]. The fluorescence lifetime is also insensitive to changes in brightness or concentration, situations where intensity measurements have difficulty [12]. Both time-resolved fluorescence and multispectral imaging are improved when integrated with a high-resolution imaging modality such as confocal microscopy. Confocal imaging allows 3-dimensional measurements in the spatial domain, and it improves localization and specificity of emitters. Confocal microscopy can lead to powerful morphological insights, such as in image-based high-content screening, which is widely used for drug discovery and the study of novel bimolecular processes [13], and is found in a wide range of disease research studies [14,15]. Despite the individual merits of spectral and lifetime imaging, these modalities are not found together in current high resolution imaging platforms in a format suitable for fast live cell imaging. Integrating FLIM and multispectral imaging into high resolution imaging platforms capable of measuring dynamic events in live cells could provide a more comprehensive understanding of cellular processes, offering a powerful tool for many disciplines of biological research.

The development of a fast multispectral confocal FLIM microscope presents challenges in live cell imaging. Conventional fast imaging platforms, such as spinning disc confocal and light sheet microscopy, use bandpass filters for spectral selection and hence confined to a single spectral channel per image and encounter limitations in optical resolution when coupled to current high-resolution wide-field time-resolved image sensors [16–19]. Though single-point multispectral confocal FLIM platforms exist [20–27], they often operate with photon count rate-limited exposure time to generate sufficient signal to accurately fit decays [28,29]. As a result, the realized acquisition times may not be suitable for tasks requiring high frame rates, long durations, and imaging on samples with low fluorescence intensity unless high-power lasers are used. Spatially parallelized confocal multispectral FLIM imaging offers the capability to conduct spectrally complex or multilabel lifetime experiments while providing higher frame rates due to its spatial and spectral multiplexing factor. This form of imaging holds significant potential for multi-time point or multi-depth (z-stack) experiments. It would allow the use of laser powers compatible with live cell imaging due to the ability to parallelize the spatial scanning thereby reducing the photon count rate requirement and provide contrast in difficult imaging situations.

Through the generation of multiple foci array and a time-gated Single-Photon Avalanche Diode (SPAD) array, we developed a technique for multiplexed temporal confocal imaging [30,31]. Given there is ample space between each foci point, it is possible to achieve spectral detection beyond using discrete bandpass filters. Here, we report on the development of the multi-spectral multipoint confocal fluorescence lifetime imaging (MS-FLIM) microscope. This work details the optical system and automated calibration procedures. Performance validation is demonstrated through examination of stained sections of fixed plant specimens, dye standards, and live mammalian cells transiently expressing fluorescent proteins showcasing FRET.

4.2 Methods

4.2.1 System Design

The optical system schematic is shown in Figure 4-1a. The system uses a frequency-doubled mode-locked tunable Ti: Sapphire (Chameleon Ultra, Coherent) capable of generating 345 nm to 510 nm laser pulses with pulse widths of 140 fs at an 89 MHz repetition rate. Laser modulation was achieved by using an electro-optic modulator (EOM) (Linios LM0202, Qioptiq) between the Ti:Sapphire laser and the frequency doubler (SHG Module, Coherent). Unwanted illumination was captured by a beam trap (BT610, Thorlabs). The output beam is expanded using a 6X beam expander (BE06R, Thorlabs) to provide a 7.2 mm ($1/e^2$) collimated illumination wavefront. The system uses a 500 μm pitch, 10x10 region of a 20x20 microlens array (MLA) (18-1453-100-000, SUSS MicroOptics) for 100-point multiplexing to enable fast acquisition times while maintaining low crosstalk between spectra. The MLA excitation image is reflected off a 442 nm long-pass dichroic (Di03-R442-t1-25x36, Semrock) and through a pair of achromatic doublets (AC508-150-A, Thorlabs) placed to form a telecentric relay, $M=1$, onto a custom-made array of 25 μm pinholes (Walthy Precision Co) to match the MLA excitation image footprint. The 25 μm pinhole in airy units varies from approximately 1.4 at 450 nanometers to 0.9 at 700 nanometers emission wavelength. The pinhole diameter was determined based on an attempt to balance the system's resulting resolution with preserving sufficient throughput for poorly excited and Stokes-shifted red fluorescence emission. Together with a pair of galvanometer window scanners (6230HM40B, Cambridge Technology) for raster scanning the 10x10 focal array in the X and Y direction, which was depicted in detail previously [31]. The system generates clean excitation spots that pass through the camera port of an inverted fluorescence microscope (DMI 6000B, Leica) equipped with a 40x/1.25 NA objective (HCX PL APO 40X / 1.25 - 0.75 Oil CS, Leica), and a temperature-controlled imaging incubation system (DeltaT, Bioptechs). The fluorescence emission, once de-scanned passes through the pinhole array, is relayed through the 442 nm long pass dichroic and a 458 nm long pass emission filter (BLP01-458R-25, Semrock) to generate a stationary confocal fluorescence array for the imaging spectrometer.

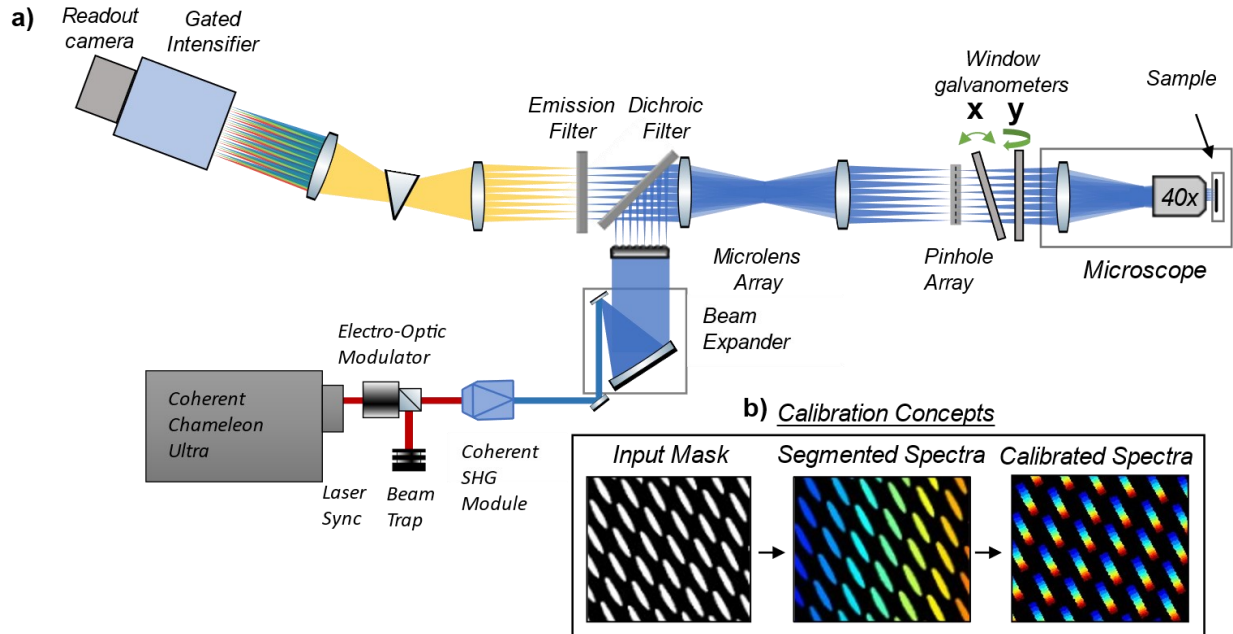


Fig. 4-1. Schematic of Multipoint Multispectral Confocal FLIM. a) Optical path of the confocal scanning system attached to an inverted fluorescence microscope. Pulsed laser emission is frequency doubled (blue) and expanded to generate multiplexed excitation with a micro lens array. The excitation is raster scanned using windows scanners. The returned fluorescence emission (Yellow) is de-scanned before being spectrally separated with an imaging spectrometer (Red, Green, Blue overlap). The resulting spectrally encoded image is amplified using a gated optical intensifier for time resolved spectral imaging. b) The spectral calibration includes the isolation of the calibration signal from the background by threshold masking (left), segmenting of spectra using watershed segmentation (middle), and calibration by reference wavelength bands to generate dispersion curves (right).

The imaging spectrometer consists of a telecentric relay, $M=2$, with a wedge prism (PS814-A, Thorlabs) placed in the center. The resulting image of 100 spectral streaks are imaged onto the gated Optical intensifier (Picostar HR, LaVision) which has a temporal gate as fast as 300 ps. An angular rotation of the spectral streaks was achieved by including a 60° rotation into the wedge prism relative to the pinhole array. The gating delay is controlled by a delay generator (Picosecond Delayer, MPD) to synchronize the gating input trigger to the laser pulsing. All sampled signal is captured by an sCMOS camera (Edge 5.5, PCO) and transferred to a controlling computer through a custom user interface. The computer synchronizes raster stepping with image acquisition and allows dynamic modification of imaging parameters such as exposure, gate delay, gate width, laser wavelength, and laser pump power. The sensor exposure duration used in these measurements is 1 ms. The sample was only exposed for 1 ms per pixel as the EOM is modulated directly by the camera's exposure signaling. The frame rate of the readout camera, however, is limited to 16 fps resulting in a 61 ms period of inactivity between exposure of the sample and the galvo scanner position step.

4.2.2 Calibration

The image of the optical streaks on the gated optical intensifier are not provided as unique discrete elements and must be extracted from the image before they can be analyzed. As a result, spatial segmentation, as well as the determination of the spectral coordinates, are required for each streak in the event of optical drift. A simplified flow chart of the calibration stage is given in Figure 4-1b

and details the process of thresholding, segmentation, and calibration. The positional calibration of each spectral streak is performed by a custom algorithm in MATLAB (R2023a) with a white light calibration image. The full image contains 100 spectral streaks that are segmented by the watershed technique [32] and sorted by position after the rotation of the pinhole array footprint is corrected. A rotation analysis is conducted using the Sobel filter [33] to identify the streak's angular orientations with respect to the pinhole array footprint, which is then processed to provide the spectral streak rotational vector. Two images at the wavelengths of 460 nm (D460/50, Chroma) and 605 nm (D605/55 chroma) are captured by placing each filter in the emission optical path sequentially and illuminating the pinhole array with the microscope's tungsten-halogen source. The spectral differences are then used to calibrate each spectrum by fitting to the expected prismatic dispersion for the material and prism geometry provided by the OEM datasheet. Thus, the collection of position coordinates, rotational orientation, and spectral coordinate vectors are determined. Pixels that qualify are sorted into spectral blocks and their coordinates saved to a calibration file. Calibration is fully automated and can be done before any imaging session quickly to ensure any drift is accounted for.

The window raster scanning pattern is a 30x30 position scan, allowing all 10x10 focal spots to image a small subregion of the field of view. Raw data output of a 30x30 raster scan consists of a series of 900 images with 2560x2160 pixels. Each image is first processed by summing pixels that correspond to specific spectra, and pinhole coordinates as provided by calibration. Each image provides a 2D array of 100 x 12, position, and spectral encoded pixels. The 900-step series of the 100 (position) by 12 (spectral) array is then sorted into the final format of a 300x300x12 (X, Y, λ) image array. These steps are repeated for each temporal gate acquired. The final set of (X, Y, λ, T) data is then converted to (X, Y, λ, τ) by rapid lifetime determination (RLD) [34], which uses two time gates to calculate the fluorescence decay lifetime:

$$\tau_{RLD} = -\frac{\Delta t}{\ln(G_2/G_1)}$$

Where Δt is the temporal separation of the beginning of the two gates with no spacing, G_1 and G_2 are the gated intensity images at the first and second time-gates, respectively. For all measurements, the first time-gate was placed 0.2 ns away from the laser IRF, which was located by scanning the gate across the time domain while measuring the convoluted fluorescence decay profile. The final images are provided as an intensity weighted FLIM Image where a pseudo color scale is used to represent the lifetime in nanoseconds, and the alpha mask represents the intensity. While two time-gates were used in the work reported here, more gates can be used for complex decays [35].

4.2.3 Sample Preparation

For an example system that contains both a broad spectrum and spectrally varying lifetime, the *Convallaria Rhizome* (Boston Electronics) was used. Two samples were imaged, one stained with Acridin-Orange, and another stained with both Safranin and Fast-Green. The excitation wavelength was 442 nm at approximately 0.25 mW at the back focal plane of the objective, corresponding to 2.5 μ W power per focus, with emission range being set to 450 nm – 700 nm. A 5x5 pixel spatial filter was applied to gate images to reduce photon count noise effects for lifetime calculation. Intensity images, as well as the alpha mask used to weigh the intensity of the lifetime images, have no spatial filter or modification. The pixel dwell time was set to 1 ms, which is also the lowest programmable exposure of the sCMOS. Temporal gates were 3 ns wide and placed with

no separation such that the second gate begins where the first ends, and the MCP voltage was 850V.

Dye Standards were used to verify the precision and accuracy of fluorescence lifetime measurement results. The fluorescence lifetime of Coumarin6 (in Ethanol) and Fluorescein (in PBS) are 2.5 ns and 4.1 ns, respectively, according to Sun et al. [36] and Zhang et al. [37]. To create a stock solution of Coumarin-6 (Sigma Aldrich, 98%, MW: 350.43g/mol), 3.5g of Coumarin-6 was weighed on a precision scale (Pioneer Analytical Ohaus PA323) and added to 10 mL of 90% ethanol, resulting in a 10 mL solution of 1M Coumarin-6. A dilution series was then performed. Specifically, 1mL of the 1M stock solution was taken and transferred into a new test tube. After, 9 mL of ethanol was added to this 1 mL aliquot resulting in a 10x dilution. The 1 in 10 dilution was repeated five times until a 10 μ M concentration of Coumarin-6 was obtained. A dilution series of Fluorescein was created by dissolving 100 mg of Fluorescein (Sigma 46955, MW = 332.31 g/mol) in 60.2 mL of phosphate buffered saline (PBS) and mixed thoroughly to create a 5 mM stock solution with a pH of 7.0. 10 mL of the 5 mM stock solution was transferred into a falcon tube containing 40 mL PBS to create a 1 mM solution, which is used as the base for samples at different concentrations (e.g., 100 μ M, 10 μ M) through a series of 10x dilutions. Once 10 μ M Coumarin-6 and 10 μ M Fluorescein were prepared, 100 μ L of each solution were pipetted into separate wells on a 384-well plate. The 384-well plate is then placed on the stage of the microscope to begin imaging. Imaging settings were consistent with the Convallaria, the gate width was set at 3 ns, the excitation wavelength was 442 nm, and the excitation power was measured to be 0.6 mW at the back focal plane of the objective corresponding to approximately 6 μ W per focus.

Uniformly distributed fluorescent proteins in live cells are great model systems and demonstrate live cell imaging with simultaneous measurement of photophysical interactions such as FRET. All DNA constructs used in this paper are publicly available on Addgene and have been used previously to as standards [18]. DNA constructs include: mVenus-pEGFP-C1 (Addgene plasmid no. 27794), mCerulean3-pEGFP-C1 (Addgene plasmid no. 54730), mCerulean3-5aa-Venus-pEGFP-C1 (Addgene plasmid no. 26394). All DNA constructs were prepared using the Monarch Plasmid Miniprep kit (NEB, T1010L) and stored at -20°C in double deionized nuclease-free water (Invitrogen AM9937).

4.2.4 Cell Maintenance

HEK293T cells (*H. sapiens*) were obtained from ATCC CRL-3216. Cells were routinely checked for mycoplasma contamination quarterly using the LookOut® Mycoplasma PCR Detection Kit (MP0035-1KT, Millipore Sigma). HEK293T cells were cultured in complete DMEM media, which is Dulbecco's Modified Eagle's Medium (DMEM) base media (11955-092, Gibco), supplemented with 10% FBS (Cat 098450, Wisent), 1 mM sodium pyruvate (11360-070, Gibco) and 1x MEM non-essential amino acids (11140-050, Gibco). HEK293T cells were maintained at 37°C, 5% CO₂, 8% O₂, and were split (1 in 20) every 2-3 days. Extra care was taken when changing media on these cells in sample plates as they easily lift off the plate, even without trypsinization. We use phenol red free media to reduce background autofluorescence signal in imaging. Thus, samples were prepared in Phenol Red Free Complete DMEM, which is Phenol Red Free DMEM F12 (319-080-CL, Wisent) supplemented with 10% FBS, 1mM sodium pyruvate and 1x MEM non-essential amino acids (11140-050, Gibco).

On day 1, a 10 cm dish of 70-90% confluent HEK293T cells was washed with 2 mL Phosphate buffered saline (PBS), then incubated in 1 mL 4x diluted (in PBS) trypsin (25200-056, Gibco) for 1 minute at 37°C. 50 μ L of resuspended cells were passed to a new 10cm dish for

continued maintenance, and 250 μL was transferred into 5 mL of complete phenol red free DMEM media and mixed by inverting the tube 5-10x to be used for cell counting. Cells were counted using a Hemocytometer (3520, Hausser Scientific). Cells were remixed by inverting after counting and diluted to 50 cells/ μL . Diluted cells were immediately seeded onto four Delta T® Heated Culture Dishes with 0.17 mm Coverslip (Cat. 10199-956, VWR), in a 1 mL volume for a total of 50 000 cells/dish. These chambers allow direct heat transfer to cells when used on a compatible stage. The four cell samples were returned to the incubator overnight to allow cells to adhere to the plate.

On day 2, within 12-18 hours of seedings, cells were transfected using the TransIT-X2 dynamic delivery system (MIR 6004, MirusBio) as described by the manufacturer and following the protocol for transfection of a 12 well plate in 1 mL total volume. In brief, DNA constructs (listed earlier for expression of 1. mCerulean3-pEGFP-C1, 2. Venus -pEGFP-C1, and 3. mCerulean3-5aa-Venus-pEGFP-C1) were each diluted to 100 ng/ μL in DNase/RNase-free water for ease of pipetting. Mirus transfection reagent and diluted DNA constructs were warmed to room temperature and vortexed before use. Unsupplemented serum-free DMEM was warmed to 37°C. We have 4 plates of cells, and prepare 4 transfection reactions: A) mCerulean3, B) Venus, C) mCerulean3-5aa-Venus and D) mCerulean3 + Venus. For each single transfection (A-C), 100 μL of serum-free DMEM, 10 μL of 100ng/ μL the corresponding DNA construct, and 3 μL of Mirus transfection reagent were added to a 1.5mL Eppendorf tube. For cotransfection sample D (mCerulean3 + Venus) 100 μL of serum-free DMEM, 5 μL of 100ng/ μL mCerulean3 DNA, 5 μL of 100 ng/ μL Venus DNA, and 3 μL of Mirus transfection reagent were added to a 1.5 mL Eppendorf tube. Each transfection reaction was vortexed briefly, burst-centrifuged, and incubated at room temperature for 15-20 minutes. The ~ 113 μL transfection reaction was then gently added drop-wise on top of the 1 mL of cells, and upon doing so each plate was labelled “A, B, C or D” for transfection sample identification. Cells were returned to incubate at 37°C, for minimum 3-5 hours, then media was gently aspirated and exchanged with pre-warmed 1mL Phenol Red Free Complete DMEM. Cells were incubated overnight.

On day 3, 10 mM HEPES was added to the media for extra buffering capacity as our stage is not equipped with CO₂ control, and the cells are handled outside of the incubator for 2-3 hours as imaging takes place. Prepare 10 mL of Phenol Red Free Complete DMEM additionally supplemented with sterile 10 mM HEPES (H0887, Sigma). For each cell sample, the media was aspirated and gently replaced with 1 mL of pre-warmed Phenol Red Free Complete DMEM + HEPES.

The sample stage (Delta T) was set to maintain the temperature of the sample at 32°C. Each cell sample was allowed to equilibrate 1 hour on stage before images were collected. Imaging settings were consistent with the Convallaria with the pixel dwell time at 1ms, the excitation wavelength set to 442 nm and the laser power lowered to a measured power of 0.25 mW at the back focal plane of the objective, or approximately 2.5 μW of power per focus, to prevent photobleaching effects. For each sample at least 5 fields of view were collected, with each field of view consisting of at least 5 cells captured per field of view.

4.3 Results and discussion

4.3.1 Fixed sample: *Convallaria*

Figure 4-2 and 4-3 illustrates images of the fixed *Convallaria* sample stained with either acridine orange (2.a-b), or Safranin and Fast-Green (3). Both samples are imaged across 12 spectral bands ranging from 450 nm to 700 nm. The spectral images were captured simultaneously with a pixel dwell time of 1 ms, resulting in a total exposure time of 1.8 s to capture all 12 spectral lifetime images. From the intensity images (Figure 4-2a), the *Convallaria* sample stained with acridine orange peaks at between 550 nm to 600 nm but is visible across all spectral bands due to the broad emission profile. The RGB image formed from all 12 spectral bands (six shown in the illustration) demonstrates three spectrally distinct regions of interest selected for analysis. Figure 4-2b demonstrates the fluorescence spectral and matching spectral-lifetime curves generated from all 12 spectral bands of the acridine orange sample. It can be observed that the fluorescence lifetime value of the *Convallaria* is spectrally complex with changes in lifetime generally increasing with wavelength. This is of interest as the *convallaria* was stained with only one fluorophore, indicating a change in spectral and lifetime properties is related to the morphology of the sample. Acridine orange is known to have a change in wavelength due to the type of nucleic acid it binds to, as well as the pH of the environment [38], and here we can identify regions which are different clearly through the wavelength as well as the lifetime spectrum.

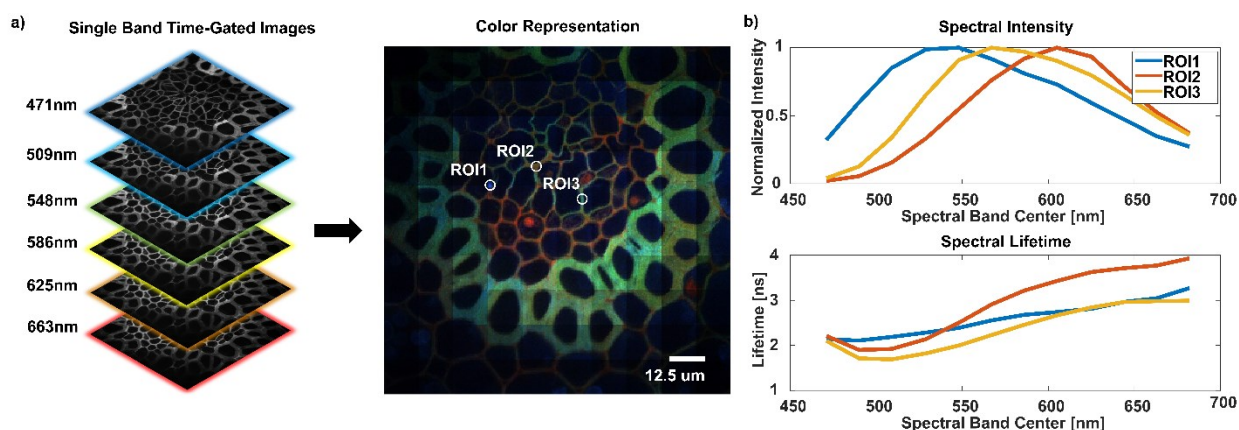


Fig. 4-2. Images show a fixed *convallaria* sample stained with acridine orange for simultaneous spectral and lifetime analysis. Spectral bands are 40 nm wide with 50 percent overlap, and pixel dwell time is 1 ms. **a)** A series of twelve spectrally separate time gated images (six displayed) reconstructed and combined to form a three-color image represented here in red, green, and blue (300×300 pixels with an image size 125×125 μm). **b)** Three spectrally distinct ROI highlighted demonstrate variations in spectra and spectral lifetime curves for a sample with a single stain.

Figure 4-3a illustrates the full field of view lifetime images (300x300 pixels) of the fixed *Convallaria* sample stained with Safranin (530 nm, 590 nm) and Fast Green (620 nm, 660 nm) [39]. Images are collected across all 12 spectral bands ranging from 450 nm to 700 nm. For all figures, an intensity weighted mask was used to modulate pixel brightness in the lifetime image (see methods). The images display negligible changes to the lifetime depending on the emission wavelength due to differences in the localization of the stains within the sample. The confocal measurements permit high resolution lifetime imaging due to the pinhole rejection of out of focus

light and allow the differentiation of small but distinct layers of the sample for each wavelength band without a

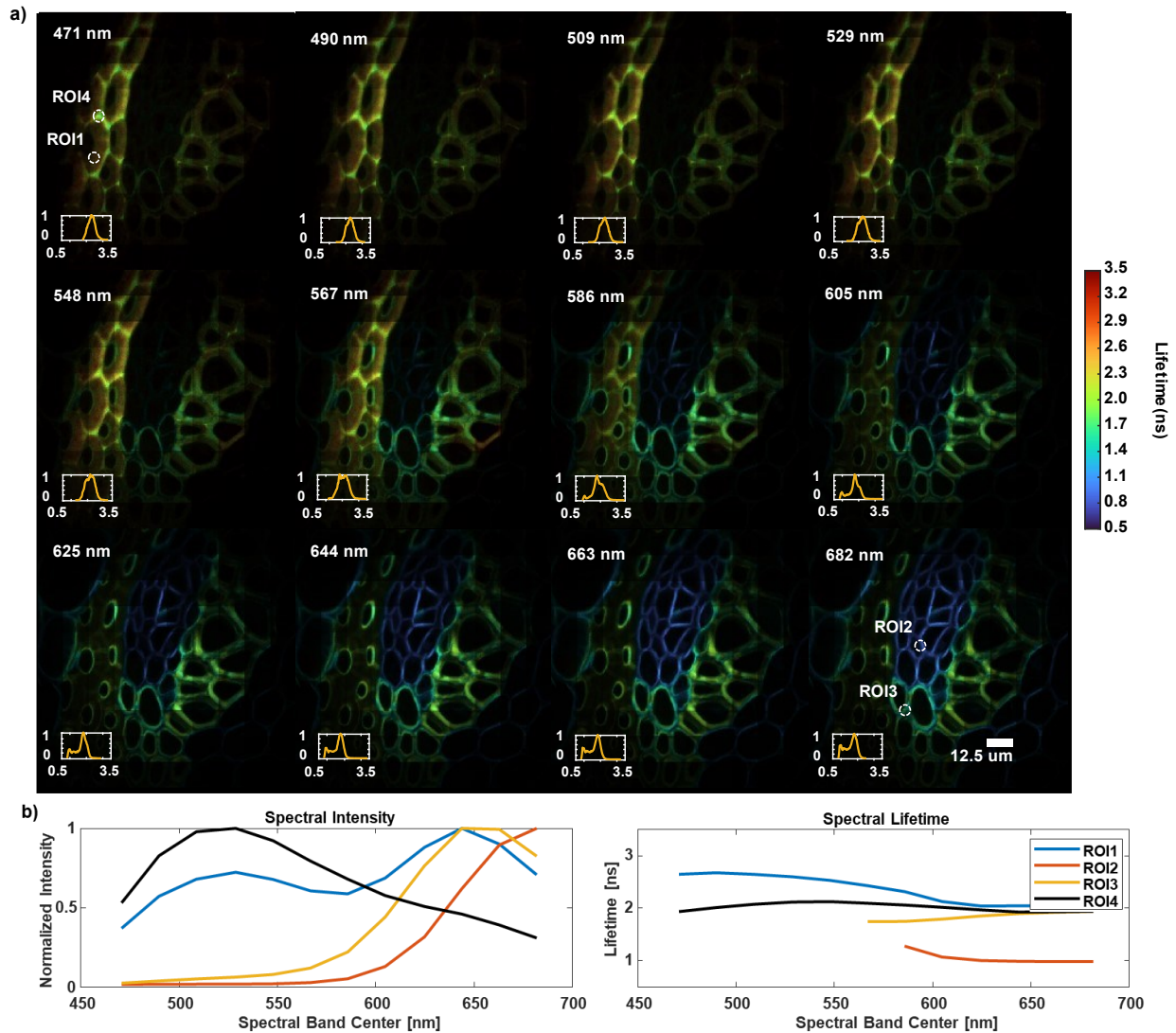


Fig. 4-3. a) A series of lifetime images taken from a convallaria stained with safranin (550 nm) and fast green (650 nm). Inserts for each wavelength are the normalized histogram of the lifetime image. Spectral bands are 40 nm wide with 50 percent overlap, and pixel dwell time is 1 ms. **b)** Four spectrally distinct ROI highlighted demonstrate variations in spectra and spectral lifetime curves. Components in ROI2 and ROI3 are excluded by threshold rules and are not present in the lifetime analysis.

compromise in image quality. Figure 4-3b illustrates the spectral and lifetime curves for four selected regions of interest which display unique spectral-lifetime characteristics. Blue-green emission is mostly absent from ROI2 and ROI3, as a result the lifetime results are excluded by threshold rules and are not presented in the lifetime analysis. The differences between regions are clear and a result of the different stains expressed in unique regions within the sample. Between the wavelength bands of 470 nm and 586 nm, Safranin is the dominant signal displayed and is mostly isolated to the endodermis, whereas Fast green is known to present in the Phloem and the Xylem with differences in the emission spectrum but emit from 586 nm to 700nm. The measured lifetimes of Safranin stain demonstrate two unique lifetimes of 2.7 ns and 2.0 ns, demonstrated in

the regions of interest 1 and 4, respectively. The measured lifetime of Fast Green is measured as either 1.8 ns or 1.0 ns, demonstrated in the regions of interest 3 and 2, respectively. These differences in lifetimes are likely the result of environmental changes within the microenvironment where the fluorophore is located, and these values align with literature-reported values [23]. It should be noted that the fixed *Convallaria* samples are not designed as a fluorescence standard for spectral and lifetime values but morphological complexity.

4.3.2 Dye standards

We chose to image two known standards to test the accuracy and precision of the lifetime estimation. We can accurately measure the fluorescence lifetime for Coumarin6 to be 2.7 ± 0.2 ns in ethanol and Fluorescein to be 4.0 ± 0.3 ns in 0.1M NaOH, at concentrations of 10 μ M as shown in Figure 4-4 a-b. The excitation wavelength is a significantly better match to Coumarin6, justifying the smaller FWHM in the lifetime distribution compared to Fluorescein. The lifetime distribution shows a slightly longer lifetime than expected by about 0.1 ns this is believed to be due to the selection of gate and potentially the influence of incomplete decay as it is known to heavily influence the accuracy of RLD generated lifetime measurements [40]. There are some spatial artifacts visible, most prominently the peripherals of the image have reduced brightness resulting in reduced lifetime accuracy and exclusion by the global thresholding procedures. This results from compounding issues such as the non-uniform excitation profile from a simple Gaussian beam expansion to imperfect telecentric relay alignment and even reduced point spread function performance for large marginal ray heights from the achromatic doublets used. This results in excitation image misalignment and pinhole coupling loss as a function of radius from the optical axis, which is present in all images. Other artifacts are the presence of a single MLA field of view having a noticeably longer lifetime, this is most probably the result of fabrication error in the pinhole array or MLA, or local laser illumination artifacts reducing the optical excitation of that individual field.

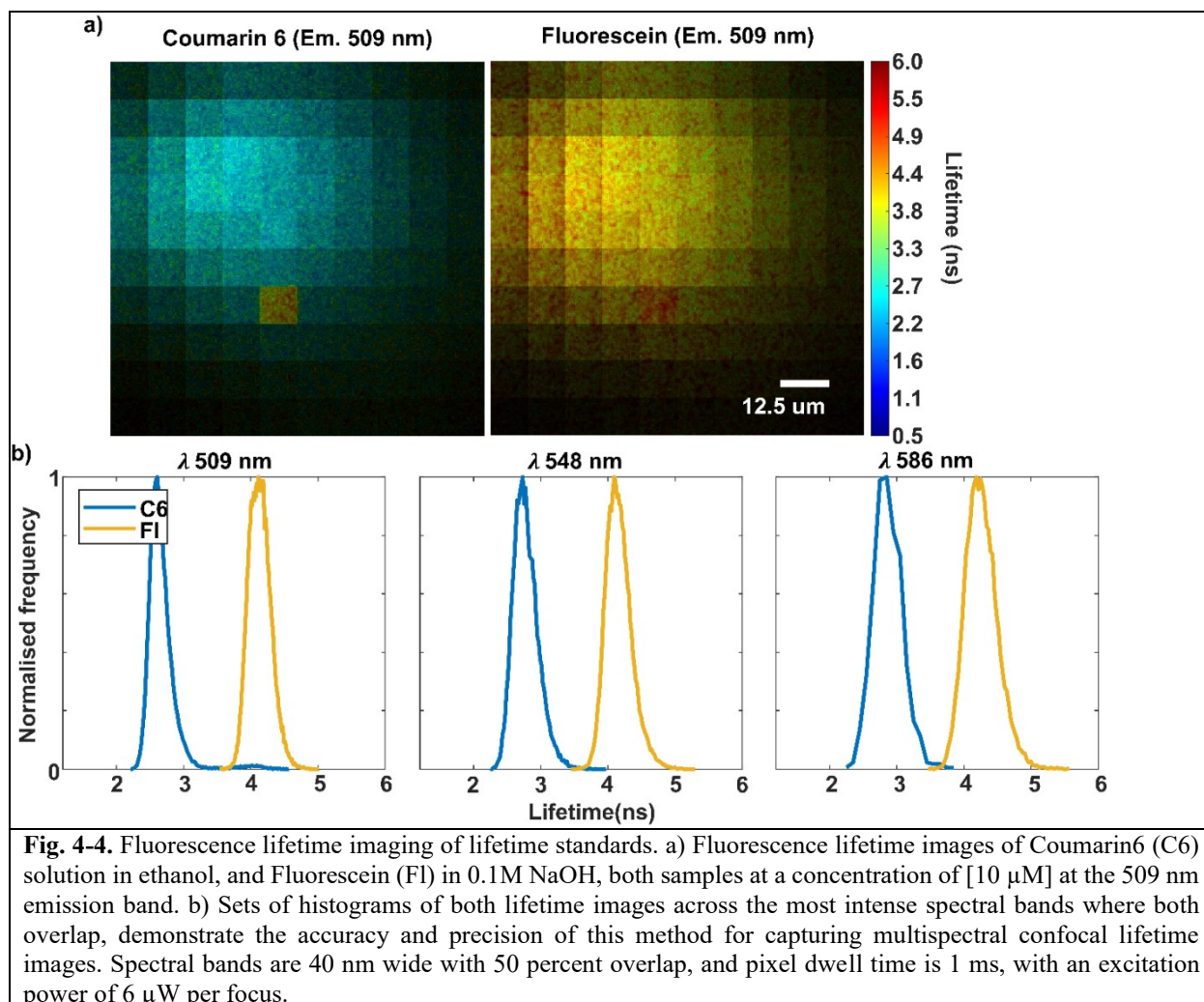


Fig. 4-4. Fluorescence lifetime imaging of lifetime standards. a) Fluorescence lifetime images of Coumarin6 (C6) solution in ethanol, and Fluorescein (FI) in 0.1M NaOH, both samples at a concentration of [10 μM] at the 509 nm emission band. b) Sets of histograms of both lifetime images across the most intense spectral bands where both overlap, demonstrate the accuracy and precision of this method for capturing multispectral confocal lifetime images. Spectral bands are 40 nm wide with 50 percent overlap, and pixel dwell time is 1 ms, with an excitation power of 6 μW per focus.

4.3.3 Live cell samples

Live cell samples of HEK293T transfected with mCerulean3, Venus, mCerulean3 and Venus, and mCerulean3-Venus linked, are imaged to characterize system performance in live cell transfection experiments. Each of these fluorophores is expressed uniformly across the cell, and as expected, we observe that the lifetime is estimated consistently across each cell (Figure 4-5 a-d). All data points in these images were collected with the same excitation wavelength (442 nm) at 1 ms of pixel dwell, demonstrating the fluorescence emission sensitivity. The lifetime images selected for mCerulean3, mCerulean3+Venus (a control), and mCerulean3-Venus, at 471 nm, demonstrate the change in donor (mCerulean3) lifetime with FRET, whereas the lifetime of Venus was demonstrated at 554 nm to show the collection of Venus emission while being excited off the peak of the excitation curve. Based on previous literature [41], the expected lifetime for mCerulean3 was 3.8 +/- 0.1 ns, for Venus was 2.9 +/- 0.1 ns, and for mCerulean3-5aa-Venus was 2.5 +/- 0.2 ns.

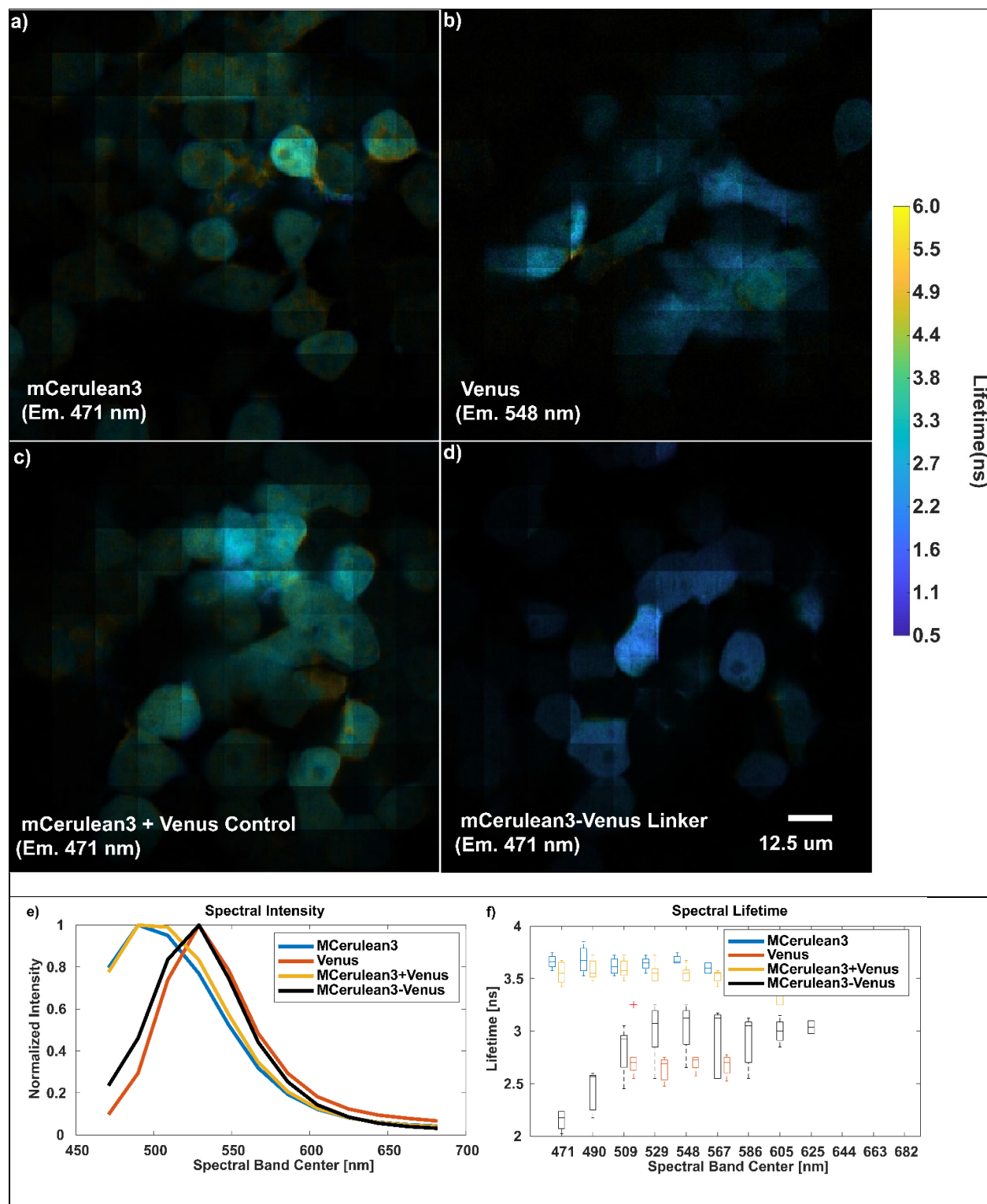


Fig. 4-5. Selected spectral lifetime images of HEK293T cells expressing (a) mCerulean3 fluorescent protein only at an emission wavelength of 471 nm (b) Venus fluorescent protein only at an emission wavelength of 554 nm (c) mCerulean3 and Venus transfected but unbound at an emission wavelength of 471 nm (d) and mCerulean3 tethered to Venus using a 13 amino-acids linker at an emission wavelength of 471 nm. e-f) Intensity and lifetime spectra of the samples over 5 fields of view with 1 ms pixel dwell time for a total exposure time of 1.8 seconds. Spectral bands

are 40 nm wide with 50 percent overlap, and pixel dwell time is 1 ms, and excitation power is 2.5 μ W per focus at 442 nm.

Figure 4-5 e-f demonstrates intensity and lifetime spectral curves for a set of 12 spectrally distinct but overlapping bands, each roughly 42 nm wide. For mCerulean3, mCerulean3+Venus, and Venus the estimated lifetimes were 3.6 +/- 0.4 ns, 3.5 +/- 0.4 ns, and 2.7 +/- 0.4 ns, respectively. They were consistently measured at different wavelengths where sufficient counts could be detected. This was expected as there is a single population of fluorophores in each of these samples for mCerulean3 and Venus, but for the control sample where they are combined, mCerulean3 is the overwhelming signal and is affected minimally by the Venus fluorescence. In contrast, mCerulean3-Venus (a FRET standard) involves both fluorophores undergoing energy transfer. Consequently, the measured lifetime in the overlapping spectral region of Venus and mCerulean3 will represent a mixed population. At such wavelengths, FRET cannot be accurately estimated using two gate RLD which computes the average lifetime and cannot separate the multi-exponential components. The mCerulean3-Venus sample over the entire spectrum represents a 4-component system (the donor (mCerulean3) lifetime, the lifetime of the donor undergoing FRET (mCerulean3-Venus), the acceptor lifetime (Venus), and the time delayed fluorescence of the acceptor (Venus) in the presence of the donor (mCerulean3)). Therefore, even though the lifetime can be estimated across the full spectrum, as shown in Figure 4-5f, these data are not useful for directly quantifying FRET. On the other hand, the spectral intensity and lifetime profiles do reveal areas where separation is possible for mCerulean3 at 470-491 nm. As expected, we observe a decrease in the lifetime of mCerulean3 when in the presence of an acceptor compared to the measured lifetime of mCerulean3 alone. The measured lifetime of mCerulean3-Venus is demonstrated as 2.3 +/- 0.3 ns when averaging wavelengths 471-491 nm. On the other hand, for wavelengths at and beyond 512 nm, the measured lifetime of cerulean-Venus is longer, 2.9 +/- 0.4 ns, demonstrating that the dominant signal at these wavelengths is coming from some combination of components as discussed. Fig. 5f notably demonstrates this, as we observe for mCerulean3-Venus a highly non-linear spectral lifetime across all spectral channels, implying a significant amount of energy being transferred out of the donor. The FRET efficiency was calculated based on the average lifetime between the 471 nm and 491 nm wavelength bands. The calculated energy transfer efficiency for this protein pair is given by $E_{FRET} = 1 - \frac{\tau_{DA}}{\tau_D}$, and is found to be 36 %.

4.4 Discussions and Conclusion

We developed a fast multispectral multipoint confocal FLIM microscope that can be used to image dynamic subcellular processes. This system simultaneously obtains 12 unique spectral channels by spectrally separating fluorescence emission onto a single-gated optical intensifier (GOI). This provides superior noise characteristics since each spectral channel for each focus is composed of 10+ pixels, with confocal resolution provided by a custom pinhole array. Our confocal performance remains unaffected by the poor spatial resolution of the microchannel plate (MCP), which is atypical for this time-gated amplification method when used in confocal time-resolved FLIM. This is due to the de-scanned nature of fluorescence capture at the sensor relaxing MCP bore hole requirements.

As the system diagrams demonstrate, the only filters are the dichroic and a long pass filter, used to isolate the optical path, and block back reflectance of excitation. This filter selection allows the spectrometer to capture all remaining fluorescence emission simultaneously, with completely

customizable spectral bands after acquisition, overlapping and non-overlapping spectral bands are entirely possible. This is because of the unique, highly oversampled readout of the fluorescence spectra from the high pixel count sensor. The large image readout of the 5.5-megapixel frame, however, does present an issue as the total data size is just over 10 GB for each FLIM image data set. The large image results in slow transfer times, limiting the raw frame capture rate to 16 fps. This limits the overall image time to under 2 minutes when including galvanometer raster step synchronization for all 900 frames requires per image. These issues can be addressed in future work by replacing the readout camera with a sensor with faster frame readout and saving images to an internal buffer.

The imaging spectrometer was designed to have a 16 nm spectral resolution at a rms spot radius of 21 μm at 650 nm, but unfortunately, the MCP intensifier has a considerably lower spatial resolution at 10 lp/mm. The loss of resolution is significant for this method as high resolutions improve the ability to deconvolve species. The resolution loss can be compensated for with the method of band shifting to remove the need for interpolation due to low spectral resolution. The additional spectral bin width has the unintended improvement in the applications of fast low light imaging, as the noise level is the sum of the several photon sensitive pixels. An improvement of the spectral resolution is possible by replacing the MCP GOI with a different technology, such as a SPAD array that has a smaller pixel size [42–44]. The SPAD array technology can also perform simultaneous multi-time gate detection that will allow resolving complex decays [45,46].

In our experiments, an intensity of 2.1 kW/cm² and a pixel exposure of 1 ms were used for imaging the live cell samples. The exposure conditions of our microscope do not predict a significant level of expected photobleaching to occur on the time scale of our exposure period, given the photobleaching characteristics of mCerulean3 and Venus fluorescent proteins [47,48]. The literature also indicates reduced photobleaching effects from pulsed illumination compared to continuous illumination [49]. Due to the sequential gate measurements of our system, photobleaching will impact our fluorescence lifetime measurement. This is because the initial gate measured will experience less photo-bleaching than subsequent gates. Multi-gate detectors that capture the fluorescence decay across all time points simultaneously will not have this issue, as photobleaching does not affect the fluorescence decay and their resulting FRET measurements. There are exceptions to fluorescent proteins that exhibit multi-exponential decays where photobleaching of decay components may not occur evenly, but there are techniques for managing the effects [50].

The power of multispectral confocal FLIM to identify unique spectral and spectral lifetime fingerprints has the potential to provide phenotypic and functional information. While it is not the intention of this study to present new novel algorithms to perform segmentation of spectral lifetime datasets, we demonstrate the power of high spatial resolution, complemented with spectral and lifetime contrast methods, to quickly identify distinct regions in fixed samples and identify molecular interactions within live cells. Fusion of these multimodal datasets with emerging technologies in machine learning presents a promising solution to identify and classify species localization, deconstruct crowded species labeling, and clarify molecular interactions through FLIM and FLIM-FRET.

This system demonstrates the first highly multiplexed multispectral confocal FLIM microscope. Through this technique we combine several technologies to offer a microscope that can extract feature rich datasets of time resolved spectra at 1.8 seconds of exposure. Spatial multiplexing with 100 points enables fast imaging with low excitation intensities preventing

photobleaching and phototoxicity. This system demonstrates the ability of time resolved spectral lifetime imaging to resolve subtle changes to sample structure or lifetime, while using excitation powers suitable for live cell imaging. We overcome spatial resolution limitations with the gated optical intensifier by de-scanning the emission image and segmenting the spectral image. This technology has the potential to significantly impact various fields including drug discovery by providing fast multidimensional imaging that can identify spatial and temporal changes in labels.

Acknowledgments. This project is supported in part by the Natural Science and Engineering Research Council (NSERC) of Canada through a Discovery Grant, a John R. Evans Leaders Fund grant from the Canadian Foundation of Innovation and Ontario Research Fund-Research Infrastructure, and a MITACS Accelerate grant.

Conflict of Interest. M. Richards, and Q. Fang declares financial interests in McFocal Bioimaging.

Author contributions.

M.R and Q.F: system conceptual design. M.R.: experiment design, construction, and development of the microscope system and calibration. All authors contributed to the cell imaging validation experiment design. E.O., A.B., and N.M., prepared biological samples. M.R, A.B, N.M. performed the biological imaging experiments. M.R processed and analysed the data. M.R., E.O., A.B., N.M. contributed to the writing of the manuscript. All authors contributed to the results analysis and discussion, as well as editing of the manuscript.

Data availability. Data underlying the results presented in this paper are not publicly available at this time but may be obtained from the authors upon reasonable request.

References.

- [1] Hiraoka Y, Shimi T and Haraguchi T 2002 Multispectral Imaging Fluorescence Microscopy for Living Cells. *Cell Struct Funct* **27** 367–74
- [2] Becker Editor W 2015 *Advanced Time-Correlated Single Photon Counting Applications* vol 111, ed W Becker (Cham: Springer International Publishing)
- [3] Sharma M 2023 *Fluorescent Proteins* vol 2564 (New York, NY: Springer US)
- [4] Garini Y, Young I T and McNamara G 2006 Spectral imaging: Principles and applications *Cytometry Part A* **69** 735–47
- [5] Acuña-Rodríguez J P, Mena-Vega J P and Argüello-Miranda O 2022 Live-cell fluorescence spectral imaging as a data science challenge *Biophys Rev* **14** 579–97
- [6] Laissue P P, Alghamdi R A, Tomancak P, Reynaud E G and Shroff H 2017 Assessing phototoxicity in live fluorescence imaging *Nat Methods* **14** 657–61
- [7] Knight M M, Roberts S R, Lee D A and Bader D L 2003 Live cell imaging using confocal microscopy induces intracellular calcium transients and cell death *American Journal of Physiology-Cell Physiology* **284** C1083–9

- [8] Zimmermann T and O'Toole P 2014 *Confocal Microscopy* vol 1075, ed S W Paddock (New York, NY: Springer New York)
- [9] Zimmermann T, Rietdorf J and Pepperkok R 2003 Spectral imaging and its applications in live cell microscopy *FEBS Lett* **546** 87–92
- [10] Stryer L 1978 Fluorescence Energy Transfer as a Spectroscopic Ruler *Annu Rev Biochem* **47** 819–46
- [11] Borst J W, Laptienok S P, Westphal A H, Kühnemuth R, Hornen H, Visser N V., Kalinin S, Aker J, Van Hoek A, Seidel C A M and Visser A J W G 2008 Structural changes of yellow cameleon domains observed by quantitative FRET analysis and polarized fluorescence correlation spectroscopy *Biophys J* **95** 5399–411
- [12] Berezin M Y and Achilefu S 2010 Fluorescence lifetime measurements and biological imaging *Chem Rev* **110** 2641–84
- [13] Zanella F, Lorens J B and Link W 2010 High content screening: Seeing is believing *Trends Biotechnol* **28** 237–45
- [14] Fraietta I and Gasparri F 2016 The development of high-content screening (HCS) technology and its importance to drug discovery *Expert Opin Drug Discov* **11** 501–14
- [15] Bickle M 2010 The beautiful cell: High-content screening in drug discovery *Anal Bioanal Chem* **398** 219–26
- [16] Hirvonen L M, Nedbal J, Almutairi N, Phillips T A, Becker W, Conneely T, Milnes J, Cox S, Stürzenbaum S and Suhling K 2020 Lightsheet fluorescence lifetime imaging microscopy with wide-field time-correlated single photon counting *J Biophotonics* **13** e201960099
- [17] Buranachai C, Kamiyama D, Chiba A, Williams B D and Clegg R M 2008 Rapid frequency-domain flim spinning disk confocal microscope: Lifetime resolution, image improvement and wavelet analysis *J Fluoresc* **18** 929–42
- [18] Poland S P, Krstajić N, Coelho S, Tyndall D, Walker R J, Devauges V, Morton P E, Nicholas N S, Richardson J, Li D D-U, Suhling K, Wells C M, Parsons M, Henderson R K and Ameer-Beg S M 2014 Time-resolved multifocal multiphoton microscope for high speed FRET imaging in vivo *Opt Lett* **39** 6013
- [19] Pian Q, Yao R, Sinsuebphon N and Intes X 2017 Compressive hyperspectral time-resolved wide-field fluorescence lifetime imaging *Nat Photonics* **11** 411–4
- [20] Day R N 2015 Measuring Förster Resonance Energy Transfer Using Fluorescence Lifetime Imaging Microscopy *Micros Today* **23** 44–51
- [21] Becker W, Bergmann A and Biskup C 2007 Multispectral fluorescence lifetime imaging by TCSPC *Microscopy Research and Technique* vol 70 (Wiley-Liss Inc.) pp 403–9

- [22] Krishnan R V., Masuda A, Centonze V E and Herman B 2003 Quantitative imaging of protein–protein interactions by multiphoton fluorescence lifetime imaging microscopy using a streak camera *J Biomed Opt* **8** 362
- [23] Esposito A and Venkitaraman A R 2019 Enhancing Biochemical Resolution by Hyperdimensional Imaging Microscopy *Biophys J* **116** 1815–22
- [24] Williams G O S, Williams E, Finlayson N, Erdogan A T, Wang Q, Fernandes S, Akram A R, Dhaliwal K, Henderson R K, Girkin J M and Bradley M 2021 Full spectrum fluorescence lifetime imaging with 0.5 nm spectral and 50 ps temporal resolution *Nat Commun* **12** 6616
- [25] Scipioni L, Rossetta A, Tedeschi G and Gratton E 2021 Phasor S-FLIM: a new paradigm for fast and robust spectral fluorescence lifetime imaging *Nat Methods* **18** 542–50
- [26] Cutrale F, Trivedi V, Trinh L A, Chiu C L, Choi J M, Artiga M S and Fraser S E 2017 Hyperspectral phasor analysis enables multiplexed 5D in vivo imaging *Nat Methods* **14** 149–52
- [27] Popleteeva M, Haas K T, Stoppa D, Pancheri L, Gasparini L, Kaminski C F, Cassidy L D, Venkitaraman A R and Esposito A 2015 Fast and simple spectral FLIM for biochemical and medical imaging *Opt Express* **23** 23511
- [28] Katsoulidou V, Bergmann A and Becker W 2007 How fast can TCSPC FLIM be made? *Advanced Photon Counting Techniques II* vol 6771 (SPIE) p 67710B
- [29] Köllner M and Wolfrum J 1992 How many photons are necessary for fluorescence-lifetime measurements? *Chem Phys Lett* **200** 199–204
- [30] Hirmiz N, Tsikouras A, Osterlund E J, Richards M, Andrews D W and Fang Q 2021 Highly Multiplexed Confocal Fluorescence Lifetime Microscope Designed for Screening Applications *IEEE Journal of Selected Topics in Quantum Electronics* **27** 1–9
- [31] Tsikouras A, Berman R, Andrews D W and Fang Q 2015 High-speed multifocal array scanning using refractive window tilting *Biomed Opt Express* **6** 3737
- [32] Bovik A 2005 *Handbook of Image and Video Processing* (Elsevier)
- [33] W. Woods J 2012 *Multidimensional Signal, Image, and Video Processing and Coding* (Elsevier)
- [34] Woods R J, Scypinski Stephen and Love L J Cline 1984 Transient digitizer for the determination of microsecond luminescence lifetimes *Anal Chem* **56** 1395–400
- [35] Sharman K K, Periasamy A, Ashworth H, Demas J N and Snow N H 1999 Error analysis of the rapid lifetime determination method for double-exponential decays and new windowing schemes *Anal Chem* **71** 947–52
- [36] Sun Y, Day R N and Periasamy A 2011 Investigating protein-protein interactions in living cells using fluorescence lifetime imaging microscopy *Nat Protoc* **6** 1324–40
- [37] Zhang X F, Zhang J and Liu L 2014 Fluorescence properties of twenty fluorescein derivatives: Lifetime, quantum yield, absorption and emission spectra *J Fluoresc* **24** 819–26

- [38] Yektaeian N, Mehrabani D, Sepaskhah M, Zare S, Jamhiri I and Hatam G 2019 Lipophilic tracer Dil and fluorescence labeling of acridine orange used for Leishmania major tracing in the fibroblast cells *Heliyon* **5** e03073
- [39] Frank J H, Elder A D, Swartling J, Venkitaraman A R, Jeyasekharan A D and Kaminski C F 2007 A white light confocal microscope for spectrally resolved multidimensional imaging *J Microsc* **227** 203–15
- [40] Ballew R M and Demas J N 1989 An error analysis of the rapid lifetime determination method for the evaluation of single exponential decays *Anal Chem* **61** 30–3
- [41] Osterlund E J, Hirmiz N, Pemberton J M, Nougarede A, Liu Q, Leber B, Fang Q and Andrews D W 2022 Efficacy and specificity of inhibitors of BCL-2 family protein interactions assessed by affinity measurements in live cells *Sci Adv* **8** 7375
- [42] Ulku A C, Bruschini C, Antolovic I M, Kuo Y, Ankri R, Weiss S, Michalet X and Charbon E 2019 A 512×512 SPAD Image Sensor With Integrated Gating for Widefield FLIM *IEEE Journal of Selected Topics in Quantum Electronics* **25** 1–12
- [43] Krstajić N, Levitt J, Poland S, Ameer-Beg S and Henderson R 2015 256×2 SPAD line sensor for time resolved fluorescence spectroscopy *Opt Express* **23** 5653
- [44] Gyongy I, Calder N, Davies A, Dutton N A W, Duncan R R, Rickman C, Dalgarno P and Henderson R K 2018 A 256×256 , 100-kfps, 61% Fill-Factor SPAD Image Sensor for Time-Resolved Microscopy Applications *IEEE Trans Electron Devices* **65** 547–54
- [45] Hirvonen L M, Nedbal J, Almutairi N, Phillips T A, Becker W, Conneely T, Milnes J, Cox S, Stürzenbaum S and Suhling K 2020 Lightsheet fluorescence lifetime imaging microscopy with wide-field time-correlated single photon counting *J Biophotonics* **13** 2015
- [46] Wayne M, Ulku A, Ardelean A, Mos P, Bruschini C and Charbon E 2022 A 500×500 Dual-Gate SPAD Imager with 100% Temporal Aperture and 1 ns Minimum Gate Length for FLIM and Phasor Imaging Applications *IEEE Trans Electron Devices* **69** 2865–72
- [47] Markwardt M L, Kremers G-J, Kraft C A, Ray K, Cranfill P J C, Wilson K A, Day R N, Wachter R M, Davidson M W and Rizzo M A 2011 An Improved Cerulean Fluorescent Protein with Enhanced Brightness and Reduced Reversible Photoswitching ed D Jones *PLoS One* **6** e17896
- [48] Lee J, Liu Z, Suzuki P H, Ahrens J F, Lai S, Lu X, Guan S and St-Pierre F 2020 Versatile phenotype-activated cell sorting *Sci Adv* **6** eabb7438
- [49] Boudreau C, Wee T-L, Duh Y-R, Couto M P, Ardakani K H and Brown C M 2016 Excitation Light Dose Engineering to Reduce Photo-bleaching and Photo-toxicity *Sci Rep* **6** 30892
- [50] Hwang W S, Song Y S and Kim D Y 2015 Fluorescence lifetime determination of photo-bleaching correlation 2015 11th Conference on Lasers and Electro-Optics Pacific Rim (CLEO-PR) vol 19 (IEEE) pp 1–2

Chapter 5. A 1Hz Multipoint Multispectral Confocal Microscope

Paper III – Multiplexed Multispectral Confocal Microscopy

MORGAN RICHARDS¹, NIKOLINA MALIC², QIYIN FANG^{1,2,*}

¹McMaster University Department of Engineering Physics, Hamilton, ON, L8S 4L8, Canada

²McMaster University Department of Biochemistry and Biomedical Sciences, Hamilton, ON, L8S 4L8, Canada

Submitted to ...

This chapter is prepared for submission to a journal for publication pending final revisions.

Introduction to Paper III

In this chapter, we describe the development and implementation of a multispectral multipoint confocal microscope capable of imaging at a real-time frame rate of 1Hz to overcome the acquisition time limitations of the multispectral microscope in the previous chapter. We demonstrate how fast multispectral confocal imaging can be achieved using a highly multiplexed design that features our improved pinhole array based 32x32 point confocal microscope, with the addition of a new sweeping mechanism to paint the spectral bands onto the sensor. This new design has achieved imaging of 22 spectral bands simultaneously onto a CMOS image sensor. In this chapter, we discuss the optical design and the steps we have taken to ensure the image quality is not limited by the new optical design. We calibrate the spectrometer and verify its accuracy and precision using simple automated procedures. We then demonstrate the performance on a fixed *Convallaria* sample to demonstrate the distinguishable spectral differences and discuss some techniques to perform automated segmentation of spectrally distinct regions.

Morgan Richards designed and constructed the optical system and new scanner controller hardware, wrote all hardware control and image processing software, created the calibration procedures, and performed scanner calibration for 1 Hz imaging. Morgan Richards and Nikolina Malic collected *convallaria* images together. Nikolina Malic assisted with aligning the optical system. Morgan Richards wrote the original manuscript draft, and all authors contributed to editing.

Contents of Paper III

Abstract:

Multispectral imaging is a powerful technique that can detect subtle differences in the fluorescence expression of a species based on its reaction to its environment. These subtle differences offer a powerful contrast agent that can be used to identify new compounds for novel medicines. Imaging with high spectral resolution is essential as often the spectral differences can shift a species' spectral band significantly. Multispectral confocal imaging is slow because single-point confocal techniques have fundamental signal collection limitations, and currently, no massively multiplexed measurement techniques offer high-resolution simultaneous multispectral measurement. Multiplexing with a pinhole array based confocal that uses window scanning offers new spatially encoded spectral measurements on dense image sensors by sweeping spectral bands with a dedicated window scanner. We present a 32x32 point multiplexed confocal microscope that captures 22 spectral bands simultaneously at a real-time image frequency of 1 Hz over the entire spectral range of 450 nm to 650 nm.

5.1. Introduction

Light microscopy has become a significant tool for studying biological systems, allowing us to explore subcellular regions in detail. Fluorescent tagging has extended the capabilities of the microscope by providing a powerful contrast agent that has a limited effect on cellular behavior [1,2]. Fluorescence allows us to localize subcellular structures to observe the effect an external agent may have on the morphology of the cell. Fluorescence spectroscopy enables the discrimination of multiple fluorescent tags to measure multilabel experiments [3]. The ability to differentiate these signals is crucial to understand complex behavior. Multilabel experiments such as those in cell painting and FRET are found in drug discovery and basic research, playing roles in phenotypic and target-based assays [4–6]. These applications provide powerful insights into the response of a cell model to the experimental compound being tested.

Improvements in the microscope's imaging resolution can improve contrast in tightly packed subcellular features. Confocal microscopy is a method of achieving diffraction-limited imaging resolution that prevents out-of-focus light from contributing to the noise in an image [7–9]. Confocal microscopy is a technique to measure the subtle changes that can occur in cellular organelle morphology. Traditional confocal microscopy, however, is a slow point-wise process that builds a picture pixel-by-pixel. Multipoint confocal microscopy techniques, such as spinning disk confocal microscopy, overcome the slow acquisition speed and divide the imaging region into subregions for parallel acquisition [10–12]. Multipoint confocal microscopy also provides a gentle method of live cell imaging for rapid measurements due to reduced excitation optical power, which leads to photobleaching and phototoxicity [10].

Due to their unique optical path, current multipoint confocal microscopes are limited to bandpass filter-based spectral selection. Multipoint multiphoton microscopy has been demonstrated to achieve spectrally resolved imaging but with limitations to the multiplexing factor due to poor efficiency and high complexity of generating multipoint excitation images [13,14]. Single photon techniques such as spinning disk confocal paint a confocal picture by rotating evenly spaced pinholes configured into a spiral. The nature of this image acquisition method leaves no room for spectral separation on an image sensor as each pixel in the final image corresponds to a one-to-

one mapping on the sensor [15,16]. As a result of the image acquisition methodology, multispectral imaging will occur with some image splitting setup [17], limiting the number of spectral bands simultaneously acquired to the number of image sensors the platform is equipped with.

Previously, we demonstrated the potential of a multispectral microscope to capture time-resolved fluorescence with our multipoint confocal microscope. The design used the sparsity of our multipoint confocal and the de-scanned fluorescence image to generate spectrally resolved fluorescence streaks. The system required an acquisition time that scaled quadratically with the image dimension, limiting its total capture time to just under 2 minutes while the required exposure was 1.8 seconds.

Here, we report on the development of a multi-spectral multipoint confocal microscope with an acquisition time that scales linearly with image dimension. This work details the optical system and automated calibration procedures. Performance validation is demonstrated by examining stained sections of fixed plant specimens.

5.2. Methods

Optical System

The schematics of the optical system design are shown in Figure 5-1. The system uses a pulsed diode laser (LDH-440M, Picoquant) that produces 440 nm excitation with pulse widths of ~1ns at a pulse repetition rate of 80 MHz. The laser output is coupled into a multimode fiber to improve the uniformity of the output excitation beam and translate it into the optical setup. The fiber output is collimated using a 300 mm lens (Thorlabs AC508-300-A) into a 1.4 cm beam to provide a collimated illumination wavefront against the microlens array (MLA). The system uses a 300 μm pitch, 32x32 MLA (18-1453-100-000, SUSS MicroOptics), for 1024-point multiplexing to enable fast sample imaging. The MLA excitation image is transmitted through a pair of achromatic doublets (Thorlabs AC508-200-A) placed to form a telecentric relay, $M=1$, and reflected off a 442 nm long-pass dichroic (Di03-R442-t1-25x36, Semrock), onto a custom pinhole array (Walthy Precision) to match the MLA excitation image footprint. The pinhole array has a square array of 25 μm diameter pinholes at 300 μm pitch. Together with a pair of galvanometer window scanners (GM-1000, Cannon) for raster scanning in X and Y [18], the system generates excitation spots that pass through the camera port of an inverted fluorescence microscope (Nikon Ti) equipped with a 40x/1.30 NA objective (Plan Fluor 40x/1.30 Oil, Nikon). The fluorescence emission, once de-scanned, passes through the pinhole array and is relayed through the 442 nm long pass dichroic. A 450 nm long pass filter (FELH0450, Thorlabs) and a 650 nm short pass filter (FESH0650, Thorlabs) were used to narrow the spectral range for imaging. The emission passes through a 4-degree wedge prism (PS811-A, Thorlabs) for spectral separation. Once the emission foci pass through the final $M=1$ relay lens, a window scanner that uses a galvo scanner (6230HM40B, Cambridge Technology) is used to perform the final scanning. The resulting spectra are imaged onto a CMOS sensor (XiQ, Ximea).

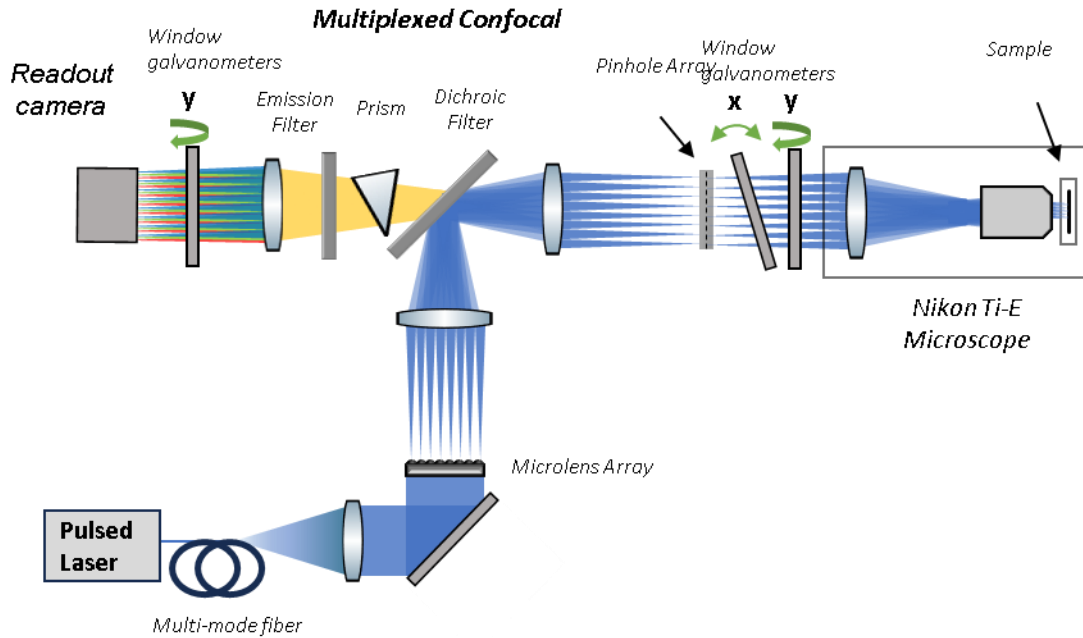


Figure 5-1. Diagram of the multispectral multipoint confocal microscope.

Synchronized Spectral Sweeping

The final sweeping of the spectra occurs using a third window scanner. This scanner will translate the spectral image at the same rate as the capture, such that both scanners are synchronized in time and angular position through a raster scan. As illustrated in Figure 5-2 a, the purpose of this mechanism is to repaint the spatial coordinate of the spectrum onto the image sensor for each row in an image acquisition. Traditionally, the 32x32 point microlens array of the scanner generates a 30x30 pixel ROI between the pitch of each microlens to ensure the sampling rate accurately captures the Nyquist limited spatial frequency. Constructing this image requires 900 raw frames from a sensor to capture the total image content. With our sweeping mechanism illustrated in Figure 5-2 b, we capture all raw frames corresponding to a single row in the image with a single sweep of the third galvo scanner. This reduces the total number of raw frames from an image sensor to just 30 for an entire high-resolution image to be generated.

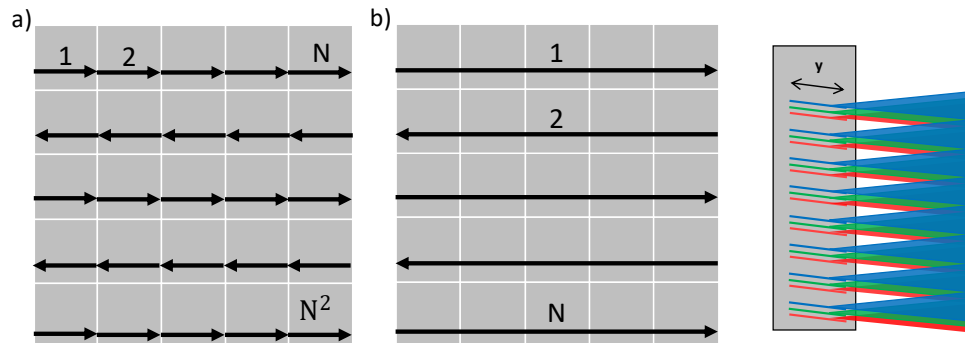


Figure 5-2. a) Example of a pixel in the final image labeled by the readout frame they originated from. b) A depiction of the sweeping behavior to paint the spectral streak onto the sensor.

The Cambridge galvo scanner was modified to convert the scanner motion from a step and stop behavior to a linear sweep motion. The scanners were driven by the DAC on a microcontroller (DUE, Arduino) to allow arbitrary waveforms to be used for scanning. An amplifier was built to increase the signal voltage to match the scanner's analog input range. Two preset scanning waveforms, one for each direction of the bi-directional sweep, were coded into the microcontroller, and upon triggering by the cannon galvo scanners, a sweep waveform would begin. This method of control is convenient as the microcontroller has direct control over both scanner and sensor exposure, allowing the two to be synchronized closely. The cannon scanner can directly influence the trigger delay for adjusting the synchronization of the rescan sweep and sensor exposure with the sample scan. And the adjustment can be done with automated adjustment and evaluation of image quality. Examples of the spectra and their sweeping behavior are given in Figure 5-3 b, where the non-swept and swept spectra are displayed. The images demonstrate the uniformity of the scanner when measuring the spectrum of a bright field illumination source (64625 HLX, OSRAM) installed on the microscope. The sweeping range of motion is carefully tuned to ensure a seamless image.

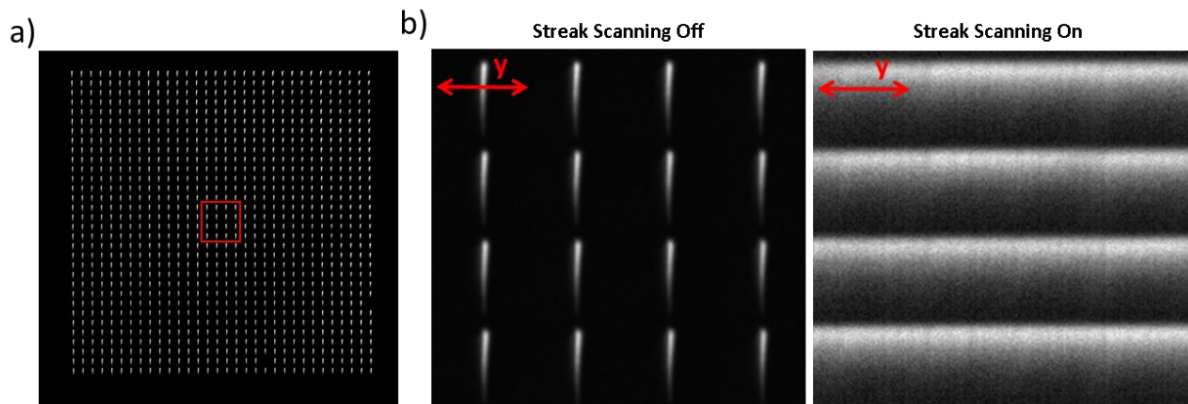


Figure 5-3. a) Full field of view for all 32x32 spectra generated with the pinhole array swept confocal spectrometer. Red ROI denotes the 4x4 region used for analysis. b) Spectral streaks with scanning off and on to demonstrate the sweeping concept. The red arrow denotes the full range of motion of the spectral streaks when undergoing displacement by the window scanner.

Swept Spectrum Resolution

The rescanned streaks must not become the limiting factor to attain the highest resolution imaging. The optical system also limits the spatial and spectral limiting resolution. The pinhole diameter acts as the slit ‘width’ of the spectrometer and the effective limiting resolution for the images. Careful alignment and verification of the streak optical quality ensures the streak width corresponds to the pinhole diameter. Figure 5-4 a illustrates this measurement where the width of the streak is carefully measured out to be 4.5 px, with a 5.5 μm pixel size corresponding to the 25 μm diameter of the pinhole. This is sampled from the center of the pinhole array image, streaks on the outermost margins of the image will have noticeably lower resolution as the off-the-shelf achromat lenses are unable to provide the diffraction-limited image quality for the entire 10x10 mm^2 field of view.

The 25 μm spot size will be the limiting feature size of the images on the sensor. The spectral bandwidth will be limited to approximately the pitch of the pinhole centers divided by the

diameter of the pinhole. For a 300 μm pitch with 25 μm pinholes, this leaves us with approximately 11 spectral bands however, because the spectral bands are sampled by over four pixels, we choose to sample at double that resolution to capture spectral variation at the Nyquist limit. To validate that the optical system has sufficient spectral resolution to match the limiting image size, a monochromatic image was captured to validate the spectral resolution. Figure 5-4 b illustrates the results of one measurement using a 532 nm laser as a monochromatic illumination source. The diameter of the image is 4.0 pixels, corresponding to a 22 μm image size. This is smaller than the pinhole image but may be explained by the source's coherence, which may result in interference patterns that modify the shape of the imaged spot.

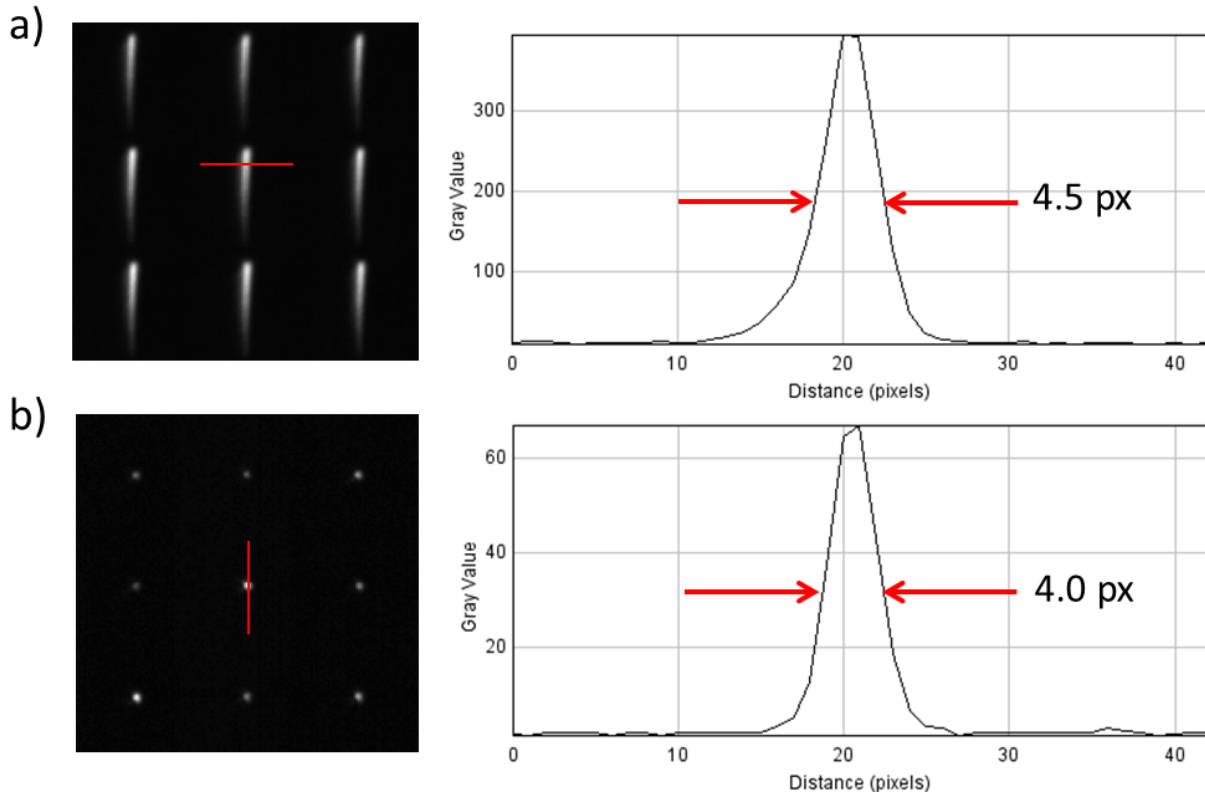


Figure 5-4. a) Isolated spectral streak with a red line identifying the placement of the cross-section highlighted. The cross-section of spectral streak for analysis of FWHM. b) Laser-generated spectral response using a 532 nm laser. A red line identifying the placement of the cross-section is highlighted. The cross-section of monochromatic spectral response for analysis of spectral FWHM.

Spectral Calibration

Spectral calibration for each row was performed to account for any minor differences in the spectral dispersion as a function of the incident angle on the prism and differences in the position of focus due to issues such as distortion. Calibration was done by fitting the results of three spectral bandpass filters to the equation for the spectral displacement:

$$Y(\lambda) = A + \frac{B}{\lambda^2}$$

Where Y is the pixel position, λ is the central wavelength of the filter, and A and B are the fitting coefficients. The source of illumination for the spectral calibration was the microscope's brightfield illumination source. The three filters selected have spectral centers evenly placed across the spectrum of interest at 483 nm (FF01-483-25, Semrock), 535 nm (AF01-535/40-25, Semrock), and 590 nm (FF01-590/36-25, Semrock).

The raw data for the fitting was extracted by analyzing the spatial profile to identify the central position of the spectral band. Figure 5-5 a illustrates the three spectral bands with false RGB coloring to simplify the position to wavelength conversion. The width of the spectral filters is non-ideal as the shape of the illumination spectra may adjust the peak position of the spectral bands. The accuracy of the fitting was tested against two lasers; a frequency-doubled Nd:YAG and a HeNe laser, with wavelengths at 532 nm and 640 nm, respectively. The cross section of the positions of each laser's peaks is demonstrated in Figure 5-5 b. The peaks are directly compared to the estimated positions from the fitting process, which are shown as vertical red and green lines. The mean error of the determined laser peak from the estimated position from the fitting process is demonstrated to be 1.6 nm, which is less than 5 nm, which corresponds to the bandwidth change of a single pixel. The fitting method is deemed to be accurate enough for accurate measurements of the fluorescence spectra.

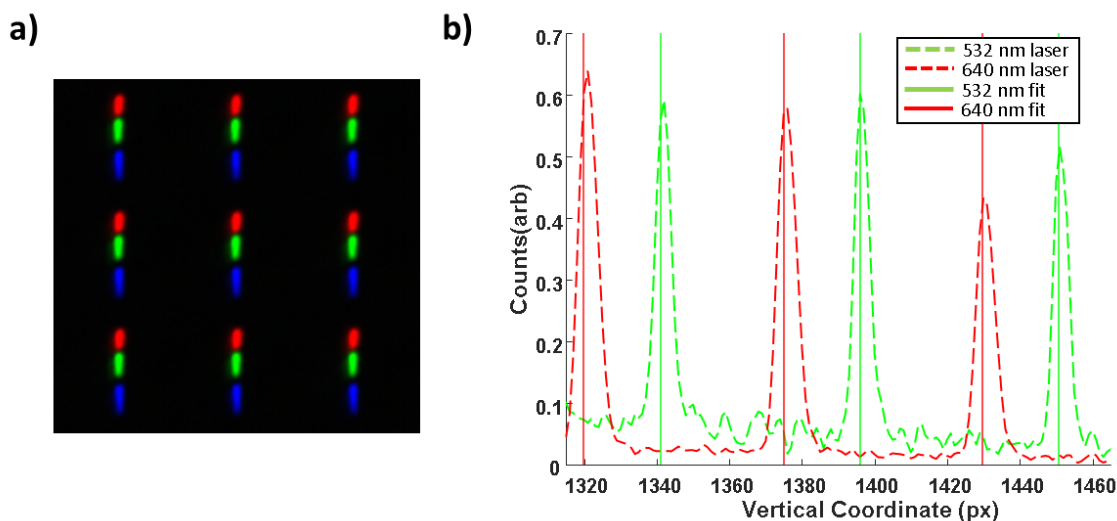


Figure 5-5. Spectral calibration. a) Band streaks as imaged onto the sensor with streak scanning converted to a three-channel image that best represents their color. b) Cross section of laser generated monochromatic spot functions for a 532 nm and 640 nm laser. Red and green vertical lines are the estimated position of the spot peaks from the tri-band calibration.

Sample: Convallaria

To demonstrate the potential of the imaging system, a Convallaria Majali's (Boston Electronics) was used to demonstrate the spatial image quality of the optical system. The Convallaria Majali's is a fixed sample that is fluorescently labeled with either two dyes, Safranin (530 nm, 590 nm) and Fast Green (620 nm, 660 nm), or a single dye, Acridine orange. Measurement of the optical power yielded approximately 0.5 mW at the objective's back focal plane, corresponding to 0.5

μW power per focus. The exposure time for this sample was 30 ms, which corresponded to 1 ms for each diffraction-limited region. Samples were analyzed using the MATLAB (R2023a) hyperspectral toolbox.

5.3. Results

Figure 5-6 illustrates the results of imaging the *Convallaria Majalis* stained with Fast Green and Safranin with the multipoint multispectral confocal microscope. Differences in localization of the dye allow spectral changes to be visually identified in the false color RGB representation (Figure 5-6a). Spectral curves allow precise identification of the two stains. Confocal imaging permits high-resolution spectral imaging due to the pinhole rejection of out of focus light and allows the differentiation of small but distinct layers of the sample for each wavelength band without compromising image quality. The differences between regions are a result of the different stains expressed in unique regions within the sample. It appears that there are 3 distinct spectral regions from the images, as illustrated in Figure 5-6 a, with spectral curves illustrated in Figure 5-6 b . ROI 2 and ROI 3 are highly correlated with the emission spectra of Fast Green and Safranin, respectively. The spectral curves indicate that there are minor differences in the 550-600nm regions, which are highlighted in ROI 1 as green-yellow in the false color image.

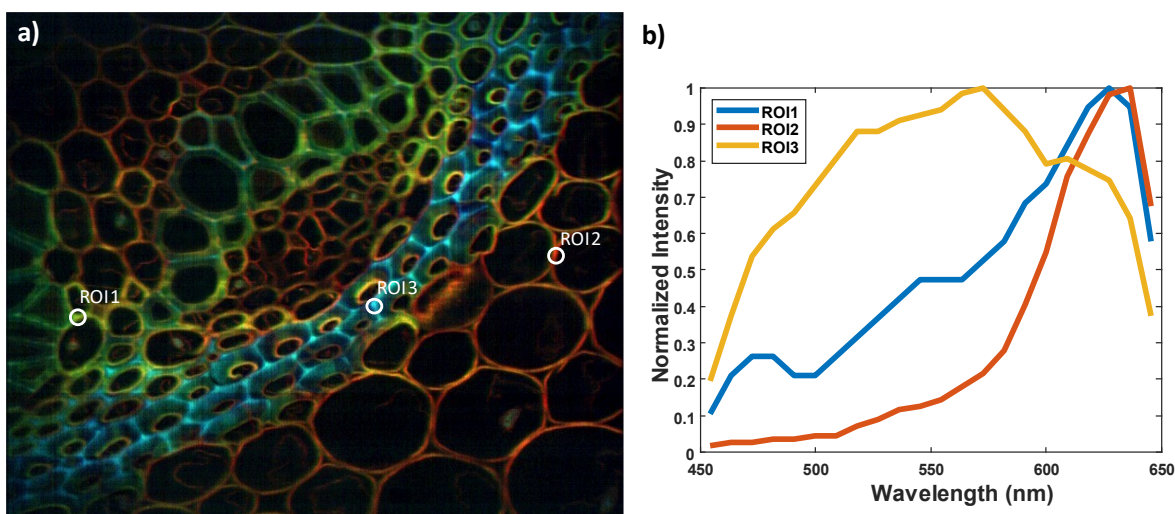


Figure 5-6. a) False-color RGB image of *convallaria Magali's* stained with Fast Green and Safranin generated from 22 distinct spectral band measurements with three regions of interest are highlighted. b) Spectral emission curves of the three selected regions of interest.

Figure 5-7 illustrates the *Convallaria* stained with Acridine orange. This *convallaria* was stained with only one fluorophore yet exhibits differences in spectral properties by the location of the staining region Figure 5-7 a. Acridine orange is known to have a change in wavelength due to the type of nucleic acid it binds to as well as the pH of the environment, and here, we can identify regions that are clearly different through the spectrum. In figures Figure 5-7 b-c we have used principal component analysis to isolate the two regions into different images. The technique

distinguishes two components that are separable. Component 1 appears to be limited to the 500-575 nm range, whereas component 2 appears to be limited to the 575-650 nm range.

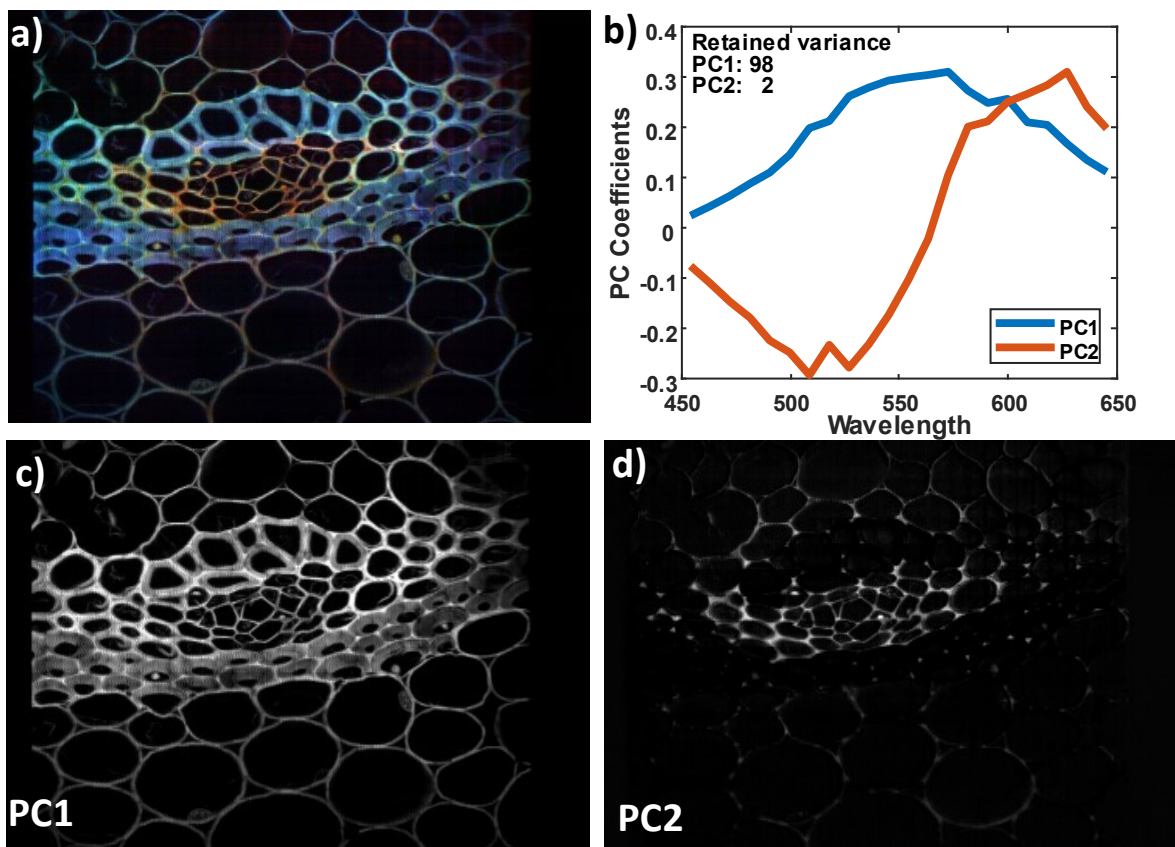


Figure 5-7. a) False-color RGB image of *Convallaria Majalis* stained with Acridine Orange over 22 spectral bands. The insert is the principal component weight by spectral band. b) Principal component coefficient analysis by wavelength. c-d) Images of the first and second principal components separated.

5.4. Discussion

We have developed a multipoint multispectral confocal microscope that uses a 32x32 pinhole array and a prism-based spectrometer to resolve confocal sections. This system obtains 22 unique spectral channels simultaneously by spectrally separating fluorescence emission onto a single image sensor. This imaging setup allows the simultaneous and efficient collection of fluorescence signals across the entire spectral emission profile using single-photon excitation. Our novel optical scanning solution enables the capture of multispectral images at a real-time frequency of 1 Hz with a sensor capable of 30 frames per second readout.

This technology stands out from previous methods due to the potential to multiplex at spot numbers several orders of magnitude larger. The size of the multiplexing array fit well with the spatial dimensions of the detector used in this research, however, at 4.5 pixels per spot the spatial sampling is higher than sampling requirements specified by Shannon-Nyquist. By

changing the magnification of the emission arm to $M=0.5$, the sampling spatial frequency requirements would still be met and allow 4x large number of foci to be sampled bringing the maximum number of multiplexed points to 4096, potentially becoming a FOV limited sampling technique. Although this system demonstrates an excellent potential to scale with the number of foci, the fundamental spectral resolution is limited both by the pinhole diameter and pinhole pitch. The diameter sets the requirement for the spatial sampling as the pixel size should be at least half the diameter of the pinhole. The pinhole spacing and the sampling frequency then determines the number of distinct spectra captured.

Simultaneous spectral band measurements are powerful for exploring multilabel and complex systems. Given the correct excitation wavelengths, a complete measurement of a system's spectral emission is possible, reducing phototoxicity and photobleaching effects on live cell measurements by preventing repeated exposure. Live cell imaging would require using a different image sensor with less noise, such as an sCMOS for low light imaging. In addition to static confocal imaging, this technique offers a potential path for a next-generation multipoint multispectral confocal FLIM. Previous multipoint multispectral confocal FLIM designs [Morgan 2024] were limited to capturing 900 readout frames to image a complete field of view. Those designs required readout of 10 GB datasets from the high-resolution sensor for a single FLIM image, limiting the image capture time to minutes. Next-generation FLIM sensors such as the PCO.FLIM.X (Excelitas) or the SPAD512² (PiImaging) are capable of video rate FLIM imaging, which would allow the creation of the first 1Hz multispectral multipoint confocal FLIM microscope while sustaining spectral and spatial resolution.

This optical system demonstrates a proof-of-concept for a spectrally resolved multipoint confocal microscope. The current multiplexing factor has not been previously demonstrated with multispectral confocal imaging. This technology has the potential to significantly impact various fields, including drug discovery, by providing a fast multispectral imaging platform that is natively compatible with next-generation image sensors for low-light and time-resolved measurements.

References

- [1] Combs C A and Shroff H 2017 Fluorescence Microscopy: A Concise Guide to Current Imaging Methods *Curr Protoc Neurosci* **79** 1–25
- [2] Balasubramanian H, Hobson C M, Chew T-L and Aaron J S 2023 Imagining the future of optical microscopy: everything, everywhere, all at once *Commun Biol* **6** 1096
- [3] Hiraoka Y, Shimi T and Haraguchi T 2002 Multispectral Imaging Fluorescence Microscopy for Living Cells. *Cell Struct Funct* **27** 367–74
- [4] Alijagic A, Scherbak N, Kotlyar O, Karlsson P, Wang X, Odnevall I, Benada O, Amiryousefi A, Andersson L, Persson A, Felth J, Andersson H, Larsson M, Hedbrant A, Salihovic S, Hyötyläinen T, Repsilber D, Särndahl E and Engwall M 2023 A Novel Nanosafety Approach Using Cell Painting, Metabolomics, and Lipidomics Captures the Cellular and Molecular Phenotypes Induced by the Unintentionally Formed Metal-Based (Nano)Particles *Cells* **12** 281

- [5] Kumar V, Chunchagatta Lakshman P K, Prasad T K, Manjunath K, Bairy S, Vasu A S, Ganavi B, Jasti S and Kamariah N 2024 Target-based drug discovery: Applications of fluorescence techniques in high throughput and fragment-based screening *Heliyon* **10** e23864
- [6] Vincent F, Nueda A, Lee J, Schenone M, Prunotto M and Mercola M 2022 Phenotypic drug discovery: recent successes, lessons learned and new directions *Nat Rev Drug Discov* **21** 899–914
- [7] Grant D M, McGinty J, McGhee E J, Bunney T D, Owen D M, Talbot C B, Zhang W, Kumar S, Munro I, Lanigan P M, Kennedy G T, Dunsby C, Magee A I, Courtney P, Katan M, Neil M A A and French P M W 2007 High speed optically sectioned fluorescence lifetime imaging permits study of live cell signaling events *Opt Express* **15** 15656
- [8] James B. Pawley 2006 *Handbook Of Biological Confocal Microscopy* ed J B Pawley (Boston, MA: Springer US)
- [9] Jonkman J, Brown C M, Wright G D, Anderson K I and North A J 2020 Tutorial: guidance for quantitative confocal microscopy *Nat Protoc* **15** 1585–611
- [10] Oreopoulos J, Berman R and Browne M 2014 Spinning-disk confocal microscopy *Methods in Cell Biology* vol 123 (Elsevier Inc.) pp 153–75
- [11] Hirmiz N, Tsikouras A, Osterlund E J, Richards M, Andrews D W and Fang Q 2020 Multiplexed confocal microscope with a refraction window scanner and a single-photon avalanche photodiode array detector *Opt Lett* **45** 69
- [12] Hirmiz N, Tsikouras A, Osterlund E J, Richards M, Andrews D W and Fang Q 2021 Highly Multiplexed Confocal Fluorescence Lifetime Microscope Designed for Screening Applications *IEEE Journal of Selected Topics in Quantum Electronics* **27** 1–9
- [13] Cha J W, Tzeranis D, Subramanian J, Yannas I V., Nedivi E and So P T C 2014 Spectral-resolved multifocal multiphoton microscopy with multianode photomultiplier tubes *Opt Express* **22** 21368
- [14] Shao Y, Qu J, Li H, Wang Y, Qi J, Xu G and Niu H 2010 High-speed spectrally resolved multifocal multiphoton microscopy *Appl Phys B* **99** 633–7
- [15] Oreopoulos J, Berman R and Browne M 2014 Spinning-disk confocal microscopy *Methods in Cell Biology* vol 123 (Elsevier Inc.) pp 153–75
- [16] Gräf R, Rietdorf J and Zimmermann T 2005 Live cell spinning disk microscopy *Adv Biochem Eng Biotechnol* **95** 57–75
- [17] Garini Y, Young I T and McNamara G 2006 Spectral imaging: Principles and applications *Cytometry Part A* **69** 735–47
- [18] Tsikouras A, Berman R, Andrews D W and Fang Q 2015 High-speed multifocal array scanning using refractive window tilting *Biomed Opt Express* **6** 3737

Chapter 6. Conclusions and Future Work

The development of a multipoint multispectral confocal fluorescence lifetime imaging microscope for live cell multidimensional imaging has been presented in this thesis. Here, I provide a summary of the presented work, discuss some of the design's shortcomings, and propose future improvements based on emerging technologies.

6.1 Summary

Microscopic imaging of fluorescently labeled live cells has been a revolutionary method for measuring cellular response to perturbations. Fluorescent labels have unique spectral and lifetime differences that can reveal complex cellular dynamics. When combined in a high-resolution confocal microscope, they offer spatial, spectral, and dynamic measurements that reveal the localization interaction. Multipoint confocal microscopy allows rapid and gentle imaging of live cells to reduce photobleaching and phototoxicity. This would enable long-duration imaging for cell models with a naturally cyclic behavior and make the technique compatible with drug discovery.

The ambition of this thesis was to produce the first implementation of a multipoint multispectral confocal FLIM microscope. It aimed to achieve one thousand or more focal point multiplexing with 50 spectral bands, each with a 10 nm resolution with overlapping bands that cover 450 nm to 700 nm. This system should be capable of making measurements at 1 Hz or faster. Current technology was compatible with producing a prototype system demonstrating this multifocal multidimensional concept. However, it fell short of its overarching expectations. This was largely a result of the technology that was selected for the demonstration system, the gated optical intensifier coupled to an sCMOS sensor.

Milestones presented in this thesis include:

- The optical system was redesigned around the pinhole array to improve the optical performance for live cell dynamic FLIM measurements. To accomplish high-speed imaging, improvements to optomechanical control, software processing, and scanner calibration were required. The new system has improved the real-time imaging speed from 3 seconds per FLIM image to 0.25 seconds per FLIM image. The new design was validated using fixed and live cell samples, and a dilution series was performed to better understand imaging performance. (Chapter 3)
- A multipoint multispectral confocal FLIM microscope was developed to capture 12 time-resolved spectral bands simultaneously within 1.8 seconds of exposure (2 minutes per FLIM image). New image processing was developed to automate the identification and calibration of spectral streaks. The system was tested using fixed samples, dye standards, and a FRET construct to capture live cell multispectral FLIM-FRET. (Chapter 4)
- An optical system was designed to capture 22 simultaneous spectral band multipoint confocal images at 1 Hz. This optical system is designed to reduce the sensor readout rate requirement from quadratic ($O(n^2)$) to linear ($O(n)$) scaling with image dimension, allowing significantly

faster image rates. Fixed samples and dye standards were used to demonstrate the imaging performance of the optical system with a CMOS image sensor. (Chapter 5)

Our implementation was limited fundamentally by the use of the gated optical intensifier. Its limited spatial resolution prevented the measurement of diffraction of limited spectra. Preventing crosstalk between spectra on the sensor required the use of a large pitch between foci, which reduced the density of foci, ultimately limiting the realization of one-thousand-point confocal measurements.

Systems	Chapter 3	Chapter 4	Chapter 5
Number of Focal Points	32x32	10x10	32x32
MLA Pitch (um)	300	500	300
Detector	Time-gated SPAD array	Gated Optical Intensifier	CMOS
Time Sampling Method	Simultaneous temporal gates	Sequential temporal gates	N. A
Temporal Gate Width (ns)	1.5 - 20	0.2 - 4	N. A
Spectral Channels	1	12	22
Spectral Resolution (nm)	40	40	20
Pulse Repetition Rate (MHz)	50	89	N.A.
Image Size (pixels)	960x960	300x300	960x960
Pinhole Diameter (AU)	1	0.9-1.4	0.9-1.4
Acquisition Time (s)	0.25	113	0.95
Sample Exposure (s)	0.20	0.9	0.9

Table 6-1. A comparison of each instrument demonstrated in this thesis.

In table 6-1, I directly compare each instrument for its spatial, spectral, and temporal capabilities, as well as the resulting image dimensions and capture times. FLIM images are captured using RLD with gated temporal image sensors. These sensors have different temporal gate widths and overall different temporal resolutions. The gated optical intensifier has a minimum gate width of 0.2 ns and SPAD of 1.5 ns. However, SPAD has a distinct advantage in that it has a timing resolution as low as 0.05 ns as SPAD technology relies on rise time to trigger digital circuitry. SPAD also has a distinct advantage as it can acquire multiple temporal gates simultaneously,

whereas the GOI can only acquire one. This means the technology is capable of measuring lifetimes more accurately and, with multiple gates, can separate multiexponential decay components. The SPAD array, however, lacks the number of spatial pixels that the GOI paired with a CMOS image sensor has thus making it currently incompatible with multispectral acquisition. As improvements in SPAD array technology continue, substitution of the GOI is expected.

The spatial resolution of each system is slightly different, as multispectral imaging requires balancing the size of the pinhole for both spatial and spectral requirements. A small pinhole improves spectral resolution as it limits feature size on the imaging spectrometer. However, a pinhole that is too small can also prevent sufficient light for red fluorescence measurement. We directly compare the pinholes in airy units to simplify spatial resolution comparisons. The pinhole diameter was chosen to satisfy both imaging at high magnification and N.A. and multispectral measurements and is found to range from 0.9 to 1.4 Airy units.

Image brightness will be sensitive to the efficiency with which the microlens array can fill the back aperture of the objective. A beam that matches the back aperture perfectly excites only the diffraction-limited volume. A beam that overfills the back aperture inefficiently excites the diffraction-limited volume as a large portion of the light is blocked. A beam that underfills the back aperture will be focused to a larger point, which will produce excitation in the out-of-focus volume, which is discarded by pinhole rejection in confocal microscopy. Currently, the $f_{\#}$ of the MLA is matched to the N.A. and magnification of the objective based on assumptions that the lens will satisfy a black box model. This may only be accurate for some lenses as back apertures may vary to account for differences in optical aberrations for unique designs.

In this work, I have demonstrated a practical set of technologies for time-resolved multispectral multipoint confocal imaging. This thesis aims to form a foundation of technologies for the widespread adoption of multispectral time-resolved fluorescence imaging in the next generation of multidimensional confocal microscopy.

6.2. Future Directions

6.2.1 Next generation time-resolved sensors for fast multispectral confocal FLIM

The next generation of multispectral confocal FLIM will rely on the advancements in image sensor technology. Critical to this next step are the temporal resolution required for time resolved fluorescence and the high resolution required for multispectral imaging.

Technologies such as SPAD arrays and multi-tap pixels offered in large resolution have become available to the market. SPAD arrays such as the SwissSPAD family of sensors are now being offered by PI imaging for the first commercially available megapixel SPAD array boasting a 512 x 512 pixel format [1,2]. This sensor technology can be designed with gate widths as low as 1 ns and features a dual temporal gate [3]. This sensor has already demonstrated its superior sensitivity for applications such as low light imaging as it offers near ideal signal to noise ratios when compared to sCMOS technology [4].

When faced with unknown samples with unpredictable signal intensities, however, SPAD arrays may not have the dynamic range required to measure both faint and bright signals simultaneously, as these sensors suffer from problems with pulse pileup [5]. As a result of the sampling problems, imaging conditions are typically tuned for sample conditions. In these situations where unknown sample behaviors are to be expected, such as in a general imaging facility, it may be ideal to choose a multi-tap frequency domain FLIM sensor such as the 1008x1008 pixel resolution PCO.FLIM X by Excelitas Technologies, which can capture up to 22 FLIM frames per second [6]. The next generation of this technology is also in development as designs have been presented pixels with an increased number of taps, such as the 4-tap and 8-tap pixels [7,8].

Multipoint Multiphoton FLIM-FRET

Two-photon fluorescence imaging of biological samples has become a significant technology for deep tissue imaging. Samples such as 3D cell cultures and in vivo imaging have gained tremendous importance in basic research and drug discovery due to their biological relevance [9–11]. Due to the high peak intensity required to observe two-photon fluorescence, pulsed lasers with ~ 100 fs pulse lengths are commonly used to achieve sufficient absorption without the high average power, which can lead to photo-thermal damage [12]. Modern diode-pumped solid-state lasers such as Ti: Sapphire technology offer more than sufficient pulse width and energy characteristics to perform multipoint multiphoton photon imaging, as they offer laser powers in excess of 2W [13,14]. The pulsed laser characteristics also act as a delta function impulse, allowing for high-quality FLIM imaging as a result.

6.2.2 Multipoint Rescan Confocal Microscopy for super resolution imaging

Rescan confocal is a revolutionary technique that allows a conventional confocal microscope to break the traditional diffraction limit of optical imaging [15]. It does so by introducing an opto-mechanically generated magnification of an image. A spatial resolution increase can be created by mechanically scanning the image at a larger spatial footprint and then collecting it. The mechanical image magnification which provides the best resolution improvement is $M=2$, and further magnification reduces the optical resolution due to the resulting image blur of the spot.

In Chapter 6, we demonstrated a mechanism that allows us to scan a fluorescence spectrum in the fast-scanning axis to achieve multispectral multipoint confocal microscopy. This optical system could be modified in two ways to achieve the same super-resolution imaging improvement. Either change the sweeping scanner's angle to permit a double image sweep length where the emission spots pass between each focus and paint the intensity profile directly on the imaging sensor. Or a second scanner can be introduced to perform $M=2$ sweeping of a quarter of the field of view of the MLA pitch, resulting in the requirement to capture 4 images per MLA pitch. Both options would be unable to capture the entire image in a single sensor readout and would need post-processing after image capture. However, this would be significant as the field

of view for rescan confocal microscopy is limited, and our confocal scanning mechanisms could offer larger fields of view at faster frame rates.

6.2.3 System Quality of Life Improvements

Packaging and Alignment

Currently, the Multipoint confocal setup is a free-space optical system that is directly built onto the optical table. We have designed and selected parts to build the system onto a portable breadboard with the aim of making the platform a modular attachment for any microscope. This involves reshaping the optical path for compactness while maintaining ease of alignment and detailing the optical alignment procedure for non-specialists. Packaging the solution into a compact package will be a dramatic improvement to the optical system as it should prevent light pollution from reaching the detection optics and prevent contamination and physical damage or accidental adjustment of optical system alignment. Currently, a new compact footprint has been designed, and items have been selected for the purpose of this task.

Confocal Scan lens for Optical Relays

Improving the optical performance of the imaging system will largely depend on the improvements to the optical system components. Namely, the largest offender for producing poor quality focal spots is the lenses used to construct the optical relays. We use Thorlabs achromats, an off-the-shelf set of components designed for the most basic imaging situations, as they offer sufficient optical performance for demonstration purposes. However, they have a rather narrow image size for truly diffraction-limited spot generation. As a result, the spots that are formed at the margins of our image planes typically exhibit a radial smear as a result of the sum of aberrations present in their optical path. Improving these marginal spots will improve coupling efficiency in the excitation arm, leading to improved fluorescence illumination uniformity throughout the sample and preventing the edge dimming present in images by increasing the edge excitation. Improving the spot quality in the emission arm will also have a similar effect on the optical system, as the emission image from the pinhole array experiences a degraded image quality post-emission relay transmission. Poor emission foci quality leads directly to reduced imaging performance in multispectral imaging and, as a result, directly limits the number of diffraction-limited spectral bands.

Improved lenses such as scan lenses or even tube lenses (although not suggested) may significantly improve the spot quality on the spots furthest from the optical axis. An example of these lenses may be the Thorlabs CLS-SL - Scan Lens, which offers a $16 \times 16 \text{ mm}^2$ diffraction limited field of view over 400-750 nm spectral range. This lens is ideal for improved optical performance but has a small effective focal length that will make alignment slightly more difficult.

Improved Dispersion Elements

Currently, a thin prism made of N-BK7 is used to produce the spectral dispersion. Although this prism is sufficient to demonstrate the basic optical concept, it lacks the performance found in many high-quality spectroscopy systems. The prism will have a larger change in refractive index for blue wavelength than red, and as a result, the spectrometer has a nonuniform spectral resolution. The prism will also produce a large angular displacement, which increases the complexity of the alignment. A direct vision geometry would simplify the alignment of the optical system as a central wavelength, such as the 532 nm from a laser diode, which could be used to design and align the entire optical system and measure the resulting spectral resolution.

Replacing this single prism with a custom-designed GRISM or a compound prism such as the dispersive Amici prism [16–20], will improve the quality of the spectrometer as it will create uniformly dispersed spectral streaks, meaning each pixel will have an equal spectral bandwidth.

Software UI improvements

Currently, a custom C++ application has been developed to control the multipoint confocal microscope. For a time, this was essential as the application was directly involved in the scanning mechanism of the confocal microscope. With the introduction of the GB-511, a controller that synchronizes the triggering of the detector and the sweeping of the scanner, the dependence on Realtime control over each element is no longer essential. A wise move would be to separate the backend and front end into separate languages and applications. The backend should be maintained as a C++ application. However, a different language may be more straightforward for image processing and visualization of datasets. Currently, most image processing occurs on MATLAB. Another motivation would be to move away from MFC, which is no longer actively developed by Microsoft. This would allow the UI design to be a separate process from backend improvement.

Multi-Wavelength Excitation

Currently, a single pulsed laser is used for all samples as the excitation wavelength. This limits the total practical application to the diverse set of samples that could be imaged on our platform. A set of at least three lasers spanning the most common wavelengths should be integrated into the system. This would be a simple upgrade, as the development of laser systems has led to single box solutions common. An example of this could be the Picoquant Prima, a three-color computer controlled light source. The three laser wavelengths are selectable between five wavelengths between 405 nm and 640 nm.

A multi-line laser source is also required for a new filter cube switcher. Currently, a single fixed cube is mounted to separate the excitation wavelengths from the emission wavelengths. This would need to be changed to have at least three positions to select from while maintaining a compact profile for integration into the enclosed system.

Deconvolution Microscopy

A significant step for many modern microscopes is post-capture image processing. One popular step is image deconvolution, which allows improved spatial resolution to be achieved [21]. Image deconvolution removes the blurring effect of the microscope point spread function to

reassign the photon counts to the proper pixel position. There are many algorithms to accomplish this task, but they are typically iterative algorithms that incrementally make improved guesses to the underlying object geometry by comparing a forward convolution with a guess and estimating the error of the result with the captured image. These algorithms take advantage of advances in GPU processing to accomplish their task quickly. Programs such as Huygens Deconvolution by Scientific Volume Imaging would be quite effective for performing deconvolution of 3D confocal image stacks.

6.3 Conclusion

The work in this dissertation has been aimed toward advancing multipoint multidimensional imaging. I have demonstrated improvements to core multipoint confocal optical design, which has led to significant improvements in optical efficiency and image quality. These changes made imaging rates of 4 Hz possible after substantial changes to hardware and software architecture and led to improvements for all future systems. Multispectral time-resolved fluorescence was demonstrated to be possible and yield full spectral lifetimes that demonstrate FRET through lifetime spectroscopy. A new method of imaging multispectral multipoint confocal images has been demonstrated to improve the image capture speed to those required for dynamic measurements. In these three systems, almost all aspects of the microscope have undergone significant changes to push the platform beyond its original goal as a 1 Hz FLIM microscope.

Future changes to this system will closely follow the developments of detection technology. With the advent of smaller pixel technologies and larger resolution, FLIM-capable image sensors, lifetime imaging will become accessible to many users in non-specialist labs. Metabolic imaging and lifetime contrast for FRET will increase in popularity as straightforward tools to probe dynamic cellular interactions.

References

- [1] Ardelean A, Ulku A C, Michalet X, Charbon E and Bruschini C 2019 Fluorescence lifetime imaging with a single-photon SPAD array using long overlapping gates: an experimental and theoretical study *Multiphoton Microscopy in the Biomedical Sciences XIX* ed A Periasamy, P T So and K König (SPIE) p 33
- [2] Ulku A C, Bruschini C, Antolovic I M, Kuo Y, Ankri R, Weiss S, Michalet X and Charbon E 2019 A 512×512 SPAD Image Sensor With Integrated Gating for Widefield FLIM *IEEE Journal of Selected Topics in Quantum Electronics* **25** 1–12
- [3] Wayne M, Ulku A, Ardelean A, Mos P, Bruschini C and Charbon E 2022 A 500×500 Dual-Gate SPAD Imager with 100% Temporal Aperture and 1 ns Minimum Gate Length for FLIM and Phasor Imaging Applications *IEEE Trans Electron Devices* **69** 2865–72
- [4] Schwartz D E, Charbon E and Shepard K L 2007 A single-photon avalanche diode imager for fluorescence lifetime applications *IEEE Symposium on VLSI Circuits, Digest of Technical Papers* 144–5

- [5] Becker W 2017 *The bh TCSPC Handbook, Pile-Up* (Becker & Hickle)
- [6] Franke R and Holst G A 2015 Frequency-domain fluorescence lifetime imaging system (pco.flim) based on a in-pixel dual tap control CMOS image sensor *Imaging, Manipulation, and Analysis of Biomolecules, Cells, and Tissues XIII* vol 9328 (SPIE) p 93281K
- [7] Shirakawa Y, Seo M-W, Yasutomi K, Kagawa K, Teranishi N and Kawahito S 2017 Design of an 8-tap CMOS lock-in pixel with lateral electric field charge modulator for highly time-resolved imaging *Silicon Photonics XII* **10108** 101080N
- [8] Seo M-W, Shirakawa Y, Kagawa K, Yasutomi K and Kawahito S 2017 A high performance multi-tap CMOS lock-in pixel image sensor for biomedical applications *High-Speed Biomedical Imaging and Spectroscopy: Toward Big Data Instrumentation and Management II* **10076** 100760V
- [9] Katt M E, Placone A L, Wong A D, Xu Z S and Searson P C 2016 In Vitro Tumor Models: Advantages, Disadvantages, Variables, and Selecting the Right Platform *Front Bioeng Biotechnol* **4** 12
- [10] Jong B K 2005 Three-dimensional tissue culture models in cancer biology *Semin Cancer Biol* **15** 365–77
- [11] Langhans S A 2018 Three-dimensional in vitro cell culture models in drug discovery and drug repositioning *Front Pharmacol* **9** 1–14
- [12] James B. Pawley 2006 *Handbook Of Biological Confocal Microscopy* ed J B Pawley (Boston, MA: Springer US)
- [13] Bewersdorf J, Egner A and Hell S W 2006 Multifocal multi-photon microscopy *Handbook of Biological Confocal Microscopy: Third Edition* **23** 550–60
- [14] Coelho S, Poland S, Krstajic N, Li D, Monypenny J, Walker R, Tyndall D, Ng T, Henderson R and Ameer-Beg S 2013 Multifocal multiphoton microscopy with adaptive optical correction *Multiphoton Microscopy in the Biomedical Sciences XIII* **8588** 858817
- [15] De Luca G M R, Breedijk R M P, Brandt R A J, Zeelenberg C H C, de Jong B E, Timmermans W, Azar L N, Hoebe R A, Stallinga S and Manders E M M 2013 Re-scan confocal microscopy: scanning twice for better resolution *Biomed Opt Express* **4** 2644
- [16] Hagen N and Tkaczyk T S 2011 Compound prism design principles, II: triplet and Janssen prisms *Appl Opt* **50** 5012
- [17] Hagen N and Tkaczyk T S 2011 Compound prism design principles, I *Appl Opt* **50** 4998
- [18] Hagen N and Tkaczyk T S 2011 Compound prism design principles, III: linear-in-wavenumber and optical coherence tomography prisms *Appl Opt* **50** 5023
- [19] Neviere M 1991 Electromagnetic study of transmission gratings *Appl Opt* **30** 4540

- [20] Nevière M, Laude J P and Maystre D 1990 Perfect blazing for transmission gratings *Journal of the Optical Society of America A* **7** 1736
- [21] De Monvel J B, Le Calvez S and Ulfendahl M 2001 Image restoration for confocal microscopy: Improving the limits of deconvolution, with application to the visualization of the mammalian hearing organ *Biophys J* **80** 2455–70